VECTRA

NEDO-10084-4
MARCH 1995

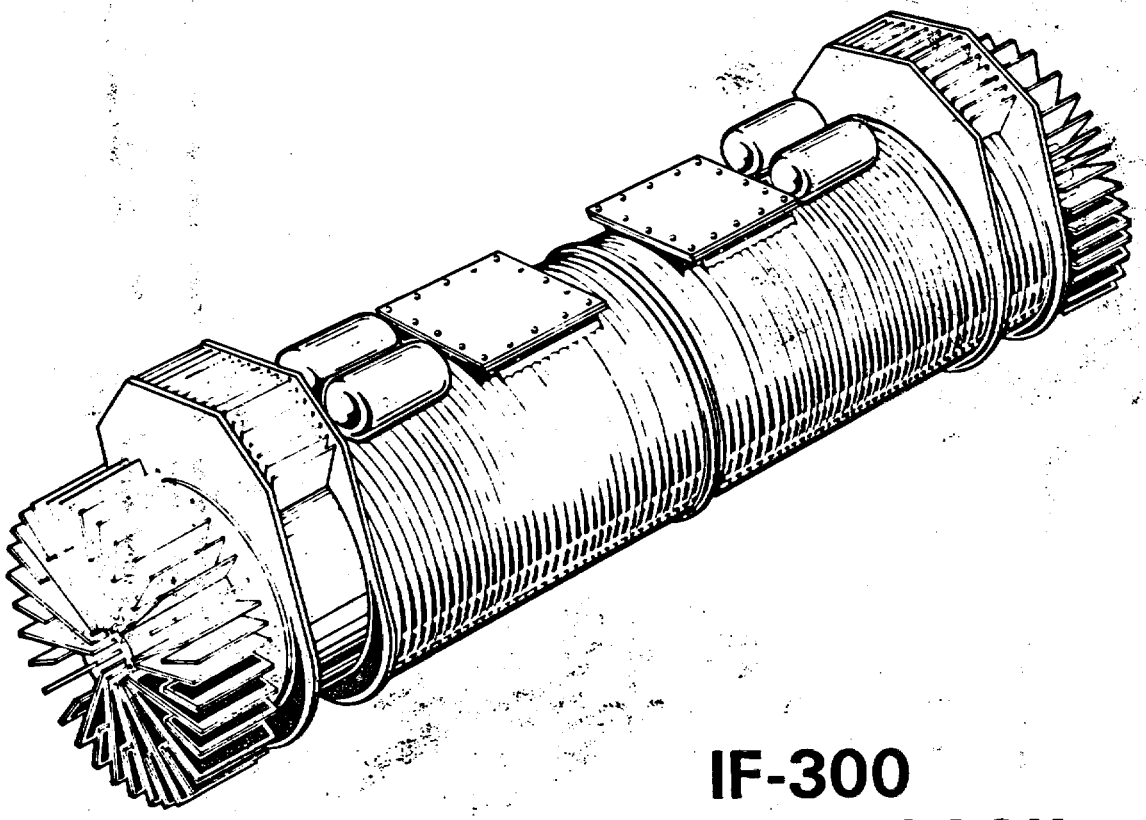

IF-300 SHIPPING CASK

CONSOLIDATED SAFETY ANALYSIS REPORT

VOLUME 1

NOTICE AND DISCLAIMER

All revision of this report through NEDO-10084-3 were prepared by General Electric Company solely for the use of the U.S. Nuclear Regulatory Commission (NRC) in licensing the IF-300 Shipping Cask. General Electric assumes no responsibility or damage which may result from any other use of the information disclosed in any revision of this report through NEDO-10084-3.

The information contained in revisions of this report through NEDO-10084-3 is believed by General Electric to be an accurate and true representation of the facts known, obtained, or provided to General Electric through May 1985. General Electric Company and the contributors to revisions of this report through NEDO-10084-3 make no express or implied warranty of accuracy, completeness, or usefulness of the information contained in this report with respect to any change of fact or law set forth therein, whether material or otherwise, and General Electric Company makes no warranty or representation, expressed or implied, with respect to the accuracy, completeness, or usefulness of the information contained in this report, other than for the licensing of the IF-300 Shipping Cask or that the use of any information disclosed in this report may not infringe privately owned rights including patent rights.

In 1988, VECTRA became the principal Licensee holder for the IF-300 Shipping Cask. VECTRA is responsible for all changes to this report starting with NEDO-10084-4.

REVISION CONTROL SHEET

TITLE: Consolidated Safety Analysis Report for IF-300 Shipping Cask

DOCUMENT NO.: NEDO-10084

AFFECTED PAGE(S)	DOC. REV.	REMARKS
1-i	3	Last revision prepared by General Electric Company. Incorporates all C of C 9001, Revision 29 references from 2/8/84 through 5/10/85. A vertical line on the right hand margin indicates a revision. "N" denotes new information while "E" denotes an editorial change.
1-1 & 1-2	"	
2-i & 2-ii	"	
2-1 - 2-15	"	
3-i & 3-ii	"	
3-1 - 3-16	"	
4-i & 4-ii	"	
4-1 - 4-21	"	
5-i - 5-vi	"	
5-1 - 5-311	"	
6-i - 6-iv	"	
6-1 - 6-82	"	
7-i - 7-ii	"	
7-1 - 7-22	"	
8-i & 8-ii	"	
8-1 - 8-22	"	
9-i & 9-ii	"	
9-1 - 9-6	"	
10-i & 10-ii	"	
10-1 - 10-15	"	
A-i/A-ii	"	
V1-i - V1-iv	"	
V1-1 - V1-52	"	
V1-A-i/ii	"	
V1-A-1 -	"	
V1-A-3	"	
V1-B-i/ii	"	
V1-B-1 &	"	
V1-B-2	"	

PAGE 1 OF 3

REVISION CONTROL SHEET

TITLE: Consolidated Safety Analysis Report for IF-300 Shipping Cask

DOCUMENT NO.: NEDO-10084

AFFECTED PAGE(S)	DOC. REV.	REMARKS
V1-C-i/ii	3	
V1-C-1 -	"	
V1-C-8	"	
V1-D-i -	"	
V1-D-vi	"	
V1-D-1 -	"	
V1-D-132	"	
V1-E-i &	"	
V1-E-ii	"	
V1-E-1 -	"	
V1-E-34	"	
V2-i - V2-iv	"	
V2-1 - V2-64	"	
V3-i - V3-iv	"	
V3-1 - V3-32	"	
VI-i/VI-ii	"	
VI-1 - VI-6	"	
i - viii	4	First revision prepared by VECTRA Technologies, Inc.
1-1	"	Incorporates C of C 9001, Revision 29 references
2-1 & 2-2	"	from 7/26/90 through 4/25/94.
2-3 & 2-3a	"	A vertical line on the left hand margin indicates a
2-4 & 2-5	"	revision.
2-8	"	
2-10 & 2-11	"	
2-14 & 2-15	"	
3-1 & 3-1a	"	
3-2a	"	
3-16	"	
4-1, 4-3, & 4-5	"	
4-9 & 4-10	"	

REVISION CONTROL SHEET

TITLE: Consolidated Safety Analysis Report for IF-300 Shipping Cask

DOCUMENT NO.: NEDO-10084

AFFECTED PAGE(S)	DOC. REV.	REMARKS
5-1, 5-3, & 5-5	4	
5-101 & 5-270	"	
6-1 & 6-1a	"	
6-2 & 6-2a	"	
6-33 & 6-35	"	
7-1 & 7-2	"	
8-1 & 8-3	"	
8-19 & 8-20	"	
9-1, 9-2, & 9-6	"	
10-4	"	
A-i/ii	"	
A-iii - A-xiii	"	
A-1-1 - A-1-10	"	
A-2-1 - A-2-338	"	
A-3-1 - A-3-86	"	
A-4-1 - A-4-5	"	
A-5-1 - A-5-92	"	
A-6-1 - A-6-131	"	
A-7-1 & A-8-1	"	
A-9-1 - A-9-13	"	
B-i/ii	"	
B-iii & B-iv	"	
B-1 - B-55	"	
C-i/ii	"	
C-iii/iv	"	
C-1 - C-14	"	

PAGE 3 OF 3

(BLANK PAGE)

NEDO-10084-3
May 1985

CONSOLIDATED SAFETY ANALYSIS REPORT FOR IF-300 SHIPPING CASK

REVISION SUMMARY

Revision and Amendment	Submittal Date(s)	Summary
NEDO-10084-3	9/84 2/85 4/85 5/85	Consolidation of previous licensing documentation and general document revision.

REVISION CODING KEY: New or changed information is indicated by vertical bars in the right margin opposite the new or changed information; "E" indicates editorial changes or corrections. Minor editorial corrections (e.g. spelling, tense, and nomenclature) are not coded.

DOCUMENT NUMBER KEY:

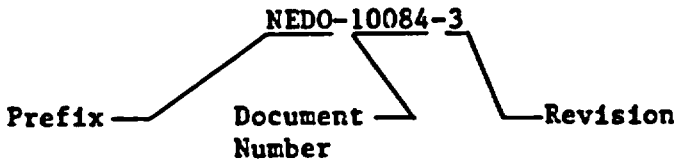

TABLE OF CONTENTS

VOLUME 1

TABLE OF CONTENTS
(Continued)

VOLUME 1
(Concluded)

TABLE OF CONTENTS
(Continued)

VOLUME 2

TABLE OF CONTENTS
(Concluded)

VOLUME 3

TABLE OF CONTENTS

I. INTRODUCTION

I. INTRODUCTION

1.1 PURPOSE

Prior to 1988, General Electric was the principle Licensee holder for the IF-300 shipping cask. Starting in 1988, VECTRA became the principle Licensee holder for this system. All references to General Electric as the principle Licensee holder in this report should currently be understood to be referring to VECTRA.

This Consolidated Safety Analysis Report (CSAR) represents the technical basis for Certificate of Compliance (C of C) Number 9001, including revisions, for the IF-300 shipping cask. This CSAR can be amended by VECTRA through the submittal of changes and/or additions which must be reviewed and accepted by the United States Nuclear Regulatory Commission (NRC).

Originally, the authorized contents of the IF-300 cask was restricted to Group I type fuel bundles, which included 14 x 14 and 15 x 15 fuel rod arrays for PWR bundles and 7 x 7 fuel rod arrays for BWR bundles.

In 1982, the C of C was amended to authorize shipment of Group II fuel bundles which had begun to replace the Group I fuel bundles in operating reactors. The Group II fuel bundles have a larger number of smaller diameter fuel rods. Group II fuel bundles have a larger number of smaller diameter fuel rods. Group II includes the 16 x 16 and 17 x 17 fuel rod arrays for PWRs and the 8 x 8 fuel rod array for BWRs.

Shipment of solid, non fissile, irradiated hardware was authorized in a 1984 amendment.

Shipments of BWR fuel with channels in a 17 element fuel basket (Volume 3, Appendix A) was authorized in a 1991 amendment and shipments of high burnup PWR fuel (Volume 3, Appendix B) was authorized in a 1994 amendment. The use of an outer plastic wrap to contain "weeping" was also authorized in a 1991 amendment (Volume 3, Appendix C).

1.2 IF-300 CASK

The IF-300 cask is designed to meet or exceed all NRC and

Department of Transportation (DOT) regulations governing the shipment of radioactive material. The primary transportation mode is by railroad, although the shipping package is designed to facilitate truck shipment on a special overweight basis for short distances. This features allows the servicing of reactor sites and other facilities which lack direct railroad access.

The IF-300 cask body is a depleted uranium shielded, stainless steel clad annular cylinder, closed at one end. Fuel is loaded into the cask through the open end and the cask is closed with a bolted and sealed head. The head construction is similar to the body of the cask.

Fuel bundles are located within the cask cavity by a removable stainless steel basket. There are several basket configurations which may be used, depending on the specific fuel being shipped. There are also two heads which permit a variation in cask cavity length. When solid, nonfissile, irradiated hardware is shipped, it is placed within a non-reusable steel liner liner built specifically for that hardware. The cask cavity is air-filled and utilizes a rupture disk device for over pressure protection.

The cask outer surface has large circumferential fins designed for impact protection. Encircling the active fuel zone is a water-filled annulus with corrugated jacket which acts as a neutron shield. The upper and lower ends of the cask are also equipped with sacrificial fins for impact protection.

The cask is cooled, when desired, by diesel engine driven blowers which maintain outer surfaces at temperatures facilitating handling. The cooling system is not required to preserve cask integrity or retain coolant. Four longitudinal ducts direct air from two blowers onto the corrugated surface.

The cask, cask supports, and cooling system are all mounted on a steel skid. Exclusion from the cask and cooling system is provided by a wire mesh enclosure which is retractable for cask removal and locks in place during transport. The skid mounted equipment forms a completely self-contained irradiated fuel and hardware shipping package.

TABLE OF CONTENTS

II. DESIGN SUMMARY

E

LIST OF TABLES

II. DESIGN SUMMARY

2.1 CASK DESCRIPTION

The VECTRA IF-300 Spent Fuel Shipping Cask is designed in accordance with the criteria of Federal Regulations 10CFR71 and 49CFR173.

Prior to 1994, the fuel loadings which could be contained in the IF-300 were as follows:

Table II-1

FUEL LOADINGS

Reactor Type	NSSS Manufacturer	No. of Bundles	Fuel Rod Array	Cladding Material	Fuel Group
BWR	General Electric	18	7 x 7	Zircaloy	I
PWR	Westinghouse	7	14 x 14	Stainless Steel	I
	Westinghouse	7	14 x 14	Zircaloy	I
	Westinghouse	7	15 x 15	Stainless Steel	I
	Westinghouse	7	15 x 15	Zircaloy	I
PWR	Combustion	7	15 x 15	Zircaloy	I
PWR	Babcock-Wilcox	7	15 x 15	Zircaloy	I
BWR	General Electric	18	8 x 8	Zircaloy	II
PWR	Westinghouse	7	17 x 17	Zircaloy	II
PWR	Combustion	7	16 x 16	Zircaloy	II
PWR	Babcock-Wilcox	7	17 x 17	Zircaloy	II

Since 1994, the IF-300 cask has also been permitted to contain 15 x 15 PWR fuel with a maximum burnup of up to 45,000 MWd/MTU with a minimum cooling time of 60 months as described in Volume 3, Appendix B.

Either BWR or PWR fuel bundles can be accommodated through the use of removable fuel baskets, spacers and two different length closure heads. In addition to irradiated fuel bundles, the IF-300 cask may be used to transport solid non-fissile irradiated hardware.

The cask weight when loaded is between 130,000 and 140,000 pounds depending on the particular type of fuel being shipped. The skid and cooling system weigh approximately 45,000 pounds.

The cask is mounted horizontally on an equipment skid during transport. Although transportation is primarily by rail, the skid is designed to accept wheel assemblies for short haul, special permit trucking. This dual-mode shipping configuration permits the use of the IF-300 cask at those reactor sites which have no direct rail access.

The cask is supported on the skid by a saddle at the head end and a cradle at the bottom end. The cradle forms the pivot about which the cask is rotated for vertical removal from the skid. There is one pickup position on the cask body just below the closure flange. The support saddle engages the cask at this section. The lifting trunnions are removed during transport. The pivot cradle trunnions are slightly eccentric to ensure the proper rotation direction for cask lay-down. The cradle is counter-weighted to remain horizontal when the cask is removed.

The cask is lifted by one of two special yokes, a normal unit and a redundant unit. Either yoke accepts the reactor building crane hook in its upper end and engages the cask lifting trunnions with its lower end. Each yoke is designed to be used with either head. The cask head is removed using four steel cables which are attached to the lifting yoke. The same yoke is used for cask uprighting and cask lifting.

All external and internal surfaces of the cask are stainless steel. The outer shell of the cask body is CG-8M (317) stainless steel. The inner shell is 317 or 216 stainless steel. The circumferential fins are 216 stainless steel and the flanges and end fins are 304 stainless steel. The fuel baskets are made of 216 and 304 stainless steel.

Gamma and fast neutron shielding, respectively, are provided in the IF-300 cask by depleted uranium metal between the cask shells and a water/ethylene glycol mixture filled annulus surrounding them. The thin walled jacket which retains the neutron shielding water is fabricated from

stainless steel and is corrugated for maximum strength and heat transfer.

The closure head is sealed with a Grayloc metallic ring. The cavity maximum normal operation pressure (LOMC) is 29 psig. However, the design working pressure is 400 psig and overpressure protection is provided by a rupture disk device designed to have a bursting pressure of 350-400 psig at 443 degrees fahrenheit. The rupture disk device is located in one of two cavity valve boxes.

Each cavity valve box is equipped with one nuclear service fill, drain, and vent valve. For ease in servicing, these valves have a quick disconnect fitting which may, as an option, be replaced by a stainless steel pipe cap or pipe plug during cask shipment.

The neutron shielding annulus is partitioned into two separate sections, each protected from overpressure by a 200 psig relief valve located in one of two neutron shielding valve boxes. Service to each section is provided annually through fill, drain, and vent valves also located in the neutron shielding valve boxes. These valves may be replaced by a stainless steel blind flange. All valve handles and/or blind flange bolts are lockwired during transit to prevent loosening.

A thermocouple well is attached to the outside of the inner shell at a point expected to be at the highest temperature. The thermocouple well emerges from the cask bottom and accepts a replaceable chromelalumel thermocouple.

The fuel bundles are contained within a removable, slotted, stainless steel basket. For the fuel baskets licensed prior to 1991, criticality control is achieved by using B_4C-filled, stainless steel tubes installed in the basket. For the channelled BWR fuel basket licensed in 1991, criticality control is achieved by using borated stainless steel poison plates (Volume 3, Appendix A). Fuel bundles are restrained axially by spacers mounted on the inside of the closure head or in the bottom of the fuel basket. The basket is centered within the cask cavity by disk spacers. Nine such spacers are mounted along the fuel basket length. Fuel bundles are inserted and removed from the basket using standard grapples. The basket is removed when the cask is to be used for the shipment of another fuel type or for cask cavity cleaning. the BWR basket has stainless steel clad uranium shielding pieces mounted on the end adjacent to the cask flange.

The outer surface of the cask body is finned for impact protection. These fins are stainless steel and are circmuferential to the cask

diameter. The cask ends and valve boxes are also finned for impact protection. All fins are welded to the cask body. The external water jacket is constructed of thin-walled material and does not contribute to the impact protection of the cask.

2.2 STRUCTURAL ANALYSIS

2.2.1 The IF-300 cask is specifically designed to meet the structural requirements of 10CFR71. Safety factors are based on allowable loads, stresses and deflections. For some components yield strength of the material is the limiting parameter; for others, ultimate strength is the true limit.

In general, for normal or slightly off-normal conditions material yield is the basis for the safety factor. It is usually under accident conditions where some components yield and take a permanent set. Under these conditions integrity of the component is the primary concern. Since almost all of the cask components are of austenitic stainless steel having good ductility, there is a significant difference between the stress required to yield the material and that needed to actually fail (break) it. Thus, for certain loadings and components ultimate strength is the safety factor basis.

2.2.2 Stress analyses have been performed for the following conditions:

- A combined 10 g axial, 5 g lateral and 2 g vertical load on the cask-to-skid tiedowns.
- With the cask acting as a beam supporting five times its weight.
- With an external pressure of 25 psig applied to the cask.
- Accidents, which include a 30 foot drop in various attitudes, a 40 inch puncture, and a 30 minute fire.
- Cask handling, in both unloading and loading operation.

- Off-normal conditions including loss-of-mechanical cooling, partial loss-of-shielding water and vandalism.

The normal transport analysis demonstrates the ability of the cask and its tiedowns to sustain both internal and external loads and maintain a yield-based safety factor greater than unity.

The cask uprighting and lifting analysis shows that no component stress level exceeds the material yield strength.

The accident analysis is divided into several parts: 1) the cavity as a pressure vessel; 2) the cask as a structure; and, 3) the cask contents.

1. The cavity sees its maximum internal pressure under accident conditions. The cavity component stresses do not exceed yield.

2. The cask body undergoes severe loading in all of the 30 foot drop orientations. There is slight flange yielding in the corner drop and slight outer shell yielding in the side drop. However, the cask remains sealed with no significant reduction in gamma shielding.

3. Group I and Group II fuel bundles were independently analyzed for the 30 foot drop. The analytical results were similar. The fuel and fuel basket undergo severe loading in the 30 foot drop and some yielding occurs. However, the extent of yielding of the fuel basket structure is limited by the short duration of the loading and the confinement of the cavity walls.

Based on allowable limits, no fuel or basket failures occur in the 30-foot drop.

The components which mitigate the 30-foot drop effects are the impact fins which protrude from the cask ends and side. These structures deform on impact in a predictable manner and limit the forces transmitted to the cask body and contents.

2.2.3 Tables II-2 and II-3 summarize the normal and accident condition "G" loadings and the structures affected.

Table II-2

NORMAL CONDITION "G" LOADINGS

E

Component	Direction/Orientation	"G" Loading
Cask Tiedowns		
Saddle & Pins, Pedestals, Cradle, Body Shell & Rings	Axial	10
	Lateral	5
	Vertical	2
Lifting		
Body Shell & Rings, Trunnions & Pins, Yoke	Cask Horizontal	3
Body Shell & Rings, Trunnions & Pins, Yoke	Cask Vertical	3

Table II-3

ACCIDENT CONDITION "G" LOADINGS

Drop Distance	Drop Orientation	Loading "G's"	Type of Analysis	Component
30 ft	Top End	356	Static[3]	Closure Flange
		560	Static[4]	BWR Fuel Basket Shielding
30 ft	Bottom End	234	Static[1]	Fuel Bundles Poison Rods
		573	Static[4]	BWR Fuel Basket Shielding
		287/127	Dynamic[5]	BWR Fuel Basket Tie Rods
30 ft	Top Corner	113.6	Static[3]	Closure Flange & Studs
30 ft	0° Side	218	Static[3]	Valve Box and Lid
		214	Static[2]	BWR Fuel Basket Shielding
		214/96	Dynamic[5]	BWR Fuel Basket Spacer Disks
30 ft	20° Side	141.2	Static[3]	Valve Box and Lid
30 ft	45° Side	184	Static[2]	BWR Fuel Basket Shielding
30 ft	90° Side	122.3	Static[1]	Fuel Bundles Poison Rods Cask Body
		137	Static[2]	BWR Fuel Basket Shielding

Notes

1. Applied load based on average cask deceleration
2. Applied load based on peak cask deceleration
3. Applied load based on 2 x average cask deceleration
4. Applied load based on 2 x peak cask deceleration
5. Applied load based on peak and plateau cask acceleration

2.2.4 The structural analyses show that the cask and tiedowns are more than capable of sustaining the loads associated with normal operation. Furthermore, with the protection provided by the impact fins the cask is capable of enduring the accident drop, puncture and pressure conditions without loss of integrity or unacceptable damage to contents.

II. DESIGN SUMMARY

2.3 THERMAL ANALYSIS

2.3.1 Design Basis Conditions

Five basic conditions of operation were analyzed. The characteristic features of each of these conditions are summarized in Table II-4. All the analyses are for a heat load of 40,000 Btu/hr and dry shipments.

Table II-4

CHARACTERISTICS OF CONDITIONS ANALYZED

Operating Condition

Parameter	Cooling	LOMC	50% SWL	30-Minute Fire	PFE
Mechanical Cooling	Yes	No	Yes	No	No
Neutron Shielding Cavity Contents	Water	Water	Water/Air	Air	Air
Solar Heat Input	No	No	No	No	Yes
Ambient Temp, °F	130	130	130	1475	130

2.3.2 Results of Design Basis Analyses

The results obtained from analyzing the above noted conditions are summarized in Table II-5 for fuels licensed prior to 1991 (for fuels licensed since 1991, see Volume 3, Appendices A and B). They are based on the use of the thermal analysis code THTD to obtain cask temperature distributions and the Wooten-Epstein correlation for a dry, air-filled, horizontal cask to obtain cladding temperatures.

Table II-5

RESULTS OF THERMAL ANALYSES

Parameter		Normal Cooling	LOMC	50% SWL	30-Minute Fire	PFE
Ambient Temp, °F		130	130	130	1475	130
Heat Load Btu/hr		40,000	40,000	40,000	40,000	40,000
Max Barrel Temp,°F		155	213	173	1274	228
Max Outer Shell Temp,°F		163	219	284	452	369
Max Inner Cavity Surface Temp, °F		173	229	292	353	377
Hottest Rod Max Temp,°F						
Gp.1	7x7 BWR	492	537	587	635	654
	15x15 PWR	503	549	601	651	670
Gp.2	8x8 BWR	498	544	595	643	662
	7x17 PWR	508	555	607	658	677
Inner Cavity Pressure, psig		14	29	70	152	267

2.3.3 Miscellaneous Thermal Conditions

The following miscellaneous thermal conditions are considered in Section VI:

- Cask operation at -40°F
- Effects of antifreeze on cask operation
- Thermal expansion of neutron shielding liquid
- Effects of residual water on cavity pressure

2.3.4 Pressure Relief and Drain, Fill, Vent Devices

a. Ruptive Disk Device: A rupture disk device designed to burst at 350-400 psig at 443°F is used to provide overpressure protection to the cask inner cavity.

b. 200 psig Pressure Relief Valve: This valve provides overpressure protection to the neutron shielding cavities.

c. 1-Inch Globe Valve: Valves of this type are used for draining, filling, and venting of the cask inner cavity and, optionally, the neutron shielding cavities.

These components are described in greater detail in Section 6.

2.3.5 Thermal Testing of the Cask

Section 6.8 discusses the details of the thermal test procedures, cask thermal acceptance criteria, and the results of tests on casks 301 through 304. The data obtained from these tests was used to determine the maximum permissible wet shipment load for each cask and to "calibrate" the thermal model.

The difference in maximum permissible wet shipment heat load between casks 301 through 304 was less than 10%. For dry shipment all casks are rated at 40,000 Btu/hr. maximum heat load.

In addition to above described beginning-of-life thermal tests, each cask has temperature measurements taken while in use. These measurements are reviewed and evaluated on an annual basis to determine if there has been any degradation in the casks ability to dissipate heat.

2.4 CRITICALITY ANALYSIS

Table II-6 summarizes the most reactive criticality conditions for the reference fuels and the configurations indicated licensed prior to 1991 (Volume 3, Appendices A and B provide details for fuels licensed since 1991). In both the BWR and PWR cases, the use of criticality control members is necessary. For fuels licensed prior to 1991, these are in the form of boron carbide-filled stainless steel tubes (as opposed to borated stainless steel poison plates described in Volume 3, Appendix A) fixed to the fuel basket components. These rods are patterned after the BWR control blade elements. Boron density is 1.75 gm/cc. The poison locations are shown in Section VII.

Table II-6

MAXIMUM k_{eff} VALUES

Fuel Type	No. of Bundles	Enrichment w/o U^{235}	k_{eff}
BWR	18	4.0	0.880
PWR	7	4.0	0.955

An infinite array of casks in air with no spacing between the casks raises the k_{eff} a very small amount thus classifying the cask fissile Class I.

Prior to making a determination of cask k-effective (k_{eff}) it was necessary to compute the most reactive fuel bundle geometry. This was done by varying rod pitch within the confines of the corresponding basket channel. To determine maximum cask k_{eff} the peak bundle geometries were placed in the appropriate cask array models and k_{eff} was computed as a function of cask cooling temperature. Peak cask reactivity is at 20°C.

2.5 SHIELDING ANALYSIS

The analysis only considers the case of 7 PWR bundles with an exposure of 35 GWD/T, a specific power of 40 kw/kg, and a 120-day cooling time. This represents a "worse" case loading of any reference fuel licensed prior to 1991 for which the cask was originally designed. Both gamma and fast neutron radiation must be considered in designing a shipping package for high exposure light water moderated reactor fuels.

2.5.1 Gamma Shielding

The gamma source arises from the decay of the radioisotopes created from the fission process during reactor operation. The source strength is a function of specific power, operating time, and cooling time. Section VIII describes the source term in detail for fuels licensed prior to 1991. Volume 3, Appendices A and B provide details for fuels licensed since 1991. Depleted uranium metal is the principal gamma shield in the IF-300 cask, although there is a significant contribution from the stainless steel inner and outer shells. The uranium is an annular casting four inches thick clad in stainless steel, and forms the cask body. Head end shielding is accomplished with three inches of stainless-clad uranium. The bottom end requires three and three-quarters of an inch of uranium.

Gamma shielding calculations were performed by computer (QAD-P5A) program considering seven groups. During horizontal transport, the nearest accessible package surface is four feet from the cask centerline, hence, one calculation considers the dose rate at a distance of six feet from this package surface (ten feet from cask centerline), along a line which bisects the cask's axis. A second calculation considers the dose rate three feet from the cask surface under accident conditions. Due to the high melting point and structural strength of uranium metal, there is no displacement of gamma shielding during the 10CFR71 accident. The gamma dose rates for the normal and accident conditions are 5.46 mr/hr and 17.6 mr/hr at their respective points of measurement.

QAD-P5A was also used to calculate the gamma dose rates at the cask ends and closure flange. The maximum end dose is 3.0 mr/hr measured 9 feet from the cask surface. The flange dose is 0.2 mr/hr measured 9 feet from the cask surface. Table II-7 tabulates the shielding results.

Table II-7

GAMMA AND NEUTRON SHIELDING RESULTS*

	R_{10} 10 ft from Cask Centerline	R_3 Accident 3 ft from Cask Surface	F_9 9 ft from Flange	T_9 9 ft from Top Head	B_9 9 ft from Bottom End
Gamma (mr/hr)	5.46	17.6	<0.2	3.0	2.8
Neutron (mRem/hr)**	3.96	440.0	<0.02	$\leq$0.6	0.4
Total (mRem/hr)	9.42	457.6	<0.22	$\leq$3.6	3.2
Regulatory Limit (mRem/hr)***	10.0	1000.0	10.0	10.0	10.0

*Locations of R_{10}, R_3, F_9, T_9 and B_9 illustrated in Figure VIII-3. E

**Includes fission in uranium shield.

***10CFR71 and 49CFR173.

2.5.2 Neutron Shielding

Fast neutrons arise primarily from the spontaneous fission of Cm 242 and Cm 244 present in high exposure (>20 GWD/T) fuel. The source strength is 3 x 10^9 neutrons/second at an average energy of ∿2 MEV. Section VIII describes this source in detail. Shielding is accomplished through the use of a 2-4 in. thick water annulus (wet cask only) followed by the 4 in. thick depleted uranium structure and finally a 5.0 to 7.0 inch thick water layer. This shielding concept employs elastic and inelastic scattering as well as capture to reduce the neutron dose rate. The dose rate points of interest are the same as those of the gamma calculations, side, end and flange. Unlike the gamma case, there is the potential for the partial loss of neutron shielding during the accident conditions. Hence, when calculating the 3 foot dose rate, the cask water, interior and exterior, is replaced by a void.

Neutron shielding calculations were performed using SN1D, a one-dimensional discrete ordinates transport code with general anisotropic scattering. This code is a modified version of ANISN written for use on the GE-635 computer. SN2D, a two-dimensional version of SN1D, was used to verify the results of approximating two-dimensional geometry in one dimension.

The normal transport neutron dose rate at a point 10 feet from the cask centerline and equidistant from the ends of 3.96 mRem/hr. The accident condition neutron dose rate 3 feet from the cask surface with no water shielding is 440 mRem/hr. The end and flange neutron dose rates were calculated based on the material thicknesses and the exposure profile of a typical fuel assembly. The latter dose rates are a factor of seven or more, less than the side dose rate. Table II-7 tabulates the shielding results.

2.5.3 Calculational Results

49CFR173 prescribes the allowable dose rates as 10 mr/hr total radiation at a point 6 feet from the vertical projection of the outer edges of the transport vehicle. Furthermore, DOT and NRC regulations specify a limit of 1 R/hr three feet from the cask surface following the hypothetical accident conditions. Table II-7 indicates that the IF-300 cask shielding meets both normal and accident shielding requirements.

2.6 FISSION PRODUCT RELEASE

For the reduced heat load of dry shipments in the IF-300 cask, the analyses of Section VI show that there is no release of any of the cask contents to the environs for either normal or accident conditions.

2.7 REGULATIONS

The IF-300 irradiated fuel shipping cask is designed to meet both the normal transport and accident conditions of the NRC and DOT. Section IX summarizes the design results in light of these regulatory criteria.

2.8 OPERATION AND MAINTENANCE

2.8.1 Operation

A complete operating manual has been written and is provided to each cask user. In addition, VECTRA offers training on cask handling prior to use. VECTRA-supplied technical assistance will also be offered in support of cask handling. The user is expected to provide all operating and health physics personnel. The user will bear the responsibility of proper cask operations.

Each shipping package will have in-transit instructions which provides guidance to the carrier personnel in the event of an abnormal condition.

2.8.2 Maintenance

Maintenance and repair of the IF-300 cask will be performed following written instructions. The same level of quality specified for the initial fabrication will be applied to maintenance and repair items. Where applicable manufacturer's recommendations or accepted industry standards will be followed. Records will be maintained on a cask-by-cask basis in accordance with regulatory requirements. An approved Quality Assurance Plan will be applied to all items of maintenance and repair.

2.9 FABRICATION AND QUALITY ASSURANCE

Since it is necessary to have some uniform and familiar set of criteria to govern equipment fabrication, General Electric had chosen the ASME Nuclear Vessel Code, Section III as guidance for the IF-300 cask fabrication and quality control. The design portion of Section III is excluded, due to the unique requirements of shipping casks.

All IF-300 basic components identified in Chapter IX are designed, fabricated, tested, used, and maintained under an NRC approved quality assurance program that satisfies requirements in 10CFR71 Subpart H "Quality Assurance" criteria for packaging and transportation of radioactive material.

TABLE OF CONTENTS

III. FUELS AND CONTENTS DESCRIPTION

LIST OF ILLUSTRATIONS

LIST OF TABLES

3.1 INTRODUCTION

The IF-300 spent fuel cask is designed as a general purpose shipping container. With its various length heads and removable fuel baskets, the IF-300 is capable of servicing all of the present and planned light-water moderated power reactors which have a building crane capacity of greater than 70 tons.

The fuels are segregated into two generic groups, BWR and PWR. Within each group is a design basis or reference fuel bundle. This assembly is a composite of parameters based on the present and projected fuel designs of General Electric, Westinghouse, Babcock & Wilcox, and expected values for present generation power reactors. These critical parameters include exposure, specific operating power, enrichment critical parameters include exposure, specific operating power enrichment, uranium content, active length, and bundle cross-section geometry. All of these are necessary inputs to a shipping cask design analysis.

Prior to 1991, the IF-300 cask was designed to ship either eighteen (18) of the BWR reference fuel bundles or seven (7) of the PWR reference fuel bundles. Since 1991, the IF-300 cask has also been permitted to ship seventeen (17) channelled BWR fuel bundles. This approach permits the shipment of any BWR or PWR fuel without specific analysis as long as it is within its respective design basis envelope.

The reference fuels and their bases licensed prior to 1991 are summarized in Table III-1. Fuel designs licensed in 1991 for the channelled BWR fuel basket are summarized in Volume 3, Appendix A, page A-1-9, Table A-1.2-2. PWR fuels with a maximum burnup of 45,000 MWD/MTU licensed in 1994 are described in Volume 3, Appendix B.

3.2 FISSION PRODUCT ACTIVITIES AND POWERS FOR THE DESIGN BASIS FUELS[1]

This section addresses Design Basis fuel licensed prior to 1991. Volume 3, Appendices A and B address fuel licensed for a 17-cell channelled BWR fuel basket in 1991 and 15x15 Westinghouse PWR fuel licensed with a maximum burnup of up to 45,000 MWd/MTU with a minimum cooling time of 60 months in 1994, respectively.

3.2.1 Design Basis for PWR Bundles

3.2.1.1 Determination of the Thermal Neutron Flux:

As a basis for design, the specific power is taken to be 40 kw/kgU, and the burn-up to be 35,000 MWd/MTU. The irradiation time is:

---

1 Calculations by Charles B. Magee; Denver Research Institute, Denver, Colorado. Results of calculations used in Table III-1.

Table III-1

CHARACTERISTICS OF EXPECTED AND DESIGN BASIS FUELS

Reactor	Type	Mfg.	Enrich. (%)	Exposure (Gwd/MTU)	Op. Pwr. (kw/kgU)	Active Length (in.)	Overall Length (in.)	Slot Envelope (in.)	Rod Array	Rod Pitch (in.)	Rod Dia. (in.)	kgU/ Assy.	Clad Mat'l	Clad Th'k (in.)
Oyster Cr. 1	BWR	GE		15	14.5	144	171 5/8	5.440	7x7	0.738	0.570	197	Zr-2	0.036
Monticello 1	BWR	GE	2.00	15.0	15.8	144	171 7/32	5.47	7x7	0.738	0.570	197	Zr-2	0.0355
Browns Ferry 1, 2, 3	BWR	GE	2.19	30.0	22.0	144	176 7/32	5.47	7x7	0.738	0.562	195	Zr-2	0.032
Group I Design Basis BWR		-	4.0	35.0	30.0	146	-	5.75	7x7	0.647 to 0.809	0.500 to 0.600	198	Zr-2	0.029 min.
Haddam Neck 1	PWR	W			21.0	120	137.66	8.420	15x15	0.553	0.422	433	SST	0.016
Turkey Pt. 3, 4	PWR	W	2.73	27.0	29.3	144	160.10	8.426	15x15	0.563	0.422	457	Zr	0.0243
H. B. Robinson 1	PWR	W	2.73	27.0	29.0	144	160.10	8.426	15x15	0.563	0.422	457	Zr	0.0243
Indian Pt. 2,3	PWR	W	2.92	27.0	32.0	144	161.38	8.426	15x15	0.556	0.422	447	Zr	0.0243
Diablo Canyon 1	PWR	W	2.67	33.0	36.9	144	160.10	8.426	15x15	0.563	0.422	457	Zr	0.0243
Palisades 1	PWR	CE	2.74	24.0	24.7	132	151	8.323	15x15	0.553	0.413	437	Zr-4	0.024
Calvert Cliffs 1	PWR	CE	2.74	30.0	28.0	132	151	8.323	14x14	0.553	0.44	437	Zr-4	0.026
Rancho Seco 1	PWR	B&W	3.09	28.2	31.8	144	165 5/8	8.522	15x15	0.568	0.430	456	Zr-4	0.026
Oconee 1, 2, 3	PWR	B&W	3.09	28.2	31.8	144	165 7/8	8.522	15x15	0.552	0.420	456	Zr-4	0.026
Point Beach 1	PWR	W	3.05	27.0	27.6	144	161.275	7.803	14x14	0.556	0.422	392	Zr	0.0243
San Onofre 1	PWR	W	3.06	30.0	21.0	120	137.66	7.813	14x14	0.556	0.402	375	SST	0.013
R. E. Ginna 1	PWR	W	3.05	27.0	27.6	144	161.275	7.803	14x14	0.556	0.422	392	Zr	0.0243
Group I Design Basis PWR		-	4.0	35.0	40.0	145	-	8.75	14x14 15x15	0.502 to 0.582	0.380 to 0.460	465	SST Zr	0.013 min. 0.020 min.
Group II Design Basis BWR		-	4.0	35.0	30.0	150	-	5.75	8x8	0.630 to 0.645	0.475 to 0.505	197	Zr-2	0.029 min.
Group II Design Basis PWR		-	4.0	35.0	40.0	144 to 150	-	8.75	16x16 17x17	0.496 to 0.507	0.374 to 0.400	475	Zr	0.020 min.

(BLANK PAGE)

$$\frac{35{,}000 \text{ MWd/MTU}}{40 \text{ MW/MTU}} = 875 \text{ days}$$

$$= 7.56 \times 10^{7} \text{ seconds}$$

The thermal neutron flux and the specific power are related as follows:

$$P = \phi \sigma_f N^{235} V$$

where

ϕ = the thermal neutron flux,
σ_f = the average microscopic fission cross-section of U^{235} (equal to 5.80×10^{-22} cm^2 per atom),
N^{235} = the number of U^{235} atoms per unit volume, and
V = the volume.

Assuming an enrichment of 3.5%, N^{235} is determined as follows:

$$N^{235} = \frac{1000 \text{ gms } (3.5 \times 10^{-2}) \ (6.023 \times 10^{23})}{(2.35 \times 10^{2}) \ V}$$

$$N^{235} = \frac{8.98 \times 10^{22}}{V} \text{ atoms per unit volume/kgU}$$

Now the power in fission/sec per kgU is given by:

$$P = \phi \ (5.80 \times 10^{-22}) \ (8.98 \times 10^{22}) \ V$$

$$P = 52.0 \ \phi \text{ fission/sec per kgU}$$

Converting from fission per second to watts:

$$P = \frac{52.0\ \phi}{3.2 \times 10^{10}} = 1.63 \times 10^{-9}\ \phi \text{ watts/kgU}$$

Thus, for a specific power of 40 kW/kgU the flux is:

$$\phi = \frac{4 \times 10^{4}}{1.63 \times 10^{-9}} = 2.46 \times 10^{13} \text{ neutrons/cm}^2 - \text{sec}$$

3.2.1.2 Total Fission Product Power and Gamma Power as a Function of Cooling Time

The compilation of Blomeke and Todd* has been used to determine the total fission product power and the gamma power for PWR assemblies as a function of cooling time under the following conditions: burnup, 35,000 MWd/MTU; specific power, 40 kW/kgU; and thermal neutron flux, 2.46×10^{13} neutrons/cm^2 - sec. The results obtained are presented in Table III-2.

(Note: The burn-up and specific power considered here are representative of the largest PWR bundles. These bundles contain 465 Kg uranium. Thus, to convert watts/kgU to watts per bundle, multiply by 465.)

Table III-2

TOTAL FISSION PRODUCT POWER AND GAMMA POWER AS A FUNCTION OF COOLING TIME FOR DESIGN BASIS PWR FUEL BUNDLES

Cooling Time (days)	Total Power (watts/kgU)	Gamma Power (watts/kgU)
90	27.6	12.6
120	21.5	9.70
150	17.7	7.52
180	15.5	6.19
210	13.3	5.30
240	11.3	4.31
270	9.95	3.76
300	9.25	3.09

*J. O. Blomeke and Mary F. Todd, "Uranium-235 Fission-Product Production as a Function of Thermal Neutron Flux, Irradiation Time, and Decay Time," Part 1, Volumes 1 and 2, Oak Ridge National Laboratory, ORNL-2127, TID-4500, Aug. 1957.

3.2.1.3 Contribution to the Decay Heat from Transuranic Elements

According to calculations by General Electric, the transuranic elements contribute 2.79 watts/kgU for a burn-up of 35,000 MWd/MTU and a cooling time of 90 days. The activity of the transuranics is mainly a function of burn-up and is essentially independent of the specific power. According to these data, the nuclides of importance are: 458 year Am^{241}, 7650 year Am^{243}, 163 day Cm^{242} and 18 year Cm^{244}. For the cooling time of concern here, it can be assumed that the Cm^{242} nuclide contributes 76% of the activity at 90 days cooling time. Assuming equal energy alphas from all the transuranic (not quite the case), the contribution of the transuranic to the thermal power as a function of cooling time can be represented by:

$$P = 0.68 + 2.11\ e^{-\lambda t}\ \text{watts/kgU}$$

where 0.68 is the contribution from the long lived nuclides and $2.11\ e^{-\lambda t}$ is the contribution from Cm^{242} with 2.11 being its contribution at 90 days cooling time and $e^{-\lambda t}$ being the fraction decayed for times greater than 90 days. The decay constant λ is equal to 0.693/163 days or 4.25×10^{-1} days $^{-1}$. Using appropriate values of t for cooling times up to 300 days the following values result. (Note: Since these nuclides decay primarily by alpha emission, the greatest part of their energy is deposited in the fuel matrix.)

Table III-3

CONTRIBUTION TO DECAY HEAT POWER FROM TRANSURANICS

Cooling Time (days)	Transuranic Power (watts/kgU)	Transuranic Plus Fission Product Power (watts/kgU)
90	2.79	30.39
120	2.53	24.03
150	2.31	20.01
180	2.12	17.62
210	1.94	15.24
240	1.79	13.09
270	1.66	11.61
300	1.54	10.79

3.2.2 Design Basis BWR Bundles

3.2.2.1 Thermal Neutron Flux

As a basis for design, the specific power for the BWR bundles is taken to be 30 kW/kgU, and the burn-up to be 35,000 MWd/MTU. The irradiation time is thus,

$$\frac{35{,}000 \text{ MWd/MTU}}{30 \text{ MW/MTU}} = 1167 \text{ days}$$

$$= 1.008 \times 10^{8} \text{ seconds}$$

In the compilation of Blomeke and Todd, used to determine the fission product activities and powers, data are given for irradiation times of 3×10^{7} seconds and 10^{8} seconds (and for shorter times). To avoid a difficult interpolation, the cooling time will be taken to be 10^{8} seconds (1160 days) and the specific power adjusted such that the burn-up remains the same, thus,

$$\text{specific power} = \frac{35{,}000 \text{ MWd/MTU}}{1160 \text{ Days}} = 30.2 \text{ MW/MTU}$$

The specific power and the thermal neutron flux are related as follows:

$$P = \phi \sigma_f N^{235} V$$

Assuming an enrichment of 2.56% (second generation TVA bundles), N^{235} per kgU is determined as follows:

$$N^{235} = \frac{1000 \text{ gms } (2.56 \times 10^{-2}) \ (6.023 \times 10^{23})}{2.35 \times 10^{2} \times V}$$

$$N^{235} = \frac{6.55 \times 10^{22}}{V} \text{ atoms per unit volume/kgU}$$

Using for the fission cross-section 5.80×10^{-22} per atom of U^{235}, the power is:

$$P = \phi\ (5.80 \times 10^{-22})\ \left(\frac{6.55 \times 10^{22}}{V}\right)$$

$$P = 38.0\ \phi \text{ fission/sec per kgU}$$

$$P = \frac{38.0\ \phi}{3.2 \times 10^{10}} = 1.19 \times 10^{-9}\ \phi \text{ watts/kgU}$$

Thus, for a specific power of 30.2 MW/MTU the flux is:

$$\phi = \frac{3.02 \times 10^{4} \text{ watts/kgU}}{1.10 \times 10^{-9}} = 2.54 \times 10^{13} \text{ neutrons/cm}^2\text{-sec}$$

3.2.2.2 Fission Product Powers and Activity from Blomeke and Todd

The compilation of Blomeke and Todd has been used to obtain the total power, the gamma power, and the activity of the gammas with energies greater than 1.7 MeV as a function of cooling time for an irradiation time of 10^8 sec (1160 days) and a thermal neutron flux of 2.54×10^{13} neutrons per cm^2 per sec. The results are given in Table III-4. The values in the table must be multiplied by 198 (there are 198 kgU in a typical BWR bundle) to obtain power per assembly. The activity of the high energy gammas has been converted to MeV per second per kgU by multiplying the number of disintegrations per second by 2.5 MeV, the assumed average energy of these gammas.

Table III-4

TOTAL FISSION PRODUCT POWER, GAMMA POWER, AND HIGH ENERGY GAMMA POWER AS A FUNCTION OF COOLING TIME FOR DESIGN BASIS BWR FUEL BUNDLES

Cooling Time (Days)	Total Power (Watts/kgU)	Gamma Power (Watts/kgU)	Greater Than 1.7 MeV Gamma Power (MeV/sec/kgU)
90	21.9	9.21	1.33×10^{12}
120	17.2	7.36	1.02×10^{12}
150	14.1	5.64	8.21×10^{11}
180	12.5	4.69	7.05×10^{11}
210	10.96	3.91	5.86×10^{11}
240	9.85	3.29	5.08×10^{11}
270	8.91	2.82	4.49×10^{11}
300	7.83	2.50	4.11×10^{11}

3.2.2.3 Contribution to the Decay Heat from Transuranic Elements

According to information obtained from General Electric, the transuranics contribute 2.79 watts/kgU to the decay heat for cooling time of 90 days. The contribution from the transuranic is a function primarily of burn-up and is not sensitive to specific power. Since the burn-up assumed for the BWR bundles is the same as that assumed for the PWR bundles, the contribution from the transuranic elements present does depend upon the initial amount of U^{238} in the fuel and, hence, upon the enrichment. The two enrichments assumed here (3.5% for PWR bundles and 2.56% for BWR bundles) are such that the initial U^{238} contents are not much different, and this small difference will be ignored. Thus, the contribution of the transuranic will be the same for the BWR bundles as for the PWR bundles, and the values as a function of cooling time reported previously are given again in Table III-5 below along with the total power.

Table III-5

CONTRIBUTION TO DECAY HEAT POWER FROM TRANSURANICS AND TOTAL DECAY HEAT POWER

Cooling Time (days)	Transuranic Power (watts/kgU)	Transuranic Plus Fission Product Power (watts/kgU)
90	2.79	24.7
120	2.53	19.7
150	2.31	16.4
180	2.12	14.6
210	1.94	12.9
240	1.79	11.6
270	1.66	10.6
300	1.54	9.37

3.3 AXIAL PEAKING FACTOR

Figure III-1 shows the various instantaneous peaking factors for a typical fuel bundle. As can be seen, the peak traverses the bundle as control rods are withdrawn. This yields an end-of-life peak to average ratio of just under 1.1. Figure III-2 is a BWR fuel rod gamma scan which also shows this flat end-of-life profile.

3.4 FUEL ACCEPTANCE

In determining if a fuel assembly type can be shipped in the IF 300 cask, it is necessary to examine several categories.

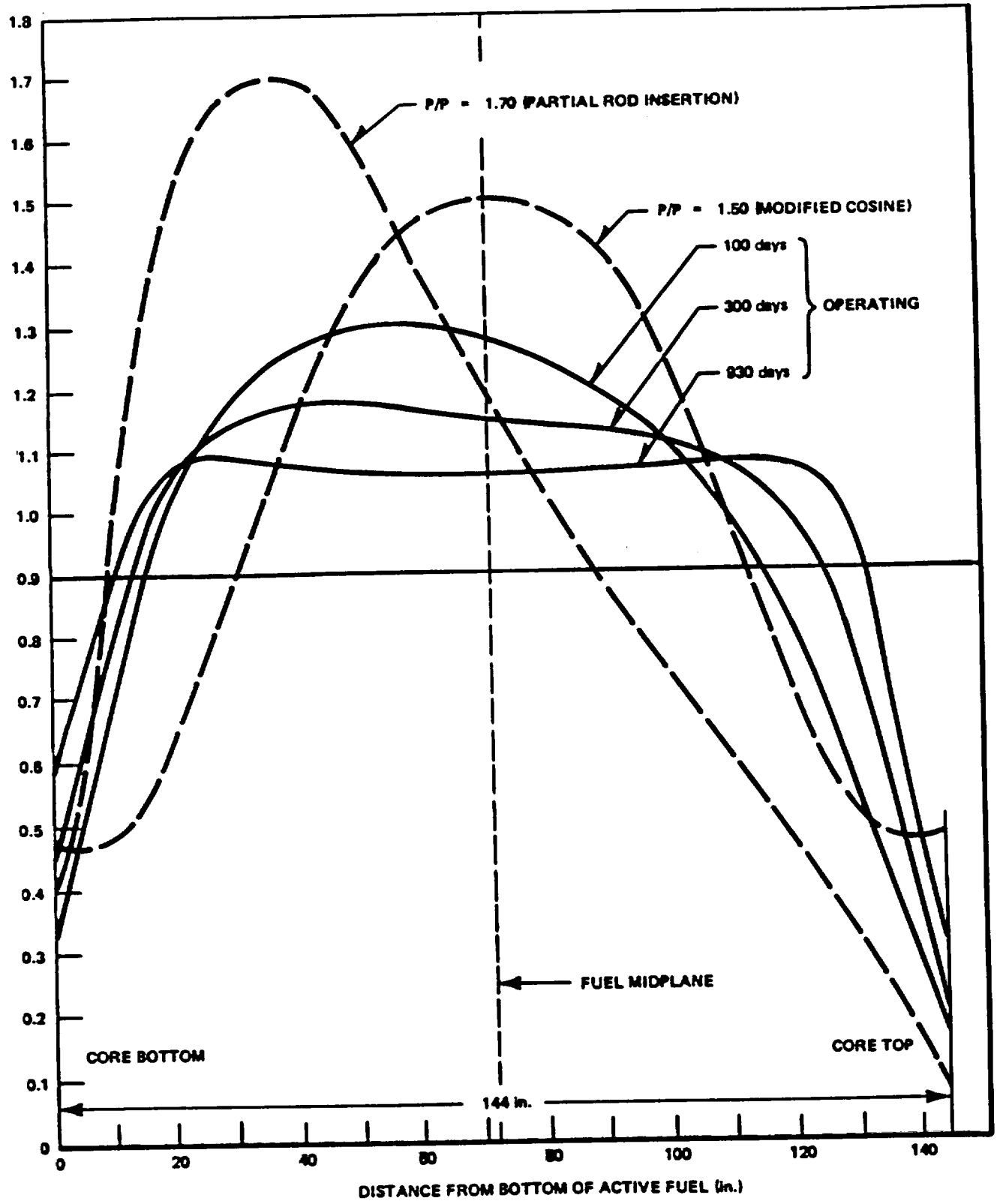

Figure III-1. Axial Local to Average Burnup and Instantaneous Power Comparisons

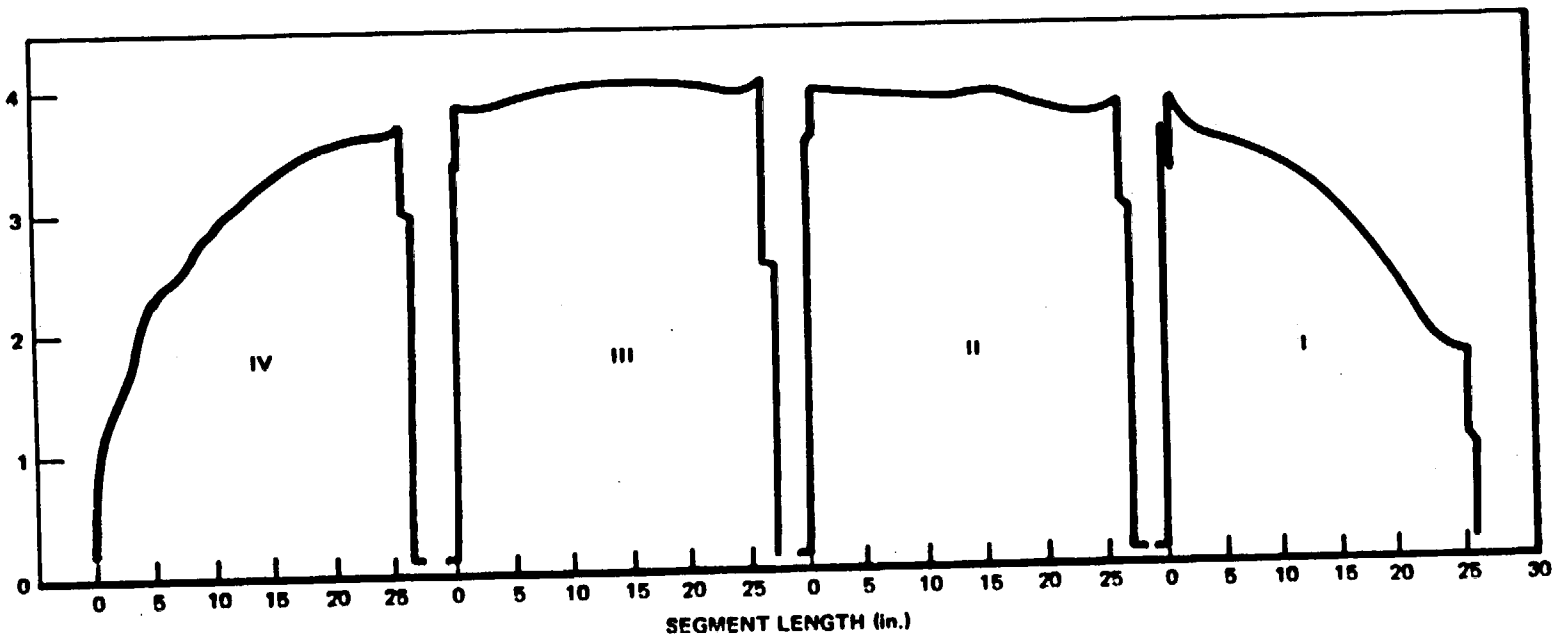

Figure III-2. Gamma Scans of the Segments of Type I Fuel From Rod F-6 Obtained with the Ge(Li) Detector Systems

3.4.1 Dimensional

The two fuel baskets and two length closure heads allow some variety in fuel dimensions. The cask envelope dimensions to which the fuel must conform are shown in Table III-6.

Table III-6
DIMENSIONS

	PWR Basket		BWR Basket	
	PWR HD.	BWR HD.	PWR HD.	BWR HD.
Maximum Length, In.	168.500	179.25	169.125	179.875
Maximum Cross-section, In.	8.75	8.75	5.75	5.75

3.4.2 Heat Transfer

Section VI describes fuel decay heat rate limits both on a per bundle and a per cask load basis.

3.4.3 Criticality

The criticality analysis of Section VII contains a parametric study of fuel bundle geometries to determine maximum cask k_{eff}. From this study comes a range of values for rod pitch and rod diameter within which any fuel shipped must fall as tabulated in Table III-1.

3.4.4 Structural

The structural evaluation of the fuel in Section V shows that those fuels examined do have the capability of resisting the drop forces without failure.

3.5 DEFECTIVE FUEL

3.5.1 Introduction

Perhaps the most difficult thing to do regarding defective fuel is to define it. Cladding integrity is not a sufficient criterion since "failures" range from pin hole perforations to complete rod separation (although the latter is a rare occurrence).

3.5.2 Shipping Defective Fuel

The vast majority of fuel failures are of the minute cladding perforation type. In general these failures are limited to certain bundles and usually to a few rods within those bundles. Often the failures are so small and far enough within a bundle that they cannot be exactly located without disassembly. Many times a bundle can only be categorized as a "possible" because of the difficulty in detecting such small leaks, and such difficulty comes at a time when the activity is at its highest, shortly after shutdown. If leaks are difficult to detect under these conditions, they are almost impossible to find after long cooling periods.

More often than not a utility will discharge bundles without segregating defective from non-defective fuel. The exceptions to this are a) if the fuel is prematurely discharged for repair; 2) if the fuel fabricator wishes to conduct studies on defects; or 3) if a gross failure is contributing to an abnormal increase in storage pool activity.

From a shipping standpoint there are two things that must be satisfied regarding defective (or any) fuel:

1. The applicable regulations must be met.

2. The cask design bases must be satisfied.

3.5.2.1 Regulations

The regulations (10CFR71, 49CFR173) governing spent fuel shipping do not speak directly to the matter of failed fuel. From the definitions contained in the regulations regarding cask contents "leaker" fuel and "non-leaker" fuel are indistinguishable. Thus, as long as the cask coolant activity limits and accident release limits can be met, leaky fuel bundles require no special handling or packaging. The C of C for the IF 300 prohibits the shipment of suspected or known failed fuel assemblies and fuel with cladding defects greater than pin holes and hairline cracks.

3.5.2.2 Cask Design Bases

Referring to subsection 3.4 above, any fuel assembly to be shipped must comply with the dimensional, thermal, criticality, and structural requirements upon which the cask design analysis was based.

From a dimensional standpoint, most leaker bundles are exactly like any other bundle. Gross rod bowing has been observed in some early fuels but it is a rarity now.

Thermally, a leaking bundle is the same as a non-leaker since the thermal output is not a function of cladding integrity. (Note: Operating power is often reduced in an area of the core which is suspected of having leakers through control rod insertion by the reactor operator. This would result in fuel characteristics (thermal, burn-up) less severe than the design basis fuel.)

Again, discounting gross bundle distortion which is rare, the bundle or cask k_∞ or k-effective is independent of cladding integrity.

From the standpoint of bundle structural integrity, again, the expected types of failures are generally insignificant since they are localized and small in size and number. There may be some further damage to the failed areas as a result of the 30-foot drop loadings but gross loss of bundle integrity will not occur.

3.5.2.3 Releases from Cask

Since the primary concern over failed fuel is what will be released under accident conditions, two things should be recognized:

(1) Each pin hole (or larger) failure has vented the accumulated fission gas in that rod long before the fuel is shipped. From the standpoint of fission gas release under accident conditions, the safest fuel to ship is that with all pins vented.

(2) Cask coolant activity is a function of fuel external contamination and anything which might escape through a failure opening.

A failed rod has operated in that condition for some time followed by a minimum of 1 year of cooling in a storage pool. It is obvious that by shipping time the failure points will have been greatly depleted of those soluble fission products which would contribute to coolant activity.

Most fuel shippers have observed that coolant water activity primarily comes from fuel external contamination ("crud") and that the contribution from leaking fuel is practically masked when performing gross measurements. This is because the very low solubility of the fuel material in water puts a practical upper limit on the quantity of

fission product activity in the coolant even if the pellets were completely exposed. Since the fission products generally must migrate through pin holes or small cracks, the rate of activity buildup in the coolant is exceedingly small.

3.6 NON-FUEL CONTENTS

3.6.1 Poison/Criticality Control Components

PWR and BWR fuel bundles occasionally contain burnable poison rods or reactivity control rods which are non-fuel bearing components. These items do not contribute measurably to the decay heat or shielding requirements of the cask and thus may be included as cask contents. No analysis of these benign components is required.

3.6.2 Residual Contamination

In the course of operation the interior cavity and fuel basket of a cask becomes contaminated with radioactive material. This residual material consists of mixed fission and activation products. Although the quantity is not always known, experience has shown that it is likely to be greater than a Type A quantity. This material may be present in both the empty and loaded cask.

3.6.3 Irradiated Hardware

Solid non-fissile irradiated hardware contained within a steel liner specifically designed for that hardware may be shipped. Limitation on weight, maximum decay heat in the package and external radiation dose rates are the same as for spent fuel shipments, except the fissionable material dose shall not exceed a Type A quantity and shall not exceed the mass limits of 10CFR71.53.

TABLE OF CONTENTS

IV. EQUIPMENT DESCRIPTION

LIST OF ILLUSTRATIONS

IV. EQUIPMENT DESCRIPTION

4.1 SHIPPING PACKAGE

General Electric drawing 159C5238 sheets 1 and 2 show the IF-300 shipping package general arrangement[1]. The package consists of five major groups: 1) The cask, part 2; 2) The tiedowns, parts 3, 18, and 19; 3) The cooling system, parts 4, 5, and 6; 4) The skid, part 15; and, 5) The enclosure, parts 7 through 14. It should be noted that some of the drawing call-outs are for information purposes only rather than to denote a safety-related material, item or dimension.

4.1.1 Cask

4.1.1.1 Body

Drawing 159C4238 sheet 4 is a cross section of the cask. The inner cavity is encircled by a 317 or 216 stainless steel cylinder 37-1/2 inches inside diameter with a one-half inch thick wall. The bottom end of the cavity is sealed with a 1-1/4 inch thick 304 stainless steel plate. The upper end is welded to the 304 stainless steel forged closure flange.

Surrounding and shrink-fitted to the inner cavity is the depleted uranium shielding material. This heavy metal assembly consists of eight or ten annular castings, each with a 38-1/2 inch ID and a four inch thick wall. The segments are approximately 16 to 20 inches long. They fit end-to-end, using an overlapping joint to prevent irradiation streaming. The shrink-fitting of shielding to cavity assures good contact for the transmission of heat. Bottom end shielding uses a 3-3/4 inch thick uranium casting.

---

1 General Electric drawings, which are currently controlled by VECTRA, are located at the end of this section.

To prevent the formation of a low melting point alloy of steel and uranium, a minimum four mil thick copper diffusion barrier exists at every uranium-steel interface. The barrier is flame sprayed on the larger pieces. Copper foil or powder may be used in some of the smaller areas. In some welded areas a copper plated back-up strip is used.

The cask outer shell is a 317 stainless steel cylinder with a 46-1/2 inch ID and a 1-1/2 inch thick wall. This outer shell is shrink-fitted to the uranium castings thus forming a composite or laminated vessel.

The cylindrical portion of the cask is encircled by a thin-walled, corrugated, stainless steel water jacket. This jacket extends axially from the upper valve box to a point slightly above the cask bottom, thus masking the active fuel zone. The water or ethylene glycol and water mixture contained in this cavity functions as a neutron shield. The jacket surface is corrugated for heat transfer purposes. The use of continuous corrugation also provides a surface which is easily decontaminated. The jacket is partitioned at the cask midlength to form two independent cavities, each rated at 200 psig and equipped with a pressure relief valve and a fill, drain, and vent valve or blind flange. Each cavity has a pair of liquid expansion tanks mounted to assure that there will be no loss from the system under the most limiting conditions. | N | E

There are four large valve boxes on the exterior of the cask body, two for the neutron shielding cavity, two for the cask cavity. The latter two are nested in the upper and lower pairs of structural rings and have lids and side members which are finned for impact and puncture protection. The lids are removable to provide access. | E

The upper (head-end) cask cavity valve box contains a one-inch stainless steel bellows seal globe valve and a rupture disk

device for overpressure protection (see Section VI for details). The lower cavity valve box contains a one-inch stainless steel bellows globe valve. Both globe valves are equipped with quick-disconnect fittings or SST caps/plugs on their outlet sides.

The cask body and valve boxes are protected from side impact by four 1-1/4 inch thick 216 stainless steel structural rings. These members are also used to support the water jacket sections. The IF-300 cask is lifted by a set of trunnions located just below the closure head flange. These items are pinned to the upper pair of structural rings (see 159C5238 Sheet 5), and are designed to be removed for transit. The upper pair of lifting rings also act as the forward support/axial restraint when the cask is in the horizontal transport position.

The lower end of the cask is equipped with 32 radially mounted impact fins. These fins are 304 stainless steel, slightly more than 1" thick. Sixteen fins are 8-1/8 inches high. The remaining sixteen are 6 inches high. All fins are welded in place.

Temperature monitoring is performed with a chromel-alumel thermocouple contained in a well entering from the bottom of the cask, located equidistant from the ends of the cask body at what is expected to be the hottest axial point.

The overall length of the cask body from fins to flange face is 184-3/16 inches. The cask cavity depth from the flange face is 169-11/16 inches. The flange face contains 32 equally spaced studs each of which is 1-3/4 inches in diameter with 8 threads per inch. The studs protrude 6-1/2 inches from the face and are made of 17-4 PH H1075 stainless steel. the flange itself is an ASTM A-182 type 304 stainless steel machined forging. There are two stainless

steel guide pins which protrude above the flange plane for initial head alignment.

4.1.1.2 Cask Heads

The IF 300 cask can be equipped with either of two heads. These heads provide two different cask cavity lengths to match the particular fuel being shipped. With the short head in place the overall cavity length is 169-1/2 inches. The long head increases the cavity to 180-1/4 inches. All PWR fuel to data can be shipped using the short (PWR) head. The longer BWR fuel necessitates the use of an extended (BWR) head.

Shielding in the heads consists of 3 inches of uranium. The outer shell and flange is a single 304 stainless steel machined casting. A circular 304 stainless steel plate is welded in place to form the inner liner and the head cover. As in the case of the body, each steel-uranium interface is isolated with a 4 mil (minimum) copper layer.

Each head has 32 radially mounted fins on the end. Sixteen fins protrude 9-1/2 inches from the surface, the remaining fins protrude 6 inches. These fins are designed to offer impact protection to the cask and contents. The fins are 304 stainless steel and are welded in place.

Due to variations in fuel lengths, it is necessary to provide some spacing scheme. There are a total of five spacer assemblies for the two heads. These spacers are mounted on circular plates which bolt to the top of the head cavity. Spacing is accomplished with struts and pads which protrude from the circular plate. Each plate is numbered and indexed to ensure proper installation. For certain BWR and PWR fuels a spacer is used in the bottom of each basket channel in addition to the head spacers. These bottom spacers elevate the fuel assemblies such that they can be easily engaged by the fuel

handling grapple for removal. A special tool is used for bottom spacer installation and withdrawal. See drawing 159C5238, Sheet 7 for a description of the spacers.

4.1.1.3 Closure

The cask body and either head are joined together using the 32 studs in the body flange and an equal number of special sleeve nuts. When the PWR head is being mounted, the short, 3½ inch-length, nuts secure it. Due to its greater length, the BWR head must utilize 13-3/4-inch-long sleeve nuts. Using the sleeve nut approach makes it possible to inter change heads without changing the studs. Two guide pins provide alignment and orientation.

Cask sealing is accomplished using a Grayloc metallic ring as shown on 159C5238 Sheet 5. The head and body flanges interlock to provide shear steps to protect the seal during impact. The seal will sustain a minimum test pressure of 600 psi at room temperature.

4.1.1.4 Fuel Baskets

There are three different fuel baskets which can be used in the IF-300 cask: a 7-cell PWR unit, an 18-cell BWR unit, and a 17-cell channelled BWR fuel unit. The 7- and 18-cell baskets are discussed in this section and are illustrated on 159C5238 Sheet 6. The 17-cell basket with its borated stainless steel poison plate design is discussed in Volume 3, Appendix A. The 7-cell basket holds the various PWR bundles and the 18-cell basket holds the various BWR fuel bundles presented in Section III for fuel description. Poison rods containing B_4C effectively cover the 7-cell PWR length 159.8 inches and the 18-cell BWR length of 167.6 inches for criticality control.

Each basket "cell" is formed from sheet stainless steel. The walls of each cell are slotted to provided coolant flow to the contained fuel. The cells are positioned by nine circular spacers placed along the basket length. These spacers or "spacer disks," also center the basket in the cask cavity. The basket cells run the full length of the fuel. When the cask is horizontal, the weight of the fuel bundle

is carried by the spacer disks. The cells are not principal load carrying members; they function as guides for ease in fuel loading.

As shown on 159C5238 sheets 6, 10 and 11 the BWR fuel basket is fitted with gamma shielding at its head-end. These assemblies consist of stainless steel-clad depleted uranium pieces and their supporting structures. The assemblies are permanently fixed to the basket. This shielding attenuates the cobalt-60 radiation from the BWR fuel bundle upper tie plates.

4.1.2 Cask Support and Tiedown

The cask support and tiedown arrangement is shown on 159C5238 sheet 5. It consists of a front saddle and a rear cradle/pedestal assembly.

4.1.2.1 Front Saddle

As illustrated (159C5238, Section B-Sheet 2, Sheet 5) the front saddle is a steel structure which is welded to the skid framing. When the cask is horizontal its upper pair of structural rings straddle the front support. There is approximately 45 degrees of circumferential contact between the cask body and the front support saddle.

This structure provides full axial restraint and partial vertical and lateral restraint of the cask. Axial restraint comes from the contact between the saddle and one of the two structural rings (depending on direction of movement). Vertical restraint is achieved by pinning the cask to the structure as illustrated on 159C5238 Sheet 5, Detail B. Lateral restraint comes from the cask-to-support contact and the tiedown pinning.

During cask rotation to the horizontal position, contact is made between the uppermost structural ring on the cask and the front edge of the saddle. The force generated by this contact draws the cask one-inch forward, out of the rear cradle. This capability of forward

movement of the cask allows it to thermally expand axially without stressing any of the tiedown or support structures.

4.1.2.2 Rear Cradle Assembly

The rear cradle assembly (159C5238 Section C-Sheet 2, Sheet 5) is a steel structure welded to the skid framing. It consists of a cylindrical cradle pivoted between two pedestals. This structure functions as a rear support and restraint as well as the rotation point for uprighting or laying down of the cask on the skid.

The lower end of the cask body fits into the cradle. When the cask is horizontal, contact with the cradle is through a "shoe" welded to the end fins and curved to match the inside of the cradle. The shoe is coated with a lubricant so that the one-inch forward movement of the cask can be achieved with a minimum of force.

Vertical and lateral restraint of the cask lower end is provided by the surrounding cradle and the pedestals. As mentioned above all axial restraint comes from the front saddle.

During cask rotation the cradle pivots in bronze bushings mounted on the pedestals. The cradle pivot point is located slightly off-center so that the cask will always tip the correct direction during loading. To keep the cradle facing upward when the cask is removed, a counter weight has been added. A spring stop prevents excessive cradle rotation.

4.1.3 Cooling System

159C5238 Sheet 1 illustrates the cooling system. This system may be used to maintain the cask at reduced surface temperatures. Neither its operation nor its installation is required for nuclear safety purposes.

Cask cooling is accomplished using an air jet impingement technique from four ducts. These ducts run the length of the cask and are 90° apart, bisecting the four quadrants. The two lower ducts are fixed to the skid. The two upper ducts lock in place during transit but move outward to facilitate cask removal.

Each duct has a single slot nozzle running its length. Small sheet metal spacers are used to segment this long slot into a number of individual nozzles. Cooling air is supplied by two Buffalo Forge Company Type BL load limit blowers. The two blowers are driven by a pair of air-cooled Deitz diesel engines.

Each engine/blower unit is independent of the other and capable of producing a minimum flow of 10,000 cubic feet of air per minute. During normal operation both units are run simultaneously, delivering ~18,000 cfm to the cask surface. Fuel tanks are located in the skid and have a total capacity of 370 gallons. This quantity will permit the continuous running of both units for a minimum of 6 days.

4.1.4 Equipment Skid

The equipment skid is designed and fabricated following standard heavy-hauling trailer practices. This structure functions as both a unitized pallet for the cask and cooling equipment and a trailer deck for special permit short haul trucking.

The skid frame uses 24-inch fabricated I-beams and the cask support attachment points are designed to sustain the 10 g, 5 g and 2 g combined load requirements of the cask tiedowns. Fuel tanks for the

cooling system diesels are incorporated into the framing. Deck plate is provided for all accessible areas. The cooling system and cask support members are attached directly to the frame. The skid is 37½ feet long, 8 feet wide and is of high strength steel construction.

Both ends of the skid are designed to accept a hydraulic "gooseneck." For transporting the package by truck, wheeled assemblies can be attached to both ends of the skid. The "goosenecks" can be used to lift the unit to a minimum road clearance of 12 inches for highway transportation.

During rail shipment, the skid sits directly on the bed of a slightly modified standard 90 ton 4-axle flat car. The skid is restrained by a tiedown system designed to comply with the load requirements of rule 88A.1.d of the Association of American Railroads Field Manual.

4.1.5 Enclosure

Exclusion from the cask and cooling system is provided by an aluminum frame and expanded metal cage as shown on 159C5238 Sheet 2. This enclosure is in three sections; two sections are over the cask and the third covers the cooling system. The two cask enclosures move along rails and telescope over the third one, which is semi-permanent, to facilitate cask removal. The enclosure ends are also semi-permanently attached to the skid. When the movable sections are retracted, the rails form a sill which protects the bottom air ducting and provides a work platform along the cask. when the sections are in place over the cask, a locking device lifts them off of their tracks and secures their movement. This device is padlocked during transit.

The cooling equipment end wall has a lockable access door for inspection. In addition, there is one small removable panel on each side of the equipment enclosure which permits access to each of the engine/blower instrument consoles. The equipment enclosure and the end walls may be removed by unbolting.

All three enclosure sections have solid roofs for sun shading. The enclosure ends are also solid. This entire enclosure makes the nearest accessible external shipping package surface approximately four feet from the cask centerline.

FIGURE WITHHELD UNDER 10 CFR 2.390

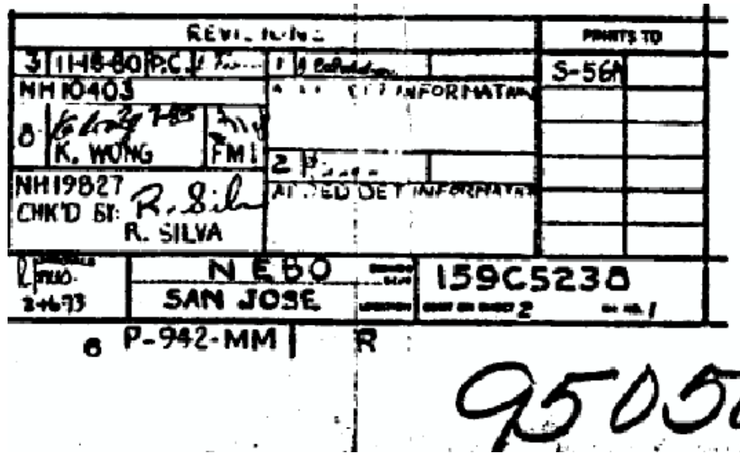

Drawing 159C52
(Sheet 1, Rev

4-11

9505080266

FIGURE WITHHELD UNDER 10 CFR 2.390

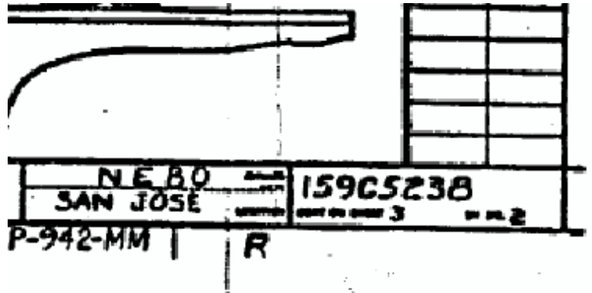

Drawing 159C5238
(Sheet 2, Rev 3)

4-12

9505080266-02

ITEM NO.	DESCRIPTION	NO REQ.
1	SHIPPING CASK & SKID ASSY	1
2	CASK GENERAL ARRANGEMENT	1 EA
3	PEDESTAL ASSEMBLY	1 RH 1 LH
4	FIXED DUCT ASS'Y	1
5	MOVABLE DUCT ASS'Y	1
6	FAN DRIVE ASS'Y	1
7	END WALL W/ ACCESS DOOR	1
8	EQUIPMENT HOOD	1
9	SMALL ENCLOSURE ASSEMBLY	1
10	LARGE ENCLOSURE ASSEMBLY	1
11	CASK END WALL	1
12	OPERATING MECHANISM ASS'Y	4
13	SIDE FRAME ASS'Y R.H.	1
14	SIDE FRAME ASS'Y L.H.	1
15	SKID FRAME ASS'Y R.H.	
16	CRADLE SPRING STOP	1
17	GASKET BOX ASS'Y	1
18	CRADLE ASS'Y	1
19	SADDLE	1
20	BARREL EXPANSION TANK	2

GENERAL NOTES

1. EXCEPT AS NOTED ALL WELDS ARE FULL PENETRATION, DEVELOPING THE FULL STRENGTH OF THE WEAKER BASE MATERIAL.
2. NUCLEAR SAFETY RELATED COMPONENTS ARE IDENTIFIED IN SECTION IX OF NEDO 10084-3 "IF-300 SHIPPING CASK - CONSOLIDATED SAFETY ANALYSIS REPORT."
3. A 1" 300 SERIES SST 300 LB. BLIND FLANGE MAY BE SUBSTITUTED FOR THE GLOBE VALVE, SNAPTITE COUPLING AND CAP IN BARREL VALVE BOXES.
4. (9) A 1" 300 SERIES SST 2000 LB. PIPE CAP MAY BE SUBSTITUTED FOR THE SNAPTITE COUPLING AND CAP IN CAVITY VALVE BOXES.

GENERAL ELECTRIC — 159C5238

UNLESS OTHERWISE SPECIFIED USE THE FOLLOWING:— APPLIED PRACTICES | SURFACES ✓ | TOLERANCES ARE REQUIRED DIMENSIONS: FRACTIONS ± | DECIMALS ± | ANGLES ±

TITLE INFORMATION DWG. I.F. 300 CASK SAFETY ANALYSIS

FIRST MADE FOR LICENSING TRANSPORTATION

159C5238 SHEET 4 OF NO. 3 REVNO. A

REVISIONS					PRINTS TO
8	NH19827	3	M.A.	9-6-77	Joseph Miller
		REDRAWN W/O CHANGE			
9	NH20900 3/14/85	4	11-6-80	PC	
		NH10403			
		5	2-10-82	PC	
		NH10469			

DRAWN J.ESKELDSON 13AUG 73 | APPROVALS R. JONES 8-13-73 | NEBO SAN JOSE | 159C5238 SHEET 4 OF NO. 3

6 P-942-MM R

Drawing 159C5238
(Sheet 3, Rev 9)

FIGURE WITHHELD UNDER 10 CFR 2.390

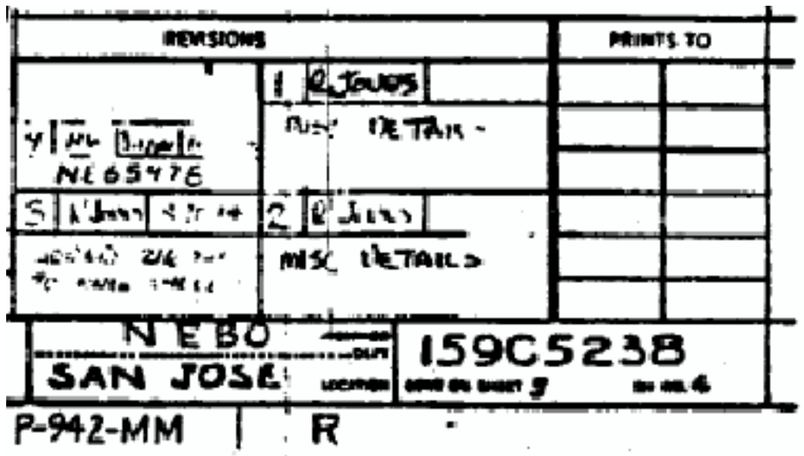

Drawing 159C5238
(Sheet 4, Rev 8)

4-14

9505080266-04

FIGURE WITHHELD UNDER 10 CFR 2.390

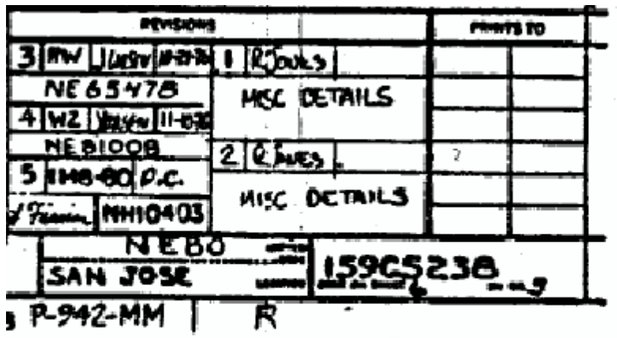

Drawing 159C5238
(Sheet 5, Rev 5)

4-15

9505080266-05

FIGURE WITHHELD UNDER 10 CFR 2.390

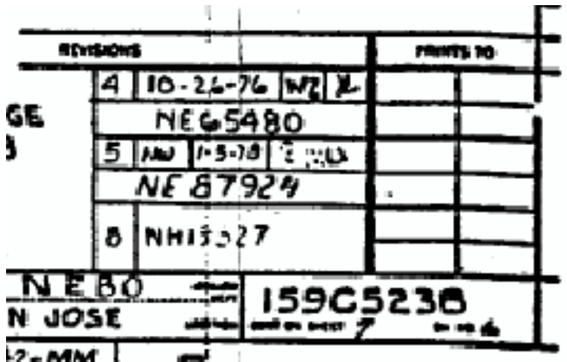

Drawing 159C5238
(Sheet 6, Rev 8)

9505080266-06

FIGURE WITHHELD UNDER 10 CFR 2.390

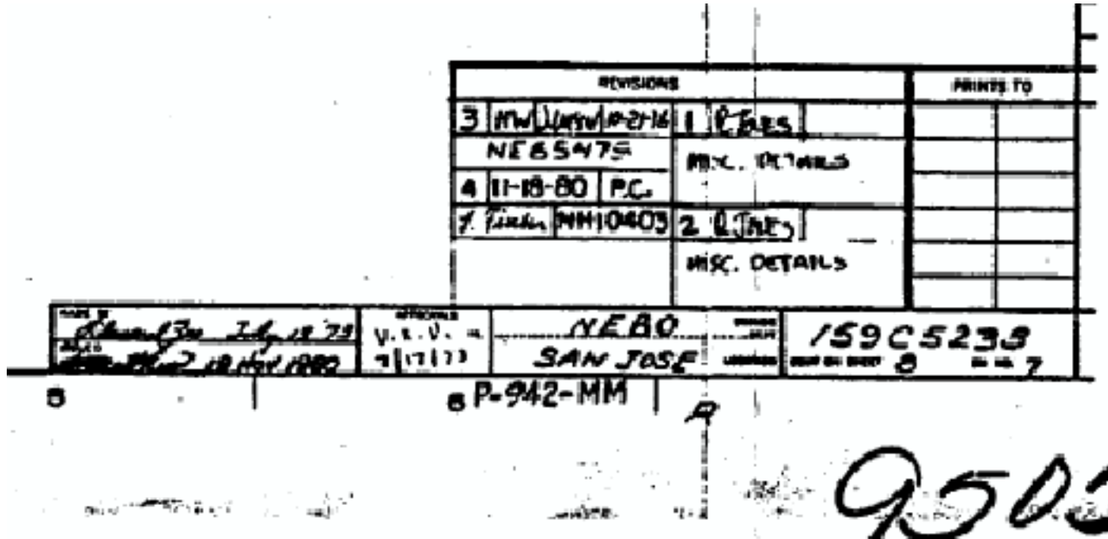

Drawing 159C5238
(Sheet 7, Rev 4)

4-17

9505080266-07

FIGURE WITHHELD UNDER 10 CFR 2.390

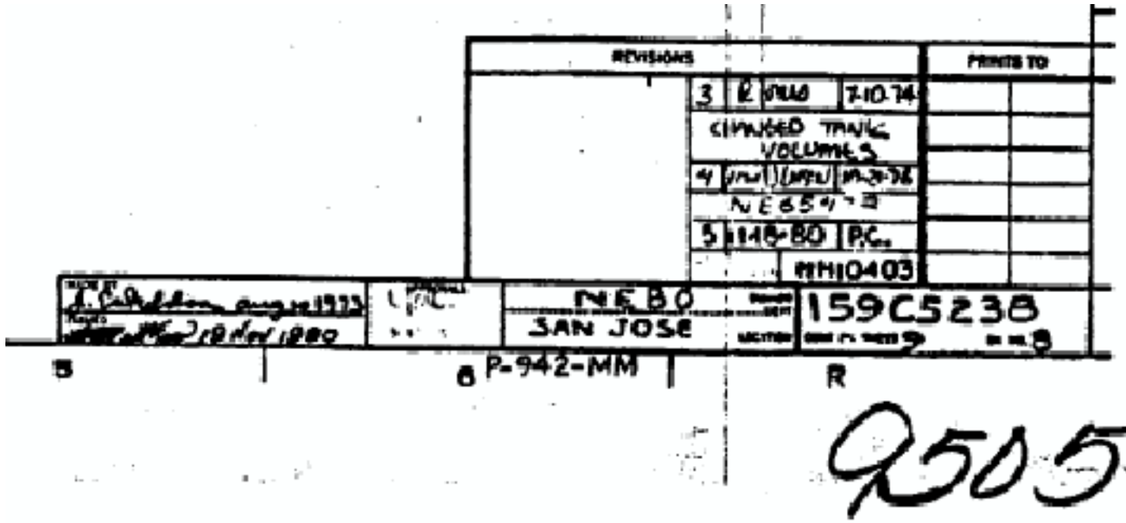

Drawing 159C5238
(Sheet 8, Rev 5)

4-18

9505080266-08

FIGURE WITHHELD UNDER 10 CFR 2.390

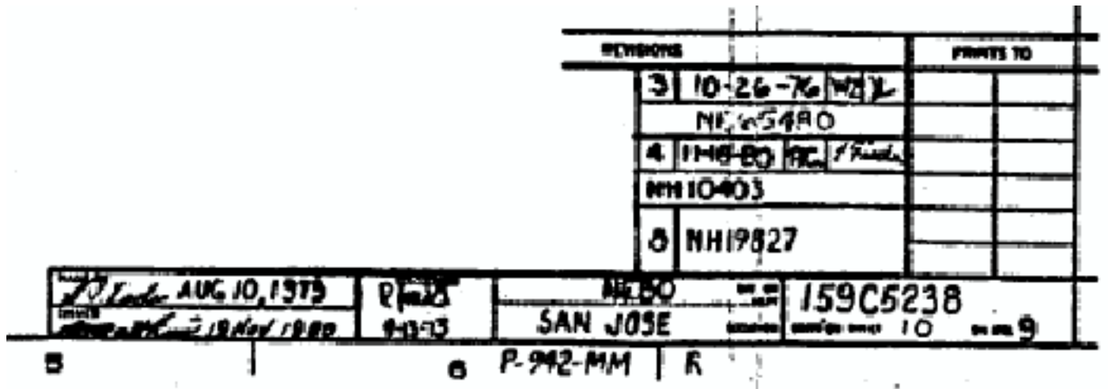

Drawing 159C5238
(Sheet 9, Rev 8)

FIGURE WITHHELD UNDER 10 CFR 2.390

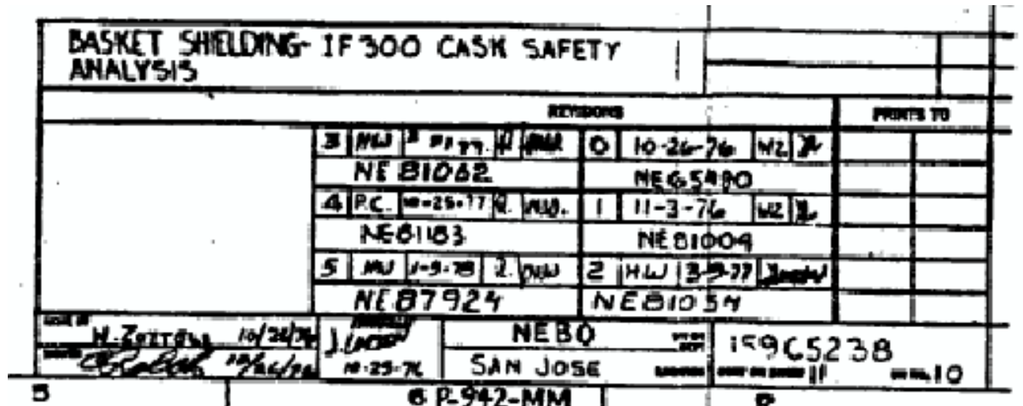

Drawing 159C5238
(Sheet 10, Rev 5)

FIGURE WITHHELD UNDER 10 CFR 2.390

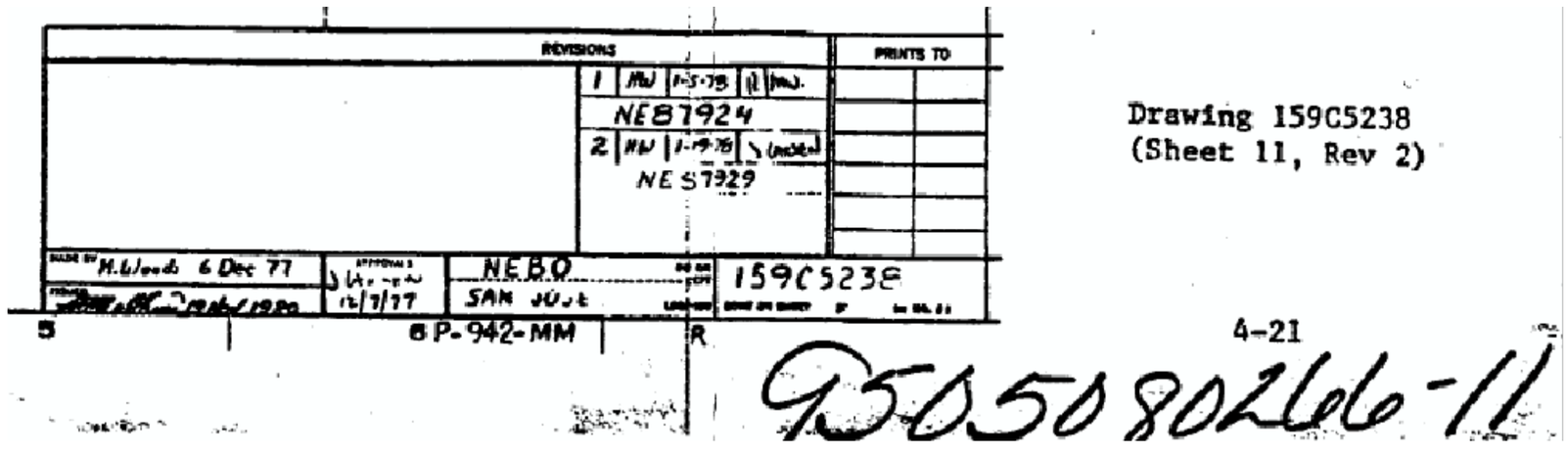

Drawing 159C5238
(Sheet 11, Rev 2)

9505080266-11

TABLE OF CONTENTS

V. STRUCTURAL INTEGRITY ANALYSIS

TABLE OF CONTENTS (CONTINUED)

LIST OF ILLUSTRATIONS

LIST OF ILLUSTRATIONS (CONTINUED)

LIST OF ILLUSTRATIONS (CONTINUED)

LIST OF TABLES

V. STRUCTURAL INTEGRITY ANALYSIS

5.1 INTRODUCTION

The structural integrity analysis of the IF-300 cask design is described in this section. This includes the 7-cell PWR and 18-cell BWR fuel baskets licensed prior to 1991. The structural integrity analysis of the 17-cell channelled BWR fuel basket licensed in 1991 is described in Volume 3, Appendix A.

All design loads specified in 10 CFR Part 71 "Packaging of Radioactive Material for Transport", as amended, plus all loads imposed by the designer of the cask are accounted for in this analysis. The best available material properties and conservative assumptions have been used in the analysis so that the element being examined can not in actuality exhibit higher stresses than those of the analysis. The acceptance criteria used for the cask require factors of safety in excess of 1.0 when subjected to each design load. The safety factor is defined as:

$$SF = \frac{\text{Allowable (load, stress, displacement, etc.)}}{\text{Calculated (load, stress, displacement, etc.)}}$$

5.2 DESIGN LOADS

The following paragraphs describe the conditions to which the cask, fuel bundles, and fuel baskets have been analyzed for the highest G-loading the cask sustains in a 30-foot drop for a given orientation.

5.2.1 Regarded as a simple beam supported at its end along any major axis, the cask shall be capable of withstanding a static load, normal to and uniformly distributed along its length, equal to five times its fully loaded weight without generating stresses in any material in excess of its yield strength.

5.2.2 The cask inner cavity shall suffer no loss of contents if subjected to an external pressure of 25 psig.

5.2.3 The internal pressure of the cask in normal operation shall be less than 200 psig.

5.2.4 The maximum internal pressure shall be 400 psig. The rupture disk device shall be designed to burst within the range of 350-400 psig at 443°F.

5.2.5 The cask shall withstand a free drop through a distance of 30 feet onto a flat, essentially unyielding horizontal surface, striking the surface in a position for which the maximum damage is expected.

5.2.6 The cask shall withstand a free drop through a distance of 40 inches striking, in a position for which maximum damage is expected, the top end of a vertical cylindrical mild steel bar mounted on an essentially unyielding, horizontal surface. The bar shall be 6 inches in diameter, with the top horizontal and its edge rounded to a radius of not more than one-quarter (1/4) inch, and of such length as to cause maximum damage to the package, but not less than 8 inches in length. The long axis of the bar shall be perpendicular to the unyielding horizontal surface.

5.2.7 Cask lifting devices which are structural parts of the package shall support three times the weight of the loaded cask without exceeding the yield stress of any material.

5.2.8 Lifting devices which are part of the cask lid shall support three times the weight of the lid without exceeding the yield stress of any material.

5.2.9 The tiedown devices for attachment of the cask to the equipment skid shall be capable of withstanding a static force, applied at the center of gravity of the cask, having a vertical component of two times the weight of the package and contents, a horizontal component along the direction in which the vehicle travels of ten times the

weight of the package contents, and a horizontal component in the transverse direction of five times the weight of the package and contents.

5.2.10 The cask body shall withstand the thermal stress conditions arising from: 1) normal cooling; 2) loss-of-mechanical cooling: 3) partial loss-of-shielding water; 4) 30-minute fire; and 5) post-fire equilibrium.

5.3 MATERIALS

Table V-1 presents the materials used in the cask, the 7-cell PWR and 18-cell BWR fuel assembly support baskets licensed prior to 1991, and miscellaneous attachments. Volume 3, Appendix A presents the materials used in the 17-cell channelled BWR fuel assembly support basket licensed in 1991.

5.3.1 Uranium Shielding Specification

The depleted uranium metal shielding material is in the form of annular castings, shrink-fitted together to form a continuous shield for the length of the cask. All casting, handling, testing and preparation for shipment are performed in accordance with General Electric Company approved specifications.

The cast material has a maximum U-235 content of 0.22%. The U-235 content of UF_6 tail material is nominally 0.20% with a $\pm$ 0.02% variation. Isotopic analysis has been performed on each casting to assure compliance with the aforementioned limit. Certified copies of the various analyses were originally provided to General Electric Company and are currently retained by VECTRA.

Table V-1

MATERIALS

Item	Materials
External water jacket	ASTM A240 Type 304
Inner shell	ASTM A296-65 CG-8M (317SST modified) or AISI 200 Type 216SST rolled plate
Shielding (casting)	Uranium, depleted metal
Outer body shell	ASTM A296-65 CG-8M (317SST modified)
Structural rings	AISI 200 Type 216
Valve box sides (castings)	ASTM A351-CF8 (304SST)
Valve box cover	AISI 200 Type 216
Bottom head outside shell	ASTM A240 Type 304
Bottom head inside shell	ASTM A240 Type 304
Top head outside shell	ASTM A240 Type 304
Top head inside shell	ASTM A240 Type 304
Top head flange (forging)	ASTM A182 304SST
Cask body flange (forging)	ASTM A182 304SST
Top head fins	ASTM A240 Type 304
Bottom head fins	ASTM A240 Type 304
Valve box fins	AISI 200 Type 216
Studs and nuts	17-4 PH H-1075/H-1025
Fuel element basket axial supports	AISI 200 Type 216
Fuel element basket channels	ASTM A240 Type 304
Basket support rings	AISI 200 Type 216
Support saddle	ASTM A516 Gr 70
Pivot cradle	ASTM A516 Gr 70
Cradle pedestals	ASTM A516 Gr 70
Block pin	AISI 4340 heat treated
Pivot cradle counter weight	Lead
Lifting trunnion blocks	AISI 4340, 304N or nitronic 40 stainless steel forgings.
Cooling ducts	6061/3003 aluminum
Enclosure	6061/6063/3003 aluminum
Skid	Tri-Ten steel

The shield material after completion of fabrication has the following nominal physical properties:

a.	Minimum Yield (0.2% offset):	35,000 psi
b.	Ultimate Tensile Strength:	60,000 psi
c.	Elongation:	6%
d.	Hardness:	Rockwell B-65
e.	Average Density:	18.82 ± 0.12 gm/cc

Samples from each heat are prepared and tested to demonstrate that the fabricated material meets the above listed physical properties. A density measurement is performed on each casting. Certified copies of each report were provided to General Electric and currently retained by VECTRA.

The porosity and soundness of all uranium castings are completely checked by coblt-60 gamma scanning. Strips of material having established thickness and density are placed at intervals on the casting surfaces to serve as reference points for checking the accuracy and sensitivity of the scanning equipment. Scanning follows procedures approved by General Electric Company.

Unacceptable porosity is defined as any area of the casting having deviation (increase) of gamma reading equivalent to a 5% decrease in the shielding thickness.

5.3.1.1 Uranium Properties

Uranium properties used in the calculations are contained in Reference 1, page 124, Figure 7.44.*

5.3.2 Fuel Basket Poison Material Specification

Criticality control in the 7-cell PWR and 18-cell BWR fuel baskets licensed prior to 1991 is provided by 0.5-inch diameter, boron carbide-filled, stainless steel tubes on 1.5-inch

* References are listed at the back of this chapter.

centers between adjacent fuel assemblies. These rods provide poison over the length of the basket and are fixed between the basket spacer disks.

Each poison tube is filled with chemically pure natural boron carbide consisting of 19.6 atomic percent B-10 and 80.4 atomic percent B-11. The minimum packed density of B_4C is 1.75 grams per cubic centimeter. The tubes may be either mechanically compacted or filled with prepressed B_4C pellets. A void space is provided in each tube to contain the small amount of helium produced in the boron-capture process.

The boron carbide columns extend well beyond the fuel active zone to compensate for any fractional settling which may occur with time. Each tube is loaded, backfilled with helium, seal welded and checked with a mass spectrometer.

The poison tube vendor is required to qualify fabrication and testing techniques prior to fabrication. Each batch of material is certified with copies of documentation retained by General Electric Company.

5.3.3 CG-8M (317 Modified) Stainless Steel

As indicated in Table V-1, the cask inner shell may be CG-8M but the outer shell must be a CG-8M centrifugal casting. The "317 modified" designation is placed on the material by the supplier (Sandusky Machine and Foundry) to indicate that a ferrite control process has been used to elevate the strength over those values tabulated in ASTM A296-65.

Properties have been derived from actual elevated temperature tests on CG-8M material as well as supplier data, as listed in Table V-2.

Table V-2

CG-8M (317 MOD.) STAINLESS STEEL PROPERTIES

Temperature, °F	Poisson's Ratio	Strength, psi Yield	Strength, psi Ultimate	Modulus of Elasticity, psi
70	0.25	54.0	92.0	27.0×10^6
200	0.27	53.3	84.7	26.7×10^6
300	0.28	39.1	72.8	26.4×10^6
400	0.29	35.8	71.2	26.0×10^6
500	0.31	33.2	71.2	25.0×10^6
700	0.31	33.2	72.4	—

$\alpha = 8.9 \times 10^{-6}/°F$ (70°F - to 500°F)

5.3.4 216 Stainless Steel

AISI 200, Type 216 is an austenitic stainless steel similar in mechanical properties and corrosion resistance to 317 stainless steel (Section 5.3.3). Type 216 stainless steel is designated ASTM A240 grade XM-17. Although it is not an ASME code material, 216 is closely related to the code-approved 300 series stainless steel. The Allegheny-Ludlum Bulletin on 216 states:

> " The AISI 200 series of austenitic stainless steels exhibit mechanical properties and corrosion resistance similar to their corresponding chromium-nickel types. Allegheny Type 216 not only has corrosion resistance equivalent to Type 316 but in some instances, particularly strong pitting media, Type 216 is superior. In addition, Type 216 offers higher strength both at room temperature and elevated temperatures (tensile strengths, creep, fatigue and stress to rupture). The low magnetic permeability of Type 216, even after severe cold working, further enhances the possible applications of this material."

5.3.4.1 Mechanical Properties

Table V-3 shows typical 216SST properties as a function of temperature. The material is hot rolled and pickled (HRAP).

Table V-4 shows typical values for Charpy V-notch impact tests on 216SST material. These data indicate that 216SST has very good impact strength under low temperature conditions.

Table V-3

216 SST PROPERTIES VS TEMPERATURE

	216 Strength, ksi	
Temperature, °F	Yield	Ultimate
70	62.4	108.8
200	58.4	100.6
400	45.9	90.9
500	-	-
600	41.7	86.8
700	-	-
800	40.1	82.8
68-212	$\alpha = 8.5 \times 10^{-6}/°F$	

Table V-4

TYPICAL VALUES - CHARPY V-NOTCH TESTS

	Charpy V-notch Impact (Ft.-lbs)	
Test Temperature	Annealed	Annealed and Sensitized
Room Temperature	223	225
-100°F	198	178
-320°F	84	71

5.3.4.2 Corrosion Resistance

The data sheets on corrosion resistance of 216 stainless steel indicate that the sensitized samples (1 hour at 1200°F) passed the Intergranular Corrosion test of ASTM A 393. If 216SST is held or slow cooled through the temperature range of 800°F-1500°F, carbides will precipitate. However, this material is not classified as being highly susceptible to sensitization. Discussions with the material developers (Allegheny-Ludlum) indicate that 216 is less susceptible than 300 series stainless steels at the same carbon content. The welding procedures followed for this material specify a maximum interpass temperature of 550°F.

To further qualify Type 216 stainless steel, intergranular corrosion tests were conducted following Practice E of ASTM A262-70 as recommended in Regulatory Guide 1.44, "Control of the Use of Sensitized Stainless Steel." A total of six welded samples were prepared for testing, two each at three different interpass temperatures. The area tested was the heat-affected zone immediately adjacent and parallel to the weld line.

The 216SST welding procedures call for an interpass temperature not to exceed 550°F. To check on the sensitization of 216 stainless steel as a function of interpass temperature, tests were conducted on samples welded using 200°F, 350°F and 550°F as interpass temperatures. The test results indicated that all samples passed Practice E of ASTM A 262-70 and there was no detectable difference between samples. Table V-5 summarizes the results. These tests confirm that Type 216 is not susceptible to stress corrosion cracking due to material sensitization.

Table V-5

RESULTS - INTERGRANULAR CORROSION TESTS

216 Stainless Steel Sample No.	Interpass Temp., of	ASTM A 262-70 Practice E
2603-4	200	Passed
2603-5	200	Passed
2604-2	350	Passed
2604-3	350	Passed
2605-2	550	Passed
2605-3	550	Passed

5.3.4.3 Inner Shell - 216 Stainless Steel

Figure V-1 shows a typical inner shell weldment using 216SST. The weld joint configurations, number of courses and dimensions may vary with vendors but the fundamental construction methodology is as shown.

5.4 VESSEL DESIGN STRESS ANALYSIS

The structural analysis of the IF 300 shipping cask is based on the determination of factors of safety as defined in Section 5.1. A factor of safety of 1.0 does not mean failure of the structure but only that the allowable limit (i.e., working stress, yield stress, ultimate stress), of the material for a specific load combination has been equalled. Factors of safety less than 1.0 are considered unacceptable for this analysis. Conservative assumptions are made where an exact analysis is either impossible or not warranted.

Nomenclature

α	-	Coefficient of Thermal Expansion
E	-	Modulus of Elasticity
ν	-	Poisson's Ratio
S	-	Elastic Section Modulus
Z	-	Plastic Section Modulus
I	-	Moment of Inertia
μ	-	Coefficient of Friction
log	-	Natural Logarithms

FIGURE WITHHELD UNDER 10 CFR 2.390

FIGURE V-1. TYPICAL INNER SHELL WELDMENT USING TYPE 216 STAINLESS STEEL

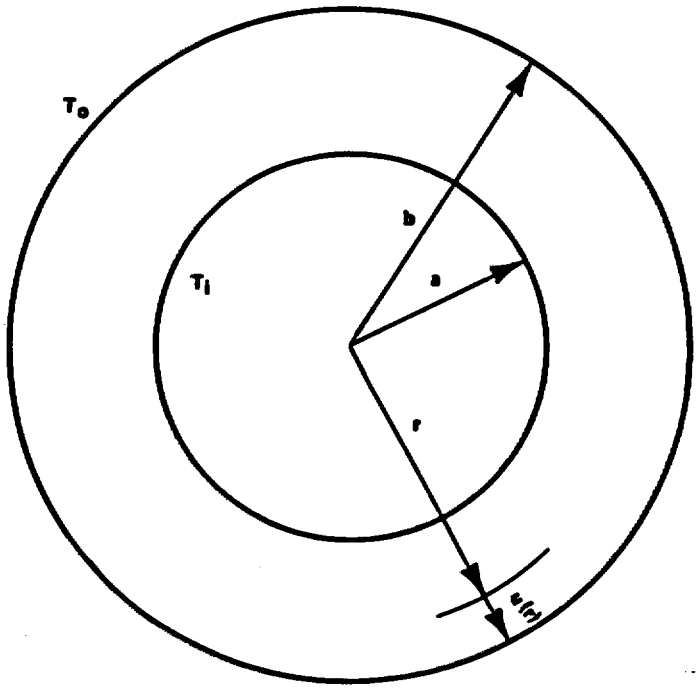

T_i = TEMPERATURE ON INNER SURFACE
T_o = TEMPERATURE ON OUTER SURFACE
u(r) = RADIAL DISPLACEMENT AT $T_i > T_o$ FOR NORMAL OPERATION LOSS-OF-COOLING, LOSS OF SHIELDING WATER, AND POST-FIRE EQUILIBRIUM CONDITIONS.

FIGURE V-2. SHELL MODEL

5.4.1 Inner Shell, Uranium, Outer Shell Stress

Stresses due to internal pressure, temperature and shrink fits of the inner shell, uranium and outer shell are analyzed in the following material (see Figure V-2):

5.4.1.1 Compatibility Formulae

a. Thick-walled Cylinder

The following equations can be written from Reference 2, Part II, Pages 228-234 for the stress due to thermal loads:

$$\sigma_r = \frac{\alpha E(T_i-T_o)}{2(1-\nu)\log(\frac{b}{a})} \left[-\log(\frac{b}{r}) - \frac{a^2(r^2-b^2)}{r^2(b^2-a^2)} \log(\frac{b}{a}) \right]$$

$$\sigma_\theta = \frac{\alpha E(T_i-T_o)}{2(1-\nu)\log(\frac{b}{a})} \left[1 - \log(\frac{b}{r}) - \frac{a^2(r^2+b^2)}{r^2(b^2-a^2)} \log(\frac{b}{a}) \right]$$

$$\sigma_z = \frac{\alpha E(T_i-T_o)}{2(1-\nu)\log(\frac{b}{a})} \left[1-2\log(\frac{b}{r}) - \frac{2a^2}{b^2-a^2} \log(\frac{b}{a}) \right]$$

and

$$u = \alpha T_o' r + \frac{r}{E}\left[\sigma_\theta - \nu(\sigma_r+\sigma_z)\right] + \frac{r\alpha(T_i-T_o)}{\log\left(\frac{b}{a}\right)} \log\left(\frac{b}{r}\right)$$

at $r = a$ & $r = b$

$\sigma_r = 0$ & $\sigma_\theta = \sigma_z$

so that

$$u(a) = \alpha T_o a + \frac{a\alpha(T_i-T_o)}{2\log\left(\frac{b}{a}\right)}\left[1 - \frac{2a^2}{b^2-a^2}\log\left(\frac{b}{a}\right)\right]$$

and

$$u(b) = \alpha T_o b + \frac{b\alpha(T_i-T_o)}{2\log\left(\frac{b}{a}\right)}\left[1 - \frac{2a^2}{b^2-a^2}\log\left(\frac{b}{a}\right)\right]$$

b. Thin-walled Shell

$$u = \alpha T_o r + \frac{r}{E}\left[\sigma_\theta - \nu(\sigma_r + \sigma_z)\right] + r\alpha(T_i - T_o)\left(\frac{b-r}{b-a}\right)$$

$\sigma_r(a) = \sigma_r(b) = 0$

$\sigma_\theta = \sigma_z$

$$\sigma_\theta(a) = \frac{E\alpha(T_i-T_o)}{2(1-\nu)}$$

$$\sigma_\theta(b) = \frac{E\alpha(T_i-T_o)}{2(1-\nu)}$$

therefore,

$$u(a) = \alpha T_o a + \frac{a\alpha(T_i-T_o)}{2}$$

$$u(b) = \alpha T_o b + \frac{b\alpha(T_i-T_o)}{2}$$

$$\sigma_r = \frac{E\alpha(T_i-T_o)}{3(1-\nu)(b-a)} \left[r - \frac{a^3}{r^2} - (1 - \frac{a^2}{r^2}) \frac{b^3-a^3}{b^2-a^2} \right]$$

Since the cask assembly is at approximately 70°F and the coefficients of linear extension (α) have 70°F as the reference temperature, the values of T_i and T_o will be adjusted as follows:

T_i = (Actual inner surface temperature - 70°F)

T_o = (Actual outer surface temperature - 70°F)

where T_{ai} = actual temperature on inner surface
T_{ao} = actual temperature on outer surface

also α_1 = coefficient of expansion corresponding to T_{ao}
α_2 = coefficient of expansion corresponding to $(T_{ai}+T_{ao})/2$

The above equations for displacement can be rewritten for a thick wall cylinder as:

$$u(a) = \alpha_1 T_o a + \frac{a\alpha_2(T_i-T_o)}{2 \log (\frac{b}{a})} \left[1 - \frac{2a^2}{b^2-a^2} \log (\frac{b}{a}) \right]$$

$$u(b) = \alpha_1 T_o b + \frac{b\alpha_2)T_i-T_o)}{2 \log (\frac{b}{a})} \left[1 - \frac{2a^2}{b^2-a^2} \log (\frac{b}{a}) \right]$$

and for a thin wall cylinder as:

$$u(a) = \alpha_1 T_o a + \frac{a\alpha_2(T_i-T_o)}{2}$$

$$u(b) = \alpha_1 T_o b + \frac{b\alpha_2(T_i-T_o)}{2}$$

Using the material properties and dimensions of the cask and writing the compatibility equations at the interface between the inner shell and the uranium and the interface between the uranium and the outer shell; considering the inner and outer shells as thin walled shells and the uranium shielding as a thick-walled shell; the following is obtained:

c. Inner Shell/Uranium Interface

$$-\frac{PR_i^2}{E_i T_i}\left(1-\frac{\nu_i}{2}\right)+\frac{P_1 R_i^2}{E_i t_i}+\frac{P_1 a_u}{E_u}\left(\frac{a_u^2+b_u^2}{b_u^2-a_u^2}+\nu_u\right)-\frac{P_2 a_u}{E_u}\left(\frac{2b_u^2}{b_u^2-a_u^2}\right)$$

$$=\delta_1+\alpha_{1i}T_{oi}b_i+\frac{b_i\alpha_{2i}(T_{ii}-T_{oi})}{2}$$

$$-\left\{\alpha_{1u}T_{ou}a_u+\frac{a_u\alpha_{2u}(T_{iu}-T_{ou})}{2\log\left(\frac{b_u}{a_u}\right)}\left[1-\frac{2a_u^2}{b_u^2-a_u^2}\log\left(\frac{b_u}{a_u}\right)\right]\right\}$$

and

d. Outer Shell/Uranium Interface

$$-\frac{P_1 b_u}{E_u}\left(\frac{2a_u^2}{b_u^2-a_u^2}\right)+\frac{P_2 b_u}{E_u}\left(\frac{b_u^2+a_u^2}{b_u^2-a_u^2}-\nu_u\right)+\frac{P_2 R_o^2}{E_o T_o}$$

$$=\delta_2+\alpha_{1u}T_{ou}b_u+\frac{b_u\alpha_{2u}(T_{iu}-T_{ou})}{2\log\left(\frac{b_u}{a_u}\right)}\left[1-\frac{2a_u^2}{b_u^2-a_u^2}\log\left(\frac{b_u}{a_u}\right)\right]$$

$$-\left[\alpha_{1o}T_{oo}a_o+\frac{a_o\alpha_{2o}(T_{io}-T_{oo})}{2}\right]$$

where

P = internal pressure (psi)

P_1 = interface pressure between inner shell and uranium (psi)

P_2 = interface pressure between outer shell and uranium (psi)

Subscripts

i = inner shell, inside diameter

u = uranium shell

o = outer shell, outside diameter

δ_1 = "Shrink fit interference" at interface of inner shell and uranium.

δ_2 = "Shrink fit interference" at interface of outer shell and uranium.

Solving the above compatibility equations for P_1 and P_2 and writing the equations for stress in the three shells as

5.4.1.2 Stress Formulae

a. Inner Shell

$$\sigma_\theta \begin{pmatrix} a_i \\ b_i \end{pmatrix} = \frac{(P-P_1)R_i}{t_i} \pm \frac{E_i \alpha_{2i} (T_{ii}-T_{oi})}{2(1-\nu_i)}$$

$$\sigma_z \begin{pmatrix} a_i \\ b_i \end{pmatrix} = \frac{PR_i}{2t_i} \pm \frac{E_i \alpha_{2i} (T_{ii}-T_{oi})}{2(1-\nu_i)}$$

$$\sigma_r = \frac{E_i \ \alpha_{2i} \ (T_{ii} - T_{oi})}{3(1-\nu_i) \ (b_i - a_i)} \left[r - \frac{a_i^3}{r^2} - \left(1 - \frac{a_i^2}{r^2}\right) \frac{b_i^3 - a_i^3}{b_i^2 - a_i^2} \right]$$

b. Uranium Shell

$$\sigma_\theta(a_u) = P_1 \frac{b_u^2 + a_u^2}{b_u^2 - a_u^2} - P_2 \frac{2b_u^2}{b_u^2 - a_u^2} + \frac{E_u \alpha_{2u} (T_{iu} - T_{ou})}{2(1-\nu_u) \log \left(\frac{b_u}{a_u}\right)}$$

$$\left[1 - \frac{2b_u^2}{b_u^2 - a_u^2} \log \left(\frac{b_u}{a_u}\right) \right]$$

$$\sigma_\theta(b_u) = P_1 \frac{2a_u^2}{b_u^2-a_u^2} - P_2 \frac{b_u^2+a_u^2}{b_u^2-a_u^2} + \frac{E_u\alpha_{2u}(T_{iu}-T_{ou})}{2(1-\nu_u)\log(\frac{b_u}{a_u})}$$

$$\left[1 - \frac{2a_u^2}{b_u^2-a_u^2} \log(\frac{b_u}{a_u})\right]$$

$$\sigma_z(a_u) = \frac{E_u\alpha_{2u}(T_{iu}-T_{ou})}{2(1-\nu_u)\log(\frac{b_u}{a_u})} \left[1 - \frac{2b_u^2}{b_u^2-a_u^2} \log(\frac{b_u}{a_u})\right]$$

$$\sigma_z(b_u) = \frac{E_u\alpha_{2u}(T_{iu}-T_{ou})}{2(1-\nu_u)\ln(\frac{b_u}{a_u})} \left[1 - \frac{2a_u^2}{b_u^2-a_u^2} \ln(\frac{b_u}{a_u})\right]$$

$$\sigma_r = \frac{\alpha_{2u}E_u(T_{iu}-T_{ou})}{2(1-\nu_u)\log(\frac{b_u}{a_u})} \left[-\log\frac{b_u}{r} - \frac{a_u^2(2-b_u)}{r^2(b_u^2-a_u^2)} \log\frac{b_u}{a_u}\right]$$

$$- P_1 \frac{a_u^2(b_u^2-r^2)}{r^2(b_u^2-a_u^2)} - P_2 \frac{b_u^2(r^2-a_u^2)}{r^2(b_u^2-a_u^2)}$$

c. Outer Shell

$$\sigma_\theta\begin{pmatrix}b_o\\a_o\end{pmatrix} = \frac{P_2R_o}{t_o} \pm \frac{E_o\alpha_{2o}(T_{io}-T_{oo})}{2(1-\nu_o)}$$

and

$$\sigma_z\begin{pmatrix}b_o\\a_o\end{pmatrix} = \pm \frac{E_o\alpha_{2o}T_{io}-T_{oo})}{2(1-\nu_o)}$$

$$\sigma_r = \frac{E_o \alpha_{2o}(T_{io}-T_{oo})}{3(1-\nu_o)(b_o-a_o)} \left[r - \frac{a_o^3}{r^2} - \left(1 - \frac{a_o^2}{r^2}\right) \frac{b_o^3 - a_o^3}{b_o^2 - a_o^2} \right]$$

5.4.1.3 Stresses During 30-Minute Fire

The previously derived relationships for shell displacement require that the shells be hotter on their ID's than on their OD's. Under fire conditions just the opposite is true, thus these equations must be modified as follows:

a. Thick-Walled Cylinder

$$u(a) = \alpha_i T_i a + \frac{a\alpha_2(T_i-T_o)}{2 \log (b/a)} \left[1 - \frac{2a^2}{b^2-a^2} \log \left(\frac{b}{a}\right) \right]$$

$$u(b) = \alpha_i T_i b + \frac{2 (T_i-T_o)}{2 \log (b/a)} \left[1 - \frac{2a^2}{b^2-a^2} \log \left(\frac{b}{a}\right) \right]$$

b. Thin-Walled Cylinder

$$u(a) = \alpha_1 T_i a + \frac{a\alpha_2 (T_i-T_o)}{2}$$

$$u(b) = \alpha_1 T_i b + \frac{b\alpha_2 (T_i-T_o)}{2}$$

The stress equations remain unchanged and the compatibility equations are only slightly modified to reflect the changes in "u".

5.4.2 Bases for Analysis

The cask shell analysis considers five thermal conditions (one normal, four off-normal) and two pressure conditions (one operating and one design). The interference fit between shells is taken at the maximum value to provide conservatism. Table V-6 summarizes the calculational bases.

Table V-6

TEMPERATURE-PRESSURE BASES FOR STRUCTURAL ANALYSIS

(See Figure V-3)

	Condition	Temperature				Cavity Pressure	
		Outer Shell Outer Dia, °F (4)	Outer Shell-Uranium Interface, °F (3)	Uranium-Inner Shell Interface, °F (2)	Inner Shell Inside Dia, °F (1)	Operating, psig	Design psig
I	Normal Cooling	230	241	278	283	55	200
II	Loss-of-Mech. Cooling	372	388	415	420	332	400
III	Partial Loss of Shield Water	580	590	612	615	332	400
IV	End-of-30 min Fire	510	428	343	330	88	400
V	Post-Fire Equilibrium	580	590	612	615	332	400

Notes

(a) Outer shell - Uranium interference fit = 0.015 in.

(b) Inner Shell - Uranium interference fit = 0.020 in.

(c) All tmperatures are for a decay heat rate of 262,000 Btu/hr.

FIGURE WITHHELD UNDER 10 CFR 2.390

FIGURE V-3. CASK BODY CROSS-SECTION

5.4.2.1 Results of Analysis:

The results of these analyses are displayed in Tables V-7 and V-8.

Table V-7

MAXIMUM STRESSES UNDER OPERATING PRESSURE

Condition No.	Inner Shell σ(ksi)*	SF	Uranium σ(ksi)*	SF	Outer Shell σ(ksi)	SF
I	-33.5	1.20	-11.1	2.61	23.3	2.04
II	-28.7	1.24	-8.9	2.88	24.5	1.48
III	-22.8	1.49	-9.6	2.17	25.1	1.35
IV	-10.6	6.85	14.2	3.87	15.9	4.49
V	-22.8	1.49	-9.6	2.17	25.1	1.35

*Negative sign denotes compressive stress.

Table V-8

MAXIMUM STRESSES UNDER DESIGN PRESSURE

Condition No.	Inner Shell σ(ksi)*	SF	Uranium σ(ksi)*	SF	Outer Shell σ(ksi)	SF
I	-32.2	1.28	-10.7	2.73	23.7	2.0
II	-28.1	1.26	-8.7	2.94	24.6	1.47
III	-22.2	1.53	-9.4	2.22	25.3	1.34
IV	15.5	4.64	15.5	3.56	16.6	4.28
V	-22.2	1.53	-9.4	2.22	25.3	1.34

*Negative sign denotes compressive stress.

5.4.3 Bottom and Top Heads

The heads are designed such that there is no gap at either of the two uranium/steel interfaces (Figure V-4). Thus, the deflection, δ, due to internal cavity pressure is common to all three components and the pressure acts on a radius, r_o, equal to the cask cavity radius of 18.75 inches.

FIGURE WITHHELD UNDER 10 CFR 2.390

FIGURE V-4. HEAD CONFIGURATIONS

5.4.3.1 Derivation of Stress Equations

The derivation of the stress relationship between the three sections is as follows (see Figure V-5):

$F_i(W)$ = Spring constant for the inner head due to load (W) on inner head.

$F_i(W_1)$ = Spring constant for the inner head due to the contact load (W_1) between the inner head and the uranium.

$F_u(W_1)$ = Spring constant for the uranium due to the load (W_2) on the uranium.

$F_o(W_2)$ = Spring constant for the outer head due to the load (W_2) on the outer head.

and

$$\delta_i = \delta_u = \delta_o = \text{Deflection}$$

$$\delta_i = \delta_w - \delta_{w1};\ \delta_u = \delta_{w1} - \delta_{w2};\ \delta_o = \delta_{w2}$$

$$\delta_i = W\left[F_i(W)\right] - W_1\left[F_i(W_1)\right]$$

$$\delta_u = W_1\left[F_u(W_1)\right] - W_2\left[F_u(W_2)\right]$$

$$\delta_o = W_2\left[F_o(W_2)\right]$$

Combining:

$$1)\quad W_1\left[F_i(W_1)\right] + W_2\left[F_o(W_2)\right] = W\left[F_i(W)\right]$$

$$2)\quad W_1\left[F_u(W_1)\right] - W_2\left[F_u(W_2) + F_o(W_2)\right] = 0$$

FIGURE WITHHELD UNDER 10 CFR 2.390

FIGURE V-5. ASSUMED LOADING DISTRIBUTION

The spring constants are given by:

$$F_x(W_y) = \frac{3a^4}{16E_x M_x^2 t_x^3} (M_x-1)(5M_x+1)$$

Where: a = cavity radius, in.
E = modulus of elasticity, psi
M = 1/ν = inverse of poisson's ratio
t = plate thickness, in.

Subscript x = o, u, or i as appropriate for the plate under consideration
Subscript y = 0, 1 or 2 for the loading under consideration

Table V-9 gives the parameters for the bottom and top heads. Note that the top head is analyzed for the BWR configuration which has the smaller outer plate thickness (1.5 in. versus 2.0 in.) of the two operational closures (BWR and PWR). Also shown are the resulting values for W_1 and W_2, the interface contact pressures.

Table V-9
HEAD SPRING CONSTANT PARAMETERS

Item	Bottom Head	Top Head (BWR)
E_i, psi	26.4×10^6	26.4×10^6
M_i	3.45	3.45
t_i, in.	1.25	1.0
E_u, psi	25.8×10^6	25.8×10^6
M_u	4.76	4.76
t_u, in.	3.75	3.0
E_o, psi	26.4×10^6	26.4×10^6
M_o	3.45	3.45
t_o, in.	1.5	1.5
W_1, psi	385	385.9
W_2, psi	25.8	47.4
W, psi	400	400

The maximum stress in each of the head segments can be determined using the following relationships:

$$\sigma_{max} = \frac{3a^2 \Delta W}{8M_x t^2_x} (3M + 1) \qquad (5.1)$$

5.4.3.2 Head Stress Calculational Result

Based on Equation 5.1, Table V-10 gives the head segment stresses and safety factors (SF) under the design cavity pressure of 400 psig.

Table V-10

HEAD STRESSES

	Bottom Head		Top Head (BWR)	
Component	Stress, ksi	SF	Stress, ksi	SF
Inner head plate	4.16	4.71	6.11	3.2
Uranium	10.81	2.40	15.92	1.6
Outer head plate	4.98	3.94	9.15	2.1

5.4.4 Cask as a Simple Beam

With the cask regarded as a simple beam supported by only the outside body shell at its ends and loaded with a uniform load equal to five times its fully loaded weight

$$\sigma_{max} = \frac{M}{Z} = \frac{(5WL/8)}{R^2 t} = \frac{17{,}100 \text{ in.-k}}{2720 \text{ in.}^3} = 6.29 \text{ ksi}$$

$$SF = \frac{54.0}{6.29} = 8.6$$

$$\tau = \frac{V}{A} = \frac{(5W/2)}{2\pi Rt} = \frac{350k}{2\pi\ (23.25)\ (1.50)} = 1.58 \text{ ksi}$$

$$SF = \frac{54.0}{1.58}\ (0.6) = 20.4$$

5.4.5 External Pressure Load - Cask Body

Checking the outer shell for elastic stability due to a 25 psig external pressure (Reference 3, Table XVI, Case 31, Page 354):

$$P' = \frac{0.807Et^2}{1r}\left[\left(\frac{1}{1-\nu}\right)^3\ \left(\frac{t}{r}\right)^2\right]$$

$$P' = 3070 \text{ psi} \qquad SF = \frac{3070}{25} = 123$$

and checking for the maximum stress due to the external pressure:

$$\sigma = \frac{pr}{t} = 400 \text{ psi} \qquad \sigma_{yield} = 54{,}000 \text{ (for 317 mod SST)}$$

$$SF = \frac{54{,}000}{400} = 135$$

5.5 30-FOOT DROP - ENERGY ABSORPTION AND DECELERATION

The thirty-foot free drop of the cask on an unyielding surface was analyzed considering 10 orientations - 2 vertical, 2 corner and 6 horizontal. The cask is protected from extensive damage by energy absorbing members which deform in a predictable manner and limit the forces imposed on the head and body.

Protection from vertically-oriented (end and corner) drops is provided by end fins. The cask head and body end are equipped with 32 radial fins as shown in Figure V-6. The fins are classified as long or short based on their standoff lengths. The 16 short fins stand 6 inches above the plane of the body bottom or head top. The 16 long fins on the bottom stand 8-1/8 inches above the bottom plane while the 16 long fins on the head stand 9-1/2 inches above the top plane. The taller fins on the head are used to reduce the load transmitted through the closure flange during impact.

Protection from horizontally-oriented drops is provided by side impact rings and, in the case of the valve boxes, rectangular fins. The body is encircled by four thick stainless steel rings which form the primary impact protection. These rings function in a manner similar to the end fins in that they deform under impact and limit the loads imposed on the cask body. For certain orientations the structural rings are supplemented by other sacrificial members to assure that all the energy is absorbed by non-vital elements of the cask.

5.5.1 Fin Bending Analysis

The fin bending analysis is based on a testing program conducted at Oak Ridge National Laboratory. The results of this program are published in USAEC report ORNL TM-1312, Vol. 9. Data from this program were correlated by General Electric for use in the IF-300 cask design and analysis. This correlation is considered proprietary and will not be exhibited in this document.

Test specimens representing single fins were mounted on an instrumented load cell and impacted by guided falling weights from various heights. Test data were recorded on an oscilloscope and photographed, from which force-time relationship graphs were plotted.

From those test results a correlation was made relating fin rotation angle, fin deflection and absorbed energy. Using this correlation, the IF 300 cask fin configuration was analyzed for energy absorption and deceleration.

To provide a degree of conservatism the decelerations were computed by dividing the drop height (360 inches) by the deformation distance computed using the correlation. Those areas in close proximity to the impact point (e.g., valve boxes, closure flange and studs) were evaluated at twice the deceleration computed using the above method.

Throughout all of the fin bending analyses it was conservatively assumed that the maximum rotation angle for a double-hinge fin was 1.5π radians

5.5.2 Corner Drop

The first drop orientation evaluated is with the cask inclined such that the center of gravity acts through the cask corner as shown in Figure V-7. The angle of inclination is slightly less than 15°. Since the cask strikes the surface at an angle with the horizontal, the fins will undergo different deformations depending on their orientations on the head (see Figure V-6 for end fin arrangement). For fins inclined at less than 10° relative to the contact surface, two hinges were assumed to be formed based on the referenced tests. For those fins hitting at an angle greater than 10°, a single hinge was assumed to form. This hinge formation behavior was observed in the ORNL tests.

The hinge closest to the cask (Figure V-8) was assumed to form at two times the fin thickness away from the surface. The hinge farthest away from the cask was assumed to form at 0.65 times the fin height away from the cask surface. These two values are based on measurements of the actual test fin profiles. The effective length of the fin hinge lines (Figure V-8) is taken as

$$L_{eff} = \frac{(L_{inner} + 2L_{outer})}{3}.$$

The average deceleration is defined in terms of drop height divided by deformation distance, (H/δ). For the analysis of the closure flange and bolting, twice the value of the average deceleration was used due to the close proximity of the flange to the point of impact. In the corner drop both long and short fins deform to absorb energy.

5.5.2.1 Fin Deformation

Assuming the cask strikes directly over small fin #1 (see Figure V-6), the first fins to contact the surface will be large fins #2. Further assuming that the total angular rotation, θ, of the hinge lines on each of the fins numbered 2 is only slightly less than the 1.5 π radian maximum, then the correlation curve of θ versus percent

FIGURE WITHHELD UNDER 10 CFR 2.390

FIGURE V-6. END FIN ARRANGEMENT

FIGURE WITHHELD UNDER 10 CFR 2.390

FIGURE V-7. ORIENTATION FOR CORNER DROP

FIGURE WITHHELD UNDER 10 CFR 2.390

SECTION B–B (FROM FIG. V–6)

FIGURE V-8. TYPICAL END FINS

deformation indicates these fins collapse to approximately 65 percent of their original height. This is the maximum fin deflection and hence the cask deceleration distance. All other fins will bend to a lesser extent since they are further removed from the point of impact. The deformation, δ, of any fin may be described as follows:

Large Fins

$\delta_1 = 7.56 \cos \phi - 2.18$ Bottom End

$\delta_1 = 7.56 \cos \phi - 1.08$ Top End

Small Fins

$\delta_s = 7.56 \cos \phi - 4.12$ Bottom End

$\delta_s = 7.56 \cos \phi - 4.58$ Top End

Where:

ϕ is the angular location of the fin referenced from small fin No. 1 (Figure V-6)

5.5.2.2 Deflection Relationship Derivation

The four equations above describe the head and body fin deflections under the 30-foot corner drop condition, assuming that initial contact is over small fin #1. Based on the fin bending correlations, it is further assumed that long fins #2 deflect to their maximum value - (65.5% of original height). All other fins will deflect a lesser amount due to their angular displacement from fin #1. There are three angles involved in this derivation. The first is the drop angle or impact angle of the cask with the ground; the second is the radial angle between fins, and the third is the angular position of the fin in question from fin #1. This last angle is a multiple of the radial angle between fins.

Refer to Figures V-6, V-7, and V-8.

a. Definitions:

δ_F = Deflection of fin, in

δ_1 = Deflection of fins #2 (max.)

R = radius from cask $\mathcal{L}$ to fin tips
= 24.75 "+6" = 30.75 (see Figure V-8)

ϕ_1 = Fin-to-fin angular spacing
= 11.25° (see Figure V-6)

ϕ_2 = Cask drop angle
= 14.226° (see Figure V-7)

ϕ = Angular position of the fin in question relative to Fin #1.

b. The formulas are derived based on two parallel planes a distance of δ_1 apart. The planes are inclined at ϕ_2 to the cask. The first plane contains the #1 fin tip (contact point-Figure V-7); the second plane contains the deflected #1 fin. The deflection of any fin, then, becomes

$\delta' = R\,\text{Cos}\phi-(R-\delta'')$
$= R(\text{Cos}\phi-1) + \delta''$

Plane A-A is normal to the contact surface. To resolve δ' to the drop angle ϕ'

$\delta' = [R(\text{Cos}\phi-1) + \delta'']\ \text{Sin}\ \phi'$

c. Long Fins

In the case of the IF-300 cask, a short fin is in the 0° position; therefore, the first long fin is displaced 11.25° from it. Thus, the δ from this displacement must be subtracted to correctly state each long fin deflection. Also, the maximum deflection, δ is measured in the correct direction (along the ϕ_2 line), and therefore, does not require angular resolution.

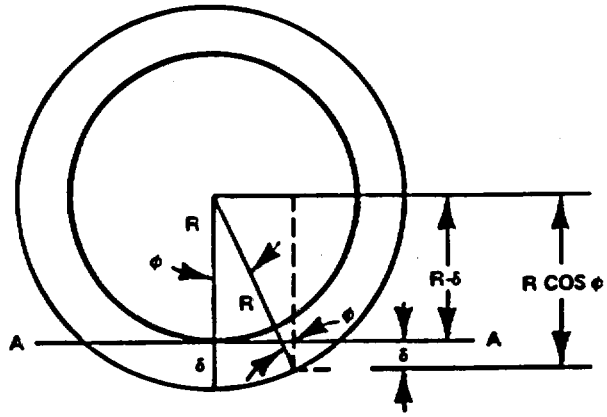

FIGURE V-9. DEFLECTION RELATIONSHIPS

Writing the above relationship for the long fins:

$$\delta_L = \delta_1 + [R(\text{Cos } -1)] \text{ Sin } \phi_2 - [R(\text{Cos } \phi - 1)] \text{Sin } \phi_2$$

As an example:

For the bottom corner drop

δ_1 = 5.24 in

Substituting:

$$\delta_L = 5.24\ [30.75\ (\text{Cos}\phi - 1)]\ \text{Sin } 14.226$$
$$-[30.75\ (\text{Cos } 11.25° - 1)]\ \text{Sin } 14.226$$
$$= 5.24 + 7.56\ \text{Cos}\phi - 7.557 - 7.412 + 7.557$$
$$= 7.56\ \text{Cos}\phi - 2.18$$

d. Small Fins

Because the small fins are shorter (2"), they are related to the long fins as follows:

$$\delta_S = \delta_L - 2\ \text{Cos } 14.226°$$
$$\delta_S = 7.56\ \text{Cos}\phi - 2.18 - 2\ \text{Cos } 14.226°$$
$$= 7.56\ \text{Cos}\phi - 4.12$$

The top head fin deflections are computed in a similar manner.

5.5.2.3 Energy Absorbed

The energy absorbed in double fin bending is described by the following:

$$E = M_p \theta$$

$$E = (\sigma_H L\ t^2 \theta)\ 1/2 \text{ in.-kips}$$

Where:

σ_H = Hinge stress of material, ksi

L = Hinge length, in.

t = fin thickness, inc.

θ = Total angular rotation of hinges, radians.

Fins Nos. 1 through 6 are the most effective in absorbing energy. Fins No. 5 and beyond impact the surface at an angle greater than 10 degrees, therefore only a single hinge is assumed to form. Tables V-11 and V-12 show the parameters used in the computations for the bottom end and top end fin corner drop analyses.

e. The energy absorbed by the fins must be equal to the cask kinetic energy. The cask kinetic energy at the moment of impact is 50,400 in.-kips.* Table V-13 shows the energy absorbed by the fins for each end of the cask as well as the cask average deceleration based on "H-over-Delta." When analyzing the closure flange and hardware a deceleration of 113.6 G's is used, twice that computed for the top corner drop.

*$1/2\ MV^2$

Table V-11

BOTTOM HEAD FIN PARAMETERS

Fin No.	No. Of Fins	Angle w/Vert. (Deg)	No. Of Hinges	ϕ (Deg)	δ (inches)	δ/h	θ (Rads)*
1 (S)	1	0	2	0	3.44	0.575	4.25
2 (L)	2	2.75	2	11.25	5.24	0.655	4.60
3 (S)	2	5.40	2	22.5	2.88	0.480	3.82
4 (L)	2	7.85	2	33.75	4.11	0.515	3.98
5 (S)	2	10.0	2	45.0	1.23	0.205	2.32
6 (L)	2	11.79	1	56.25	2.02	---	0.686

*Values of θ obtained from correlation of fin bending test data.

Table V-12

TOP HEAD FIN PARAMETERS

Fin No.	No. Of Fins	Angle w/Vert. (Deg)	No. Of Hinges	ϕ (Deg)	δ (inches)	δ/h	θ (Rads)*
1 (S)	1	0	2	0	2.98	0.497	3.90
2 (L)	2	2.75	2	11.25	6.34	0.667	4.67
3 (S)	2	5.40	2	22.50	2.41	0.402	3.45
4 (L)	2	7.85	2	33.75	5.21	0.549	4.15
5 (S)	2	10.0	2	45.00	0.77	0.128	1.77
6 (L)	2	11.79	1	56.25	3.12	---	0.79
7 (S)	2	13.12	1	67.50	---	---	---
8 (L)	2	13.95	1	78.75	0.40	---	0.17

*Values of θ obtained from correlation of fin bending test data.

Table V-13

CORNER DROP CALCULATIONS

Item	Impact End	
	Bottom Head	Top Head
Short fin energy abs. in.-kips	26,000	22,600
Long fin energy abs. in.-kips	24,300	27,400
Total energy abs, in.-kips	50,300	50,000
Cask kinetic energy, in.-kips	50,400	50,400
Percent error	0.2	0.8
Maximum deformation, in.	5.24	6.34
Drop Height, in.	360	360
Deceleration, "G"	68.7	56.8

5.5.3 End Drop

The end drop is the second orientation evaluated. The cask is positioned such that its cask axis is perpendicular to the impacting surface. All 16 long end fins come in contact with the surface simultaneously. Using the same fin bending correlation as in the corner drop, the total plastic hinge rotation, final deformation, and subsequent deceleration are shown in Table V-14. It should be noted that only the 16 long fins crush since the deformation distance is less than the difference in fin heights. The deceleration difference (178 versus 234) is due to the taller fins (9.5 in. versus 8 in.) on the closure end.

Table V-14

END DROP DECELERATIONS

Item	Impact End	
	Head	Body
θ (radians)	2.24	2.24
δ (inches)	2.02	1.54
Deceleration (G's)	178	234

5.5.4 Side Drop

Six side orientations were analyzed for the 30-foot drop criterion. These six positions are shown by the circled numbers on Figure V-10. Impact protection is provided by a number of structural members. The principal structures are four heavy rings arranged in pairs at either end of the body. A finned valve box is nested between each of the two pairs of impact rings. A 90-degree arc ring is mounted on the cask body midway between the valve boxes but on the opposite side. These structures are shown on Figures V-10 and V-11.

Energy absorption computations utilize the same correlation employed in the vertical drop analyses. As shown in Figure V-10 the structural rings and fins were assumed to form two hinges with the hinge closest to the cask forming at two times the fin thickness away from the cask surface. The second hinge formed at 0.65 times the fin height away from the cask surface. The effective hinge length of the circular structural rings was computed as follows:

$$L_{eff} = \frac{2L_o + L_i}{3}$$

where: L_o = length of outer hinge line

L_i = length of inner hinge line (See Figure V-10)

This is based on the fact that the outer hinge absorbs approximately two-thirds of the energy and the inner hinge absorbs the remaining one-third. This is consistant with the corner drop analysis.

Referring to Figure V-10, Table V-15 presents a listing of the six side orientations and their respective energy absorbing members.

FIGURE WITHHELD UNDER 10 CFR 2.390

FIGURE V-10. STRUCTURAL RING, FIN, AND VALVE BOX ARRANGEMENT

FIGURE WITHHELD UNDER 10 CFR 2.390

FIGURE V-11. CASK SIDE STRUCTURAL RINGS AND FINS – VIEW A-A

Table V-15

ENERGY ABSORBING MEMBERS
(Refer to Figure V-10)

Orientation	Energy Absorbing Member
0°	Structural Rings, Valve Box Fins
20° (valve box corner)	
45°	
90°	
135°	, Partial Ring
180°	, Partial Ring

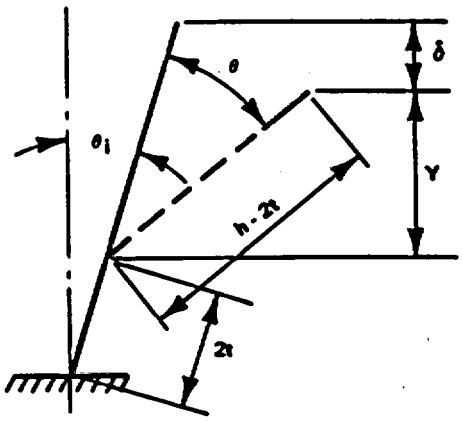

FIGURE V-12. SINGLE HINGE BENDING

5.5.4.1 0° Orientation Side Drop

This is a direct drop on the valve boxes. Energy is absorbed by deformation of the four structural rings and the valve box lid fins. As can be seen in Figure V-11 structural rings are angled outward from the valve box (5 degrees). This angle will cause the fins to collapse away from the box in an unobstructed direction. The lid fins are inclined from the vertical hence they undergo various angular rotations depending on their location. Fin pairs 1, 2 and 3 strike the surface at less than 10 degrees and form a double hinge. Fin pairs 4 through 7 are inclined at an angle greater than 10 degrees and only fail in single hinge bending. The energy absorbed by the bending of a 216 SST fin or ring is given by:

$$E = 55 L_e t^2 \theta \text{ in.-kips} \qquad (5.2)$$

where:

L_e = effective hinge length, in.

t = fin thickness, in.

θ = hinge rotation, radians

Referring to Figure V-12, for single hinges

$$\theta = \left[\cos^{-1}\left(\frac{Y}{h - 2t}\right)\right] - \theta_i \qquad (5.3)$$

where:

$Y = (h - 2t) \cos \theta_i - \delta$

h = fin height, in.

θ_i = fin inclination, rad

δ = fin deformation, in.

For double hinges θ is derived from the fin bending correlation curves.

Table V-16 contains a summary of the 0° side drop calculation parameters. The resulting cask deceleration is:

$$\text{"G"} = \frac{360}{3.3} = 109$$

Table V-16

0° ORIENTATION PARAMETERS

Fin No.	Fin thk,in.	No. of Fins	h, in.	θi deg	δ, in.	δ/h	(h-2t), in.	Y, in.	No. of hinges	θ, rad
1	9/16	1	7.0	0	3.3	0.472			2	3.78
2	9/16	2	7.02	4	3.3	0.470			2	3.77
3	9/16	2	7.07	8	3.3	0.467			2	3.76
4	9/16	2	7.15	12	3.3		6.025	2.59	1	0.916
5	9/16	2	7.28	16	3.3		6.15	2.62	1	0.853
6	9/16	2	7.45	20	3.3		6.325	2.64	1	0.791
7	3/4	2	7.90	24.2	1.55		6.40	4.29	1	0.413
Struc. Rings	1-1/4	4	16	5	3.3	0.206			2	2.35

Table V-17

20° ORIENTATION PARAMETERS

Fin No.	Fin thk,in.	No. of Fins	h, in.	θi deg	δ, in.	δ/h	(h-2t), in.	Y, in.	No. of hinges	θ, rad
2	9/16	1	7.02	17.1	0.5		5.895	5.13	1	0.216
3	9/16	1	7.07	13.1	1.5		5.945	4.28	1	0.537
4	9/16	1	7.15	9.1	2.6	0.364			2	3.27
5	9/16	1	7.28	5.1	3.6	0.494			2	3.89
6	9/16	1	7.45	1.1	4.8	0.644			2	4.56
7	3/4	1	7.90	3.1	4.0	0.506			2	3.95
8	3/4	1	7.16	7.3	2.7	0.377			2	3.33
9	3/4	1	7.03	11.4	1.45		5.53	3.97	1	0.571
10	9/16	1	6.94	15.6	0.25		5.815	5.35	1	0.129
Struct. Ring	1-1/2	4	18.95	5	5.1	0.269			2	2.75

5.5.4.2 20° Orientation Side Drop

This side orientation has the impact point directly on the corner of the valve box lid. As in the previous case the cask kinetic energy is absorbed by the structural rings and the box fins. The energy absorbed is computed using equations 5.2 and 5.3 as before. Table V-17 gives the fin bending parameters. The resulting cask deceleration is:

$$\text{"G"} = \frac{360}{5.1} = 70.6$$

5.5.4.3 45° Orientation Side Drop

This side orientation places the point of impact directly on the valve box side castings. As in the two previous cases, the cask energy is dissipated by the deformation of structural rings and valve box fins. Formulas 5.2 and 5.3 describe this energy absorption. Table V-18 gives the calculational parameters. The resulting cask deceleration is:

$$\text{"G"} = \frac{360}{4.8} = 75$$

Table V-18

45° ORIENTATION PARAMETERS

Fin No.	Fin thk,in.	No. of Fins	h, in.	θi deg	δ, in.	δ/h	(h-2t), in.	Y, in.	No. of hinges	θ, rad
5	9/16	1	7.28	29	1.9		6.155	3.49	1	0.461
6	9/16	1	7.45	25	4.2		6.325	1.53	1	0.890
7	3/4	1	7.90	20.8	4.8		6.40	1.18	1	1.022
8	3/4	1	7.16	16.7	4.8		5.66	0.63	1	1.168
9	3/4	1	7.03	12.5	4.8		5.53	0.60	1	1.244
10	9/16	1	6.94	8.3	4.8	0.692			2	4.77
11	9/16	1	6.88	4.2	4.8	0.698			2	4.78
12	9/16	1	6.86	0	4.8	0.70			2	4.80
Struct	1-1/4	4	15.17	5	4.8	0.316			2	3.01

5.5.4.4 90° Orientation Side Drop

In this side drop position, only the four impact fins contact the surface. The relative angle of fins to ground is zero degree, hence each undergoes a double hinge formation. Rearranging equation 5.2 and solving for θ gives a hinge rotation of 3.54 radians. From the fin bending correlation, the following is obtained:

$$\frac{\delta}{h} = 0.42$$

where: δ = deformation
h = fin height
= 7 inches

Therefore: $\delta = (0.42)(7) = 2.94$ inches
and: Deceleration, "G" $= \frac{360}{2.94}$
$= 122.3$

5.5.4.5 135° Orientation Side Drop

In this orientation the four 1-1/4-inch thick structural rings and a portion of the 1-1/4-inch thick partial ring absorbs the cask energy. Each ring undergoes double bending. At the assumed maximum hinge rotation, θ, of 4.72 radians 98.3 percent of the cask kinetic energy is absorbed. In reality the hinge can rotate somewhat more than 4.72 radians where unobstructed and therefore the slight residual kinetic energy (1.7%) will be dissipated in further ring deformation. At 4.72 radians the deceleration distance is:

$\delta/h = 0.71$
$\delta = (0.71)(7.0) = 4.97$ inches

and the deceleration is:

"G" $= \frac{360}{4.97} = 72.4$

5.5.4.6 180° Orientation Side Drop

In this position the four 1-1/4-inch thick structural rings and the full 1-1/4-inch thick partial ring act to absorb the cask energy. Using the rearranged version of equation 5.2, θ is calculated to be 4.32 radians. The deflection and deceleration, using the fin bending correlation for double hinging is:

$\delta/h = 0.60$
$\delta = (0.60)(7.0) = 4.20$ inches

therefore "G" $= \frac{360}{4.2} = 85.7$

5.5.5 Deceleration Summary

Table V-19 summarizes the deceleration values for the two vertical and six side drop orientations. The table also indicates that the cask kinetic energy has been effectively dissipated in each case. The 0° side orientation deceleration, 109 "G" is doubled when evaluating the stress in the valve box structure. The top corner drop deceleration, 56.8 "G" will is doubled when evaluating the closure flange.

Table V-19
30-FOOT DROP DECELERATION
SUMMARY

Orientation	$E_{KE,in-k}$	$E_{ABS,in-k}$	% ERROR*	$\delta_{in.}$	"G"
0° Side	50400	51160	1.5	3.3	109
20° Side	↓	50600	0.4	5.1	70.6
45° Side		50220	-0.36	4.8	75
90° Side		50400	0	2.94	122.3
135° Side		49560	-1.7	4.97	72.4
180° Side		50400	0	4.20	85.7
Top End		50400	0	2.02	178
Bottom End		50400	0	1.54	234
Top Corner		50000	-0.8	6.34	56.8
Bottom Corner		50300	-0.2	5.24	68.7

* Negative Sign Indicates Residual Kinetic Energy.

5.6 30-FOOT DROP - COMPONENT STRESSES

There are several critical components which must be analyzed for structural integrity under certain 30-foot drop loadings. Specifically these are: 1) the closure flange and hardware; 2) the cavity valve boxes; 3) the fuel baskets; and 4) the fuel assemblies.

5.6.1 Cask Closure

The cavity closure consists of stepped 304 stainless steel flanges held together with 32, 1-3/4-8 NC high strength (17-4-PH) studs and nuts. Sealing is accomplished using a Grayloc Seal Ring. The flange configuration is illustrated in Figure V-13.

5.6.1.1 Top End Drop

In the top end drop, the flange is placed in compression along its full circumference. The loading is assumed to equal the body weight times twice the top end deceleration, or:

$$F = (120^{k}) \ (2 \times 178)$$

$$= 42720 \text{ kips}$$

The contact area is bounded by the seal rib i.d. and the flange o.d. This value is as follows:

$$A_c = \frac{\pi}{4} \left[(OD)^2 - (ID)^2 \right]$$

$$= \frac{\pi}{4} \left[(49.5)^2 - (41.0)^2 \right]$$

$$= 604 \text{ in.}^2$$

FIGURE WITHHELD UNDER 10 CFR 2.390

FIGURE V-13. CAVITY CLOSURE

therefore:

$$\sigma c = \frac{F}{A_c}$$

$$= \frac{42720^{k}}{604 \text{ in.}^2}$$

$$= 70.7 \text{ ksi}$$

Dynamic compressive yield of 304 SST = 70 x 1.25 = 87.5 ksi

$$\text{Safety Factor} = \frac{87.5}{70.7} = 1.24$$

5.6.1.2 Corner Drop

In the corner drop the cask is inclined at an angle such that the action line of the center of gravity passes through the lid corner. As illustrated on Figure V-14, this angle is 14.226°. The forces involved are also shown. These forces are derived from the following assumptions:

a. Twice the average deceleration is applied to the cask body weight.

b. The average deceleration is applied to the cask contents.

When the cask impacts there are several forces acting. At the point of contact the fins produce a force equal to:

$$F_R = (2 \times 120 + 20) \text{ "G" kips}$$

$$= 260 \text{ "G" kips}$$

The axial resultant of this force is 252 "G" kips which places the flanges in compression. From this value is subtracted the sum of two times the head weight and one times the contents axial component; or:

FIGURE WITHHELD UNDER 10 CFR 2.390

FIGURE V-14. CORNER DROP LOADS

$$F = \left[252^{k} - (17.7^{k} + 19.38^{k})\right] \quad \text{"G"}$$

To yield a net compressive force on the flange from the drop of:

$$F_{net} = 214.92 \text{ "G" kips}$$

This force is further reduced by subtracting away those non-drop related forces which tend to pry the flanges apart, namely: 1) internal pressure, 264 k; and 2) seating force, 375 k.

There is also a moment acting to rotate the body relative to the head. This moment acts about the flange parting line. Its force term is the vector sum of the transverse components of the impact force and twice the head weight. This moment is as follows:

$$M = (88.425") \ (64.0^{k} - 4.49^{k}) \text{ "G"}$$

$$M = 5260 \text{ "G"}$$

thus the net forces on the flange are:

$$P = 214.92 \text{ "G"} - \left[(0.2 \times \pi \times 20.5^{2}) + 375^{k}\right]$$

$$P = 214.92 \text{ "G"} - 639^{k}$$

$$M = 5260 \text{ "G"}$$

The design approach is to permit localized yielding of the studs and flange as long as those studs in the elastic portion of the flange are of sufficient strength to hold an internal pressure of 400 psig and maintain a tight joint after the drop. The design of the Grayloc bore seal is such that relative axial displacement of the mating flanges, such as would occur should there be localized yielding, will not destroy the ring's ability to retain pressure.

Bolting material is 1-3/4-8 NC, 17-4 PH stainless steel heat treated to 125 ksi yield strength at 200°F. The stress area of each stud is 2.08 square inches. There are 32 studs in the closure.

Flange material is 304 stainless steel having a static compressive yield strength of 70 ksi. Dynamic yield will be approximately 25 percent above this value.

The following is a derivation of the flange and stud stress relationship:

a. Derivation

Figure V-15 shows the basic relationship between components for the cask closure. This forms the analytical model for the flange stress analysis.

Referring to Figure V-15:

σ_1 = yield stress of flange

σ_2 = yield stress of bolts

$$\sigma' = \left(\frac{R_o - \bar{X}}{R_o - \bar{X} - d}\right) \sigma_1$$

$$\sigma'' = \sigma' - \sigma_1 = \left(\frac{d}{R_o - \bar{X} - d}\right) \sigma_1$$

$$\theta = \cos^{-1} (\bar{X}/R_o)$$

$$\phi = \cos^{-1} (\bar{X}/R_1)$$

$$\theta' = \cos^{-1} \left[(R_o - d)/R_o\right]$$

$$\phi' = \cos^{-1} \left[(R_o - d)/R_1\right]$$

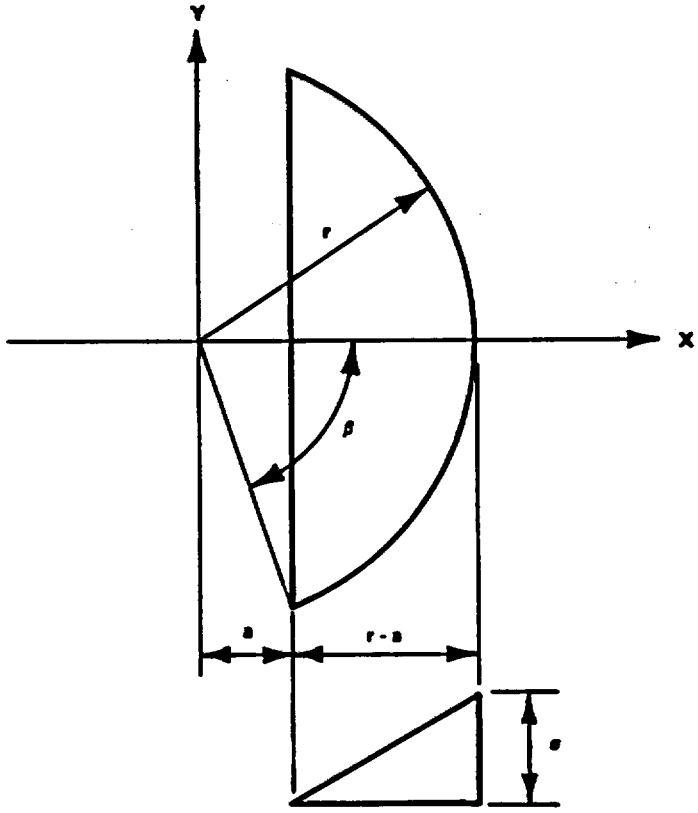

FIGURE V-15. BEARING ON FLANGE

Force and Moment produced by bearing stress on flange (Figure V-15)

$$F = \frac{\sigma r^3}{r-a} (\text{Sin } \beta - 1/3 \text{ Sin}^3 \beta - \beta \text{ Cos } \beta)$$

$$M_y = \frac{\sigma r^4}{r-a} (\beta/4 - 1/4 \text{ Sin } \beta \text{ Cos } \beta - 1/6 \text{ Sin}^3 \beta \text{ Cos } \beta)$$

$$\beta = \text{Cos}^{-1} (a/r)$$

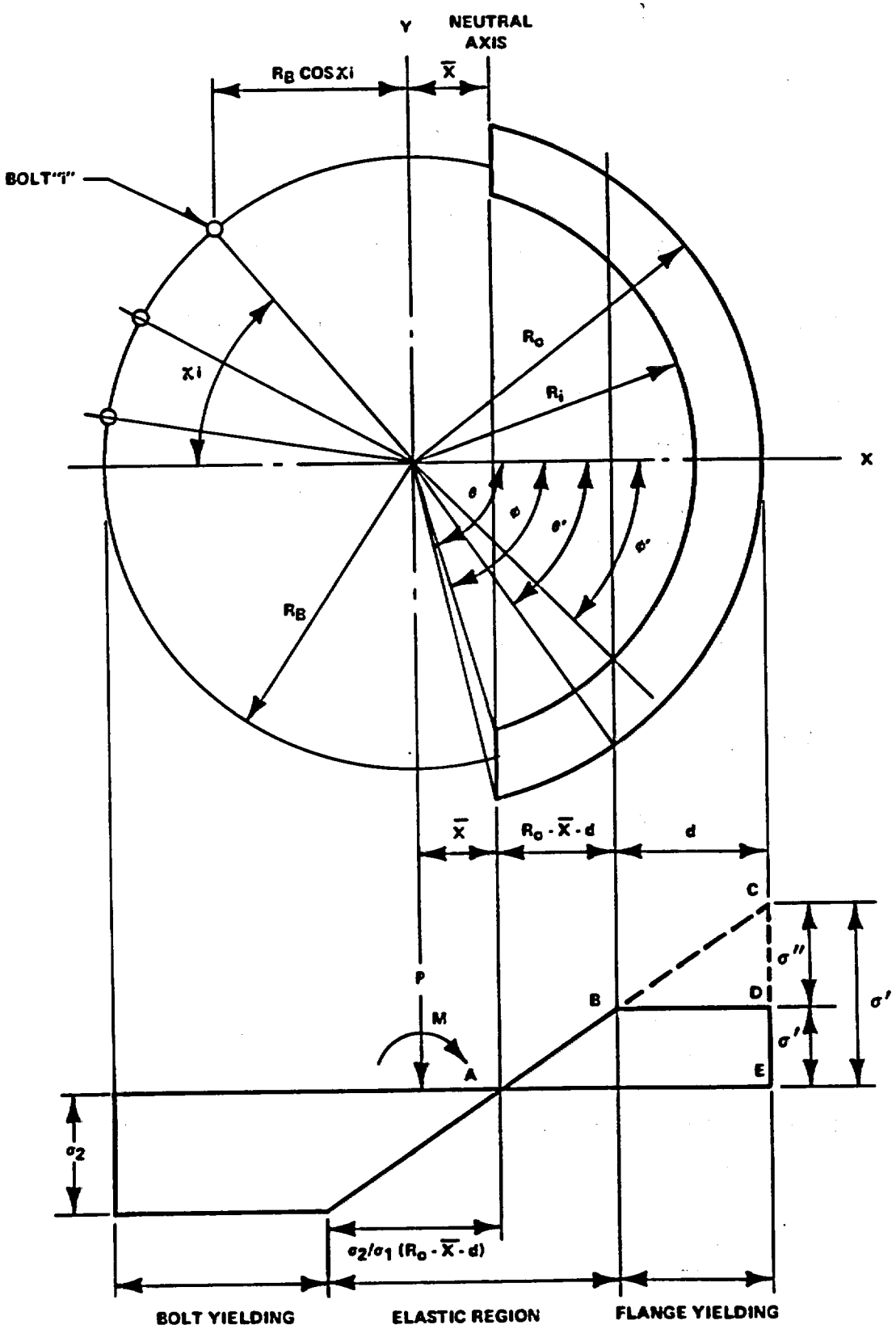

FIGURE V-16. CLOSURE MODEL

Let $d' = R_o - \bar{X} - d$

Noting that $\frac{\sigma'}{R_o - \bar{X}} = \frac{\sigma_1}{d'}$ and that $\frac{\sigma''}{d} = \frac{\sigma_1}{d'}$,

Define

$$F(\beta,r) = \sigma_1 r^3 (\sin\beta - 1/3 \sin^3 \beta - \beta \cos \beta)/d'$$

$$M(\beta,r) = \sigma_1 r^4 (\beta/4 - 1/4 \sin\beta \cos\beta - 1/6 \sin^3\beta \cos\beta)/d'$$

Force and Moment Produced by Bearing Stress Described by Triangle ACE in Figure V-16.

$\underline{-R_o \leq \bar{X} < -R_i}$

$$F_1 = F(\theta, R_o) + \pi \sigma_1 R_i^2 \bar{X}/d'$$
$$M_1 = M(\theta, R_o) - \pi \sigma_1 R_i^4/4d'$$

$\underline{-R_i \leq \bar{X} \leq R_i}$

$$F_1 = F(\theta, R_o) - F(\phi, R_i)$$
$$M_1 = M(\theta, R_o) - M(\phi, R_i)$$

$\underline{R_i < \bar{X} \leq R_o}$

$$F_1 = F(\theta, R_o)$$
$$M_1 = M(\theta, R_o)$$

Force and Moment Produced by Bearing Stress Described by Triangle BCD in Figure V-16.

$\underline{-R_o \leq R_o - d < -R_i}$

$$F_2 = F(\theta', R_o) + \pi \sigma_1 R_i^2 (R_o - d)/d'$$
$$M_2 = M(\theta', R_o) - \pi \sigma_1 R_i^4/4\, d'$$

$-R_i \leq R_o - d \leq R_i$

$$F_2 = F(\theta', R_o) - F(\phi', R_i)$$
$$M_2 = M(\theta', R_o) - M(\phi', R_i)$$

$R_i < R_o - d \leq R_o$

$$F_2 = F(\theta', R_o)$$
$$M_2 = M(\theta', R_o)$$

Net force and moment produced by bearing stresses:

$$F_c = F_1 - F_2$$
$$M_c = M_1 - M_2$$

If flange has fully yielded (i.e., $d = R_o - \bar{X}$), the following equations apply:

Define

$$F'(\beta,r) = \sigma_1 r^2 (\beta - \sin\beta \cos\beta)$$
$$M'(\beta,r) = 2\sigma_1 r^3 \sin^3\beta/3$$

$-R_o \leq \bar{X} \leq R_i$

$$F_c = F'(\theta, R_o) - \pi \sigma_1 R_i^2$$
$$M_c = M'(\theta, R_o)$$

$-R_i \leq \bar{X} \leq R_i$

$$F_c = F'(\theta, R_o) - F'(\phi, R_i)$$
$$M_c = M'(\theta, R_o) - M'(\phi, R_i)$$

$R_i < \bar{X} \leq R_o$

$F_c = F'(\theta, R_o)$
$M_c = M'(\theta, R_o)$

Forces and moments produced by stresses in bolts

Let A_i = Area of Bolt "i"
m = Number of Stressed Bolts

If $\bar{X} + R_B \cos \alpha_i < 0$, no stress exists in bolt

Define $d'' = \frac{\sigma_2}{\sigma_1} (R_o - \bar{X} - d) = \frac{\sigma_2}{\sigma_1} d'$

Considering bolts for which $\bar{X} + R_B \cos \alpha_i \geq 0$.
If either $d' = 0$ (section is fully yielded), or $\bar{X} + R_B \cos X_i \geq d''$, the following equation's apply:

$F_i = \sigma_2 A_i$
$M_i = F_i R_B \cos \alpha_i$

For all other bolts
$F_i = (\bar{X} + R_B \cos \alpha_i) \sigma_2 A_i / d''$
$M_i = F_i R_B \cos \alpha_i$

Summing up the forces and moments on all stressed bolts:

$$F_T = \sum_{i=1}^{m} M_i$$

$$M_T = \sum_{i=1}^{m} M_i$$

Equilibrium Equations:

1) $M = M_C + M_T$
2) $P = F_C - F_T$

These equations can be solved by a trial-and-error process to determine the location of the neutral axis and the extent of flange and bolt yielding.

b. Results

Figure V-17 shows the stress, load and moment distribution for the corner drop case.

In this configuration a small portion of the flange has yielded, however none of the studs reach their yield stress. There are only 6 studs in the yielded flange area; these are assumed to lose their holding capability. The remaining 26 studs are in the elastic portion of the flange and continue to exert sufficient force to keep the closure sealed. The studs must be capable of seating the seal ring and resisting the post accident pressure of 400 psig.

$$F = 375^{k} + 528^{k}$$
$$= 903^{k}$$

$$A_s = (26 \text{ studs})\ (2.08 \text{ in}^2/\text{stud})$$
$$= 54 \text{ in}^2$$

$$\sigma_t = \frac{F}{A} = \frac{903^{k}}{54}$$

$$= 16.7 \text{ ksi}$$

$$SF = \frac{125 \text{ ksi}}{16.7 \text{ ksi}} = 7.5$$

Cask closure integrity will remain following the 30 foot corner drop.

FIGURE WITHHELD UNDER 10 CFR 2.390

FIGURE V-17. FLANGE AND BOLT ANALYSIS FOR 30" CORNER DROP

5.6.2 Cavity Valve Box

As the energy absorbing members deform while dissipating the cask kinetic energy, the valve box fins impart a force to the valve box structure (lid and sides). These members must be examined for integrity.

5.6.2.1 Valve Box Lid

The 0° drop places the maximum load on the valve box lid. The 0° average deceleration will be assumed increased by a factor of two due to its close proximity to the impact point.

$$F = \frac{2 \times E_{Fin}}{\delta_{Fin}}$$

$$= \frac{2 \times 55 \times 14 \times 0.5625^2 \times \theta_{Fin}}{\delta_{Fin}} \qquad \text{(from equ. 5.2)}$$

$$= \frac{488\ \theta_{Fin}}{\delta_{Fin}}$$

Table V-20 gives the forces for each of the lid fins. Note the lid symmetry.

Table V-20

LID FIN FORCES

FIN NUMBER	θ_{1rad}	$\delta_{1in.}$	F_{kips}
1	3.78	3.3	560
2	3.77	3.3	558
3	3.76	3.3	556
4	0.916	3.3	135.6
5	0.853	3.3	126
6	0.791	3.3	117

From Table V-20:

$0.5\ F_1 + F_2 + F_3 = 1394k$

$F_4 + F_5 + F_6 = 378.6k$

Distribute the 1394k and 378.6k loads as uniform loads W_1 and W_2 on the valve box cover plate illustrated in Figure V-18.

$$W_1 = \frac{378.6}{6.73 \times 12.5} = 4.5 \text{ ksi}$$

$$W_2 = \frac{1394}{5.77 \times 12.5} = 19.32 \text{ ksi}$$

(Assuming: $A_{W_2} = 12.5 \times 32.75 \tan 10°$)

Rotation of yield lines:

$$\theta_1 = \frac{1}{(12.5-a)}$$

$$\theta_2 = \frac{1}{b} + \frac{1}{c}$$

$$\theta_3 = \frac{1}{d} + \frac{1}{e}$$

FIGURE WITHHELD UNDER 10 CFR 2.390

FIGURE V-18. VALVE BOX LID

where:

$$b = \frac{6.25\ \sqrt{6.25^2 + (12.5-a)^2}}{(12.5-a)}$$

$$c = \frac{(12.5-a)\ \sqrt{6.25^2 - (12.5-a)^2}}{6.25}$$

$$d = \frac{a\ \sqrt{6.25^2 + a^2}}{6.25}$$

$$e = \frac{6.25\ \sqrt{6.25^2 + a^2}}{a}$$

Length of yield lines:

$$L_1 = 12.5 \text{ in.}$$

$$L_2 = \sqrt{6.25^2 + (12.5-a)^2}$$

$$L_3 = \sqrt{6.25^2 + a^2}$$

Now:

m = yield moment/unit length

$$= \sigma_Y \frac{t^2}{4}$$

Internal work, W_i

$$W_i = M\ (L_1\theta_1 + 2L_2\theta_2 + 2L_3\theta_3)$$

Substituting:

$$W_i = M\ \left(\frac{25}{12.5-a} + \frac{12.5}{a} + 4\right)$$

External work $(a \leq 6.73)$

$$W_e = \frac{6.25}{3} W_1 a + 2 \left[\frac{6.25^2}{3} W_1 + (W_2-W_1) \frac{5.77}{2} \times \frac{5.77 \times 6.25}{12.5-a} \times \frac{5.77 \times 6.25}{3 \times 6.25 \times (12.5-a)} \right] + \frac{6.25\, W_2 \times (12.5-a)}{3} - (W_2-W_1) \times (12.5-a-5.77) \times \left(6.25 - \frac{5.77 \times 6.25}{12.5-a}\right) \times \left(5.77 + \frac{12.5-a-5.77}{3}\right) \Big/ (12.5-a)$$

External work $(a \geq 6.73)$

$$W_e = \frac{6.25}{3} W_1 a + (W_2-W_1) \times (a-6.73) \times \left(6.25 - \frac{6.73 \times 6.25}{a}\right) \times \left(6.73 + \frac{a-6.73}{3}\right) \Big/ a + 2 \left[\frac{6.25^2}{3} W_2 - (W_2-W_1) \times \frac{6.73}{2} \times \left(\frac{6.73 \times 6.25}{a}\right) \times \left(\frac{6.73 \times 6.25}{3 \times a \times 6.25}\right) \right] + \frac{6.25}{3} W_2 (12.5-a)$$

Applying the virtual work theorem:

$$W_i = W_e$$

Solving by trial and error for the value of "a" which maximizes "m" the following is obtained:

$$a = 6.9"$$
$$m = 58 \text{ in.-k/in.}$$

For $\sigma_y = 58.4$ ksi and t=2 in.

$$m = 58.4 \times \frac{2^2}{4} = 58.4 \text{ in.-k/in.}$$

$$\therefore SF = \frac{58.4}{58} = 1.01$$

5.6.2.2 Valve Box Side Walls

For 0° drop attitude:

$$P_1 = P_2 = 452k$$
$$P_3 = 1352k$$

This drop is the worst loading for walls 1, 2 and 3.

$$\sigma_{1,2} = \frac{452}{12.5x1} = 36.2 \text{ ksi}$$

$$k\ell/r = \frac{2x7.5}{0.289} = 51.9$$

$$\sigma_u = 58 \text{ ksi}$$

$$SF = \frac{58}{36.2} = 1.6$$

$$\sigma_3 = \frac{1352}{2.0x12.5} = 54.2 \text{ ksi}$$

$$k\ell/r = \frac{2x7.5}{0.578} = 25.9$$

$$\sigma_{cr} = 70 \text{ ksi}$$

since $\sigma_{cr} > \sigma_{yp}$ use 58.0 ksi

$$SF = \frac{58.0}{54.2} = 1.08$$

5.6.2.3 Valve Box Lid Corner

The following analysis examines the box overturning and the lid bolting shear stresses from the 20° corner drop. Table V-21 lists the individual fin forces.

Table V-21

CORNER DROP FIN FORCES

FIN No.	θ_1 rad	δ_1 in.	F_1 kips
2	0.216	0.5	210.6
3	0.537	1.5	175.0
4	3.27	2.6	614.0
5	3.89	3.6	528.0
6	4.56	4.8	464.0

The total force is 1991.6 kips. The horizontal component of this force is:

$$F_H = 1991.6 \sin 21.07^\circ = 716 \text{ kips}$$

The lid is held in place by the following:

4 - 1"-8UNC socket head cap screws
6 - 1½" ϕ down pins

Material of both items is 17-4 PH stainless steel heat treated to a yield strength of 145 ksi minimum.

$$\text{Area} = 4 \times 0.551 + 6 \times 1.227 = 9.567 \text{ in.}^2$$

$$\tau = \frac{F}{A} = \frac{716}{9.567} = 74.8 \text{ ksi}$$

$$SF = \frac{145 \times 0.577}{74.8} = 1.12$$

Assume that the fin forces are transmitted to the cask outer shell by the 304 SST side castings only (conservative). Figure V-19 and Table V-22 show the forces involved.

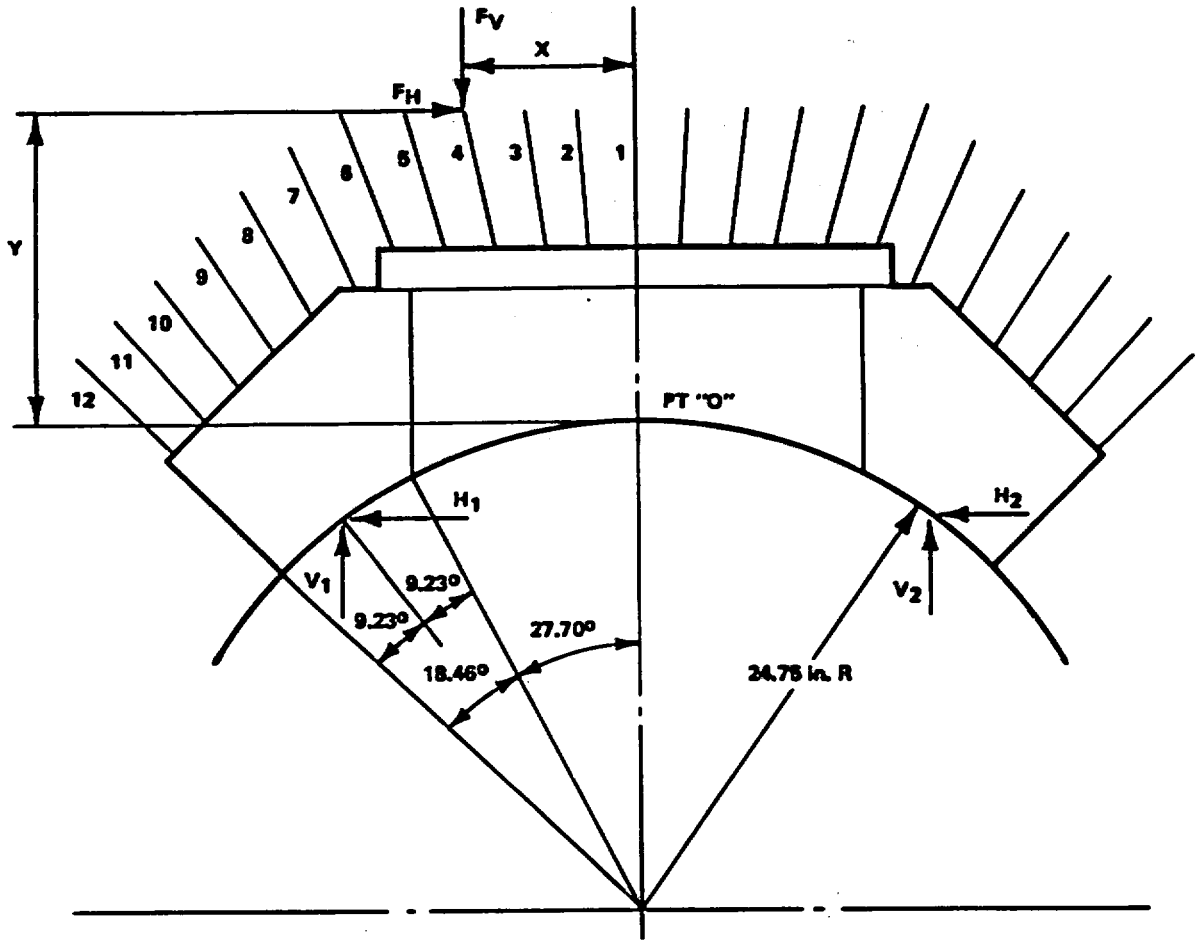

FIGURE V-19. VALVE BOX CORNER DROP

Table V-22

SIDE BLOCK FORCES

FIN No.	X (in.)	Y (in.)	F_H (kips)	F_V (kips)	+ $M_{"0"}$ (in.-kip)
2	2.84	16.0	75.8	196.6	654
3	5.73	16.0	62.9	163.2	72
4	8.66	16.0	220.8	573.0	-1424
5	11.70	16.0	190.0	492.6	-2720
6	14.83	16.0	167.0	433.0	-3748
7	17.48	14.25	308.0	797.0	-9550
8	19.78	11.90	384.0	996.0	-15152
9	22.0	9.70	122.8	318.4	-5810
10	24.1	7.65	90.6	235.0	-4968
Σ			1621.9	4204.8	-42646

Assume H_2 = 1/2 Σ horizontal forces on lid = 358k

H_1 = H_2 + Σ horizontal forces on block = 358 + 906 = 1264k

$\Sigma F_V = V_1 + V_2$

or, $V_1 + V_2 = 4205k$

$\Sigma M_o = 0$

or, $1264\ (4.95) + 14.85\ V_1 + 358\ (4.95) - 14.85\ V_2 - 42646 = 0$

Solving:

$V_1 - V_2 = 2330k$

$V_1 = 3267k$

$V_1 = 938k$

Forces normal to shell at point 1:

= 3267 x 0.799 + 1264 x 0.601 = 3372k

Forces tangential

= 3267 x 0.601 - 1264 x 0.799 = 954k

Arc length on block

= 24.75 x 0.322 = 7.97 in.

Minimum weld, Box-to-shell:

$A_W = 2\ (14 \times 7.97 - 10 \times 3.97) = 143.6\ in.^2$

Design weld area not including divider plate:

$A_D = [(8.25 \times 14.625) - (12.625 \times 5.25) + 2 \times 11.98 \times 1] \times 2$
$= 156.67\ in.^2$

$SF = \frac{156.67}{143.6} = 1.09$

5.6.2.4 Conclusion

The valve box lid and side structures have been examined under both the 0° and corner drop (20°) orientations. The calculations show that the forces involved are distributed such that the box retains its integrity (all SF > 1.0) and thereby protects the contents.

5.6.3 Fuel Bundle Support Structure - 30-Foot Drop

The IF-300 shipping cask is designed to accommodate either BWR or PWR fuel bundles through the use of interchangeable support structures known as fuel baskets.

The 18 bundle BWR basket (Figure V-20) and the 7 bundle PWR basket (Figure V-21) consist of a series of square, thin walled channels running the length of the cask cavity. Each channel holds a single

FIGURE WITHHELD UNDER 10 CFR 2.390

FIGURE V-20. BWR 18 CELL FUEL BASKET

FIGURE WITHHELD UNDER 10 CFR 2.390

FIGURE V-21. PWR 7 CELL FUEL BASKET

fuel bundle and passes through nine circular spacer disks and a top plate. The disks are positioned along the structure length to support the fuel bundle weight laterally and are tied together axially with four 2-1/4-inch diameter 216 stainless settl bars. Each channel is slotted to permit free circulation of the cask coolant. All basket components are either 216 or 304 stainless steel, except for the internal shielding added to the top of BWR baskets as described below.

Criticality control is provided by 1/2-inch diameter by 0.020-inch wall thickness, boron carbide filled, stainless steel tubes lining the interior gaps between the fuel channels. These elements are similar to the absorber rods used in GE BWR control rod blades and are fabricated to the same specifications.

The BWR and PWR fuel basket configurations are analyzed for impact resulting from a 30-foot drop of the cask onto a flat, unyielding surface. Five cask orientations are considered: three horizontal (0 degrees, 45 degrees, and 90 degrees) and two vertical (top and bottom end). Corner drop orientations are not considered because the decelerations associated with corner drops are significantly less than for other orientations (see Table V-19, page 5-48).

The forces that are applied to the fuel baskets are based on cask decelerations which were determined for the internal shielding analysis of Appendix V-1. These decelerations, and the corresponding orientation of the cask upon impact, are shown in Figure V-22.

The BWR horizontal and vertical drop analyses are performed first, followed by the PWR analyses. All calculations assume a temperature of 200°F.

Cask No.	Orientation	Peak G's	Plateau G's
1	0 degrees	204	91
2	45 degrees	153	68
3	90 degrees	133	59
4	top end	280	124
5	bottom end	287	127

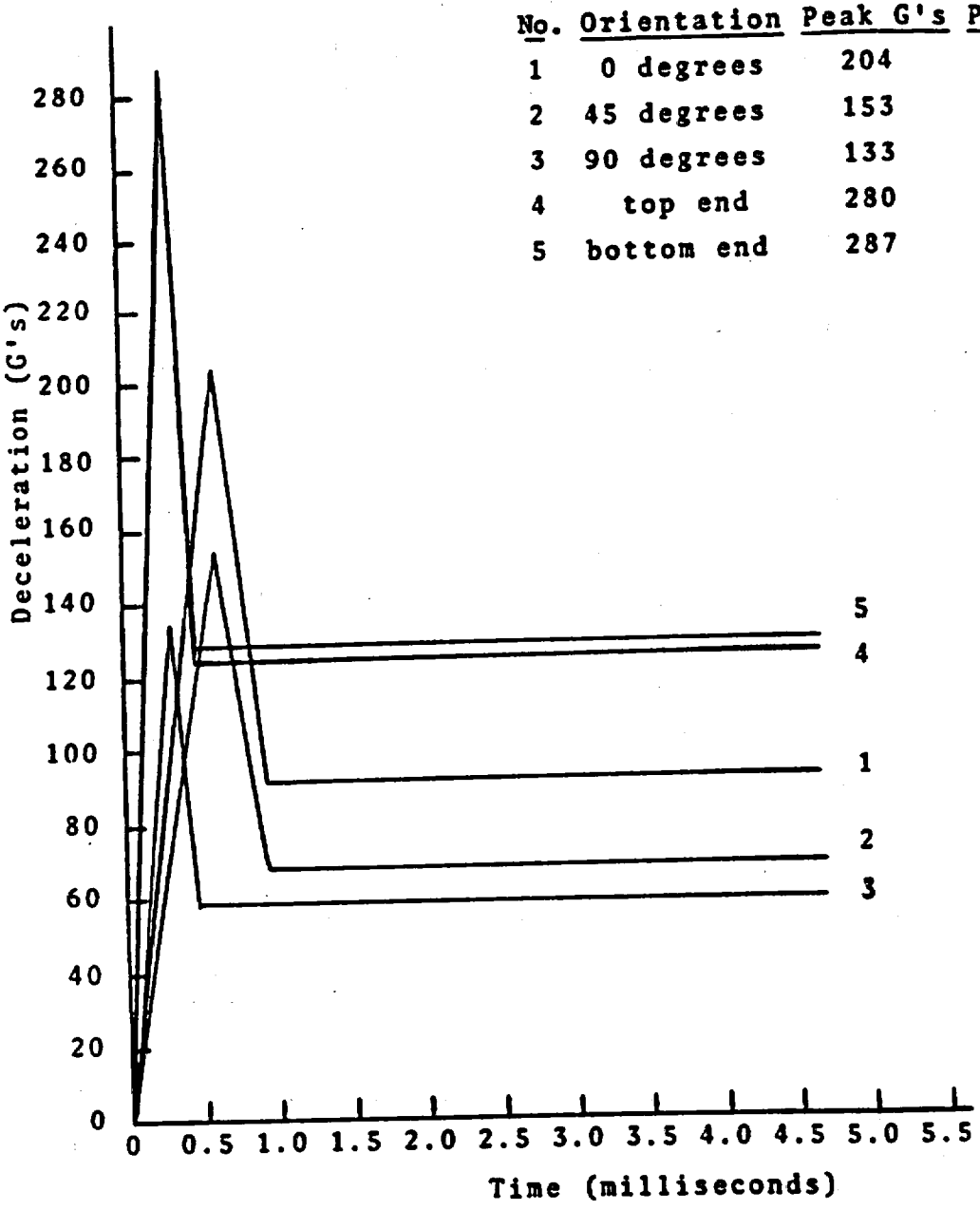

FIGURE V-22. CASK DECELERATION VS. TIME*

*Based on Figure 5 and Table 7 of Appendix V-1.

5.6.3.1 BWR Basket - (Figure V-20)

a. Internal Shielding Safety Analysis Report

In 1977 a design change was made to the BWR baskets to incorporate gamma shielding structures at the upper end of the basket. A safety analysis report (NEDO-21796, "BWR Basket Internal Shielding Safety Analysis Report") was written and submitted for NRC review in January 1978. This safety analysis report (NEDO-21796) is self-contained in that it addresses structural, shielding, heat transfer, criticality, fabrication and quality assurance. NEDO-21796 is reproduced in its entirety as Appendix V-1 of this CSAR.

b. BWR Basket Horizontal Drop Analysis

The BWR basket is designed such that the axially positioned spacer disks approximately coincide with the fuel rod spacers of the fuel bundles. The weight of the fuel bundles is transmitted directly to the spacer disks, as the channels are not load bearing members. The channels serve only as guides for the fuel bundles as they are lowered into the cask. The spacer disk material is 216 stainless steel.

The static load on each spacer disk, and the top plate, is determined by applying concentrated and distributed loads representing the fuel basket and fuel bundle weights to a finite beam computer model of the fuel basket. Reaction forces are then calculated by the computer at the support points (spacer disks and top plate) corresponding to the fuel basket and fuel bundle weights transmitted through each support point under static conditions. The maximum calculated static weight for a BWR spacer disk is 2365 pounds, which occurs at the second to bottom spacer disk. The static load at other fuel basket support points does not exceed 2070 pounds. Figure V-23 shows the axial position of the spacer disks and the top plate.

FIGURE WITHHELD UNDER 10 CFR 2.390

FIGURE V-23. BWR SPACER DISK & TIE ROD

The decelerations shown in Figure V-22 are based on rigid body motion assumptions. Since the axial position of the spacer disk with the maximum static load approximately coincides with the lower set of structural rings, the decelerations to be applied to that spacer disk must be increased by 5% to account for the "effective" mass of the cask being slightly less than that of a perfectly rigit body. This same factor was used in, and derived for, the internal shielding analysis described above. Decelerations at the middle of the cask are less than those which occur at the structural rings due to the greater relative displacement of the cask center before rebound.

i. Bearing Stresses

For bearing stress calculations, the stress distribution between the spacer disk and cask cavity wall is ellipsoidal in shape, as shown in Figure V-24. The contact length and resulting stress are calculated with the following equations:

$$b = 2.15 \sqrt{PD_1D_2/E(D_1 - D_2)}$$

$$S_{max} = 0.591 \sqrt{PE(E_1 - D_2)/D_1D_2}$$

where:

b = length of rectangular contact patch

S_{max} = maximum bearing stress

P = maximum applied load

E = modulus of elasticity

D_1 = cask cavity inside diameter

D_2 = fuel basket outside diameter

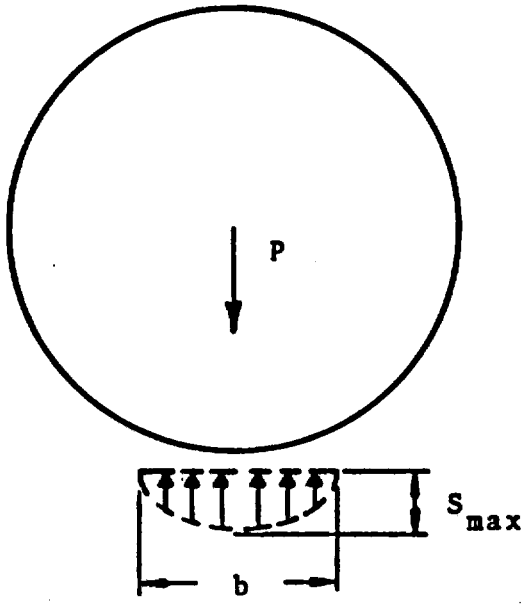

FIGURE V-24. CONTACT PRESSURE DISTRIBUTION

The maximum applied load for bearing stress calculations is determined as follows:

$$P = (2365) \times (204) \times (1.05) = 506.6 \times 10^3 \text{ lbs}$$

where:

2365 lbs is the maximum spacer disk load

204 G's is the maximum horizontal cask deceleration

1.05 is the cask amplification factor

Using this load, the values of b and S_{max} are 25.6-inches and 25.9 ksi, respectively. Therefore, the factor of safety for the most limiting spacer disk, under bearing stress from the cask cavity wall, is 2.24 based on a 200°F yield strength of 58.4 ksi (Table V-3).

ii. Spacer Disk Internal Stresses

Appendix V-3 documents a static analysis of the BWR spacer disk for three horizontal drop orientations: 0 degrees, 45 degrees, and 90 degrees, as depicted in Figure V-20. From the static analysis it was determined that the 0 degree drop case was the most limiting condition. The following discussion summarizes a dynamic analysis of the 0 degree drop case which is also documented in Appendix V-3.

The 0 degree drop analysis uses the ANSYS finite element model shown in Figure V-25.* Uniformly distributed loads based on the 0 degree drop deceleration vs. time history from Figure V-22 are applied to each fuel cell. The sum of these loads is determined by multiplying the maximum spacer disk static load (2365 lbs) by the 0 degree drop decelerations of Figure V-22, and increasing the resulting load by 1.05 to account for variations in the cask behavior from perfectly rigid body motion. The total applied load is given in Table V-23.

Table V-23. Peak and Plateau Spacer Disk Loads

Cask Orientation	Peak Load	Plateau Load
0 degrees	506.0 kips	226.0 kips

*The interface between the spacer disk and the cask cavity wall is assumed to be at the bottom of the model.

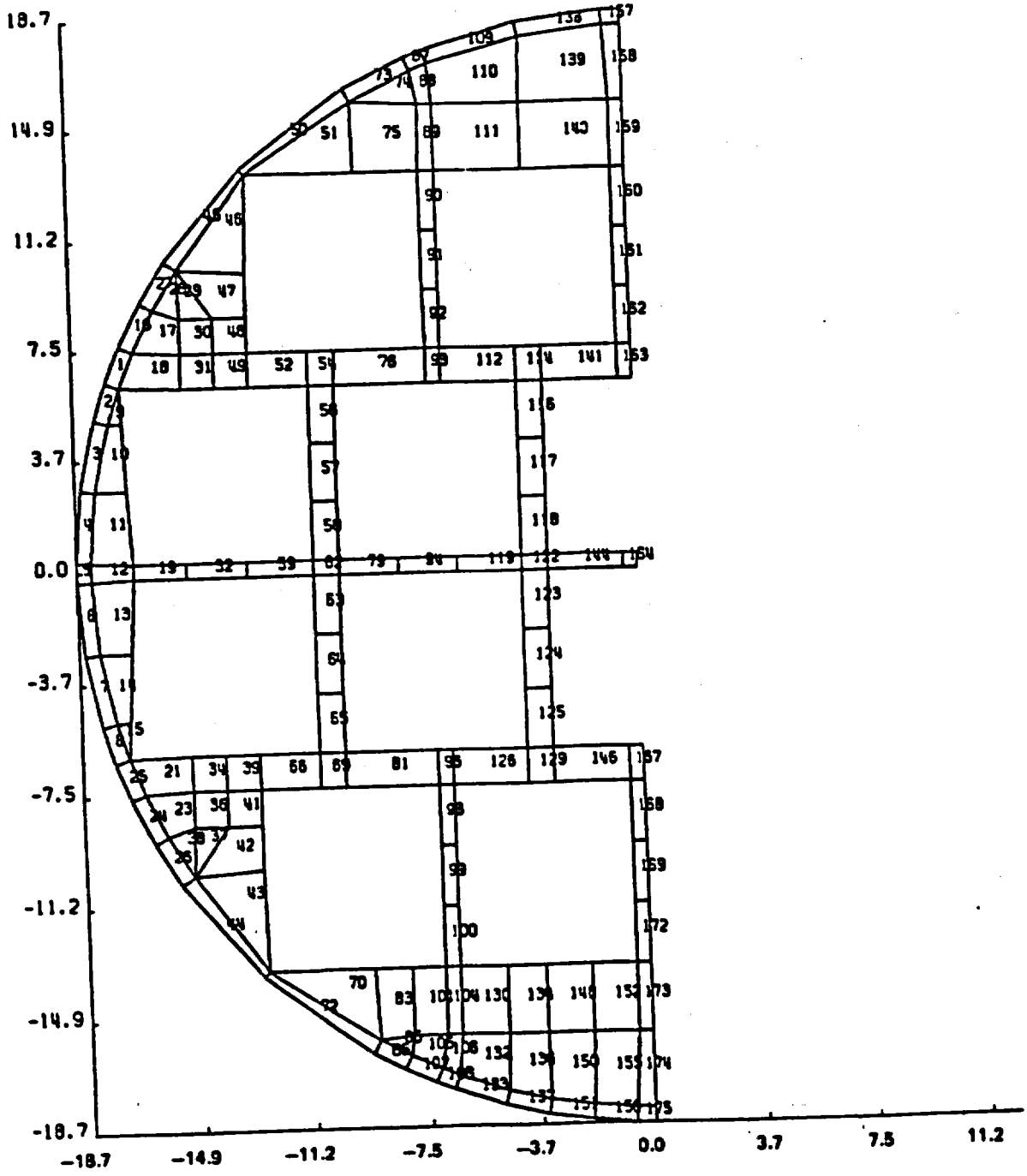

FIGURE V-25. ANSYS FINITE ELEMENT MODEL OF SPACER DISK FOR 0 DEGREE DYNAMIC ANALYSIS

The plateau load is maintained for approximately 14 milliseconds, after which the energy of the initial impact has been absorbed by the cask.

In order to correctly model the interface between the spacer disk and the cask cavity wall, gap elements are used at the perimeter of the ANSYS spacer disk model. As the load applied to the spacer disk increases, the gaps adjacent to the initial contact area start to close, thereby causing a redistribution of the reaction forces which occur at the spacer disk perimeter.

The results of this analysis indicate yielding of elements 96 and 167 only. These elements develop maximum equivalent strains of 0.543 and 0.243 percent, respectively, with maximum effective stresses of less than 60 ksi for both elements. For members potentially subject to buckling, peak compressive stresses occur at elements 98 (23.9 ksi) and 172 (41.5 ksi).

To determine the critical buckling stress for these members, a static buckling analysis of their geometries was done using the finite element computer program ADINA* and pinned-pinned end conditions. The critical buckling stresses thereby determined (45 ksi for element 98 and 52 ksi for element 172) are greater than the predicted compressive stresses by 96 percent and 25 percent respectively, so that buckling of these members is not predicted. Several conservative assumptions provide greater safety than indicated by the calculated margin. These are:

*ADINA is a general purpose finite element computer program which is particularly well suited to large displacement nonlinear problems. It was developed by K.J. Bathe and E.L. Wilson. Publications by the program developers and others were reviewed and the applicability of ADINA to dynamic buckling problems affirmed. (Ref. 25, 26, 27, 28)

- The increase in yield strength that is normally associated with high strain rates is ignored. The dynamic critical buckling is estimated to be at least twice as high as the static critical buckling stress if a 7 ksi increase in yield strength per decade of strain rate from 10^{-5}-in/in/sec to 10^{2}-in/in/sec is assumed.

- The maximum spacer disk load used (2365 lb) is at least 14 percent higher than the load for any other spacer disk.

- The strength of the poison rod header bar assemblies is not taken into account.

- The cell spacer depth normal to the spacer disk plane is assumed to be 4-inches. In reality there is a 7-inch depth of solid material before the circulation vents are encountered.

- The energy absorption capabilities of the cell assemblies, fuel rods and fuel rod spacers are ignored.

- The critical buckling stresses are obtained assuming both cell spacers and disk ligaments have pinned ends. In reality the end conditions are closer to being fixed.

- The total weight of the spacer disk and its associated components (fuel rods, poison rods, header bars, cell assemblies, etc.) is used to calculate the pressure applied to simulate the load. In reality only the weight of the fuel rods and the cell assemblies is applied to the inside surface of the spacer disk cells. This results in an overestimate of the load applied to the cells.

- The post-buckling capabilities that would resist collapse if the buckling point were encountered are not accounted for.

Data supporting additional margin is reported in Appendix V-1. The results of impact tests on fins having slenderness and aspect ratios similar to those of the cell spacers and disk ligaments show the dynamic critical buckling stress to be significantly higher than the static critical buckling stress.

Since only two elements of the spacer disk model exceed their yield strength, no significant deformation is predicted in the 0 degree drop. And since the 0 degree drop case is the most limiting horizontal drop orientation, cask drops in other orientations would result in lower stresses and deformations than those described above.

c. BWR Basket Vertical Drop Analysis

i. Tie Rod Buckling Analysis

In order to provide a means of axial location for the spacer disks, as well as resistance to axial loads, each fuel basket has four 2-1/4-inch diameter 216 stainless steel bars (tie rods) running full length. These bars extend from the bottom of the cask cavity to the closure head when the fuel basket is installed in the cask. Figure V-23 shows the basket spacer disk and tie rod arrangement for the BWR configuration.

Each circular spacer disk is welded to the four tie rods as shown in Section B-B of Figure V-23. The end clearance between the closure head and the tie rods is sized such that there is no interference due to thermal expansion under any normal or accident condition.

The tie rods are analyzed for dynamic buckling with an ADINA finite element computer model of one tie rod. The model, shown in Figure V-26, uses 23 elements over a span of 22.75-inches (the maximum) and conservatively assumes that the tie rod is pinned at both ends at the location of the spacer disks. The bi-linear stress-strain

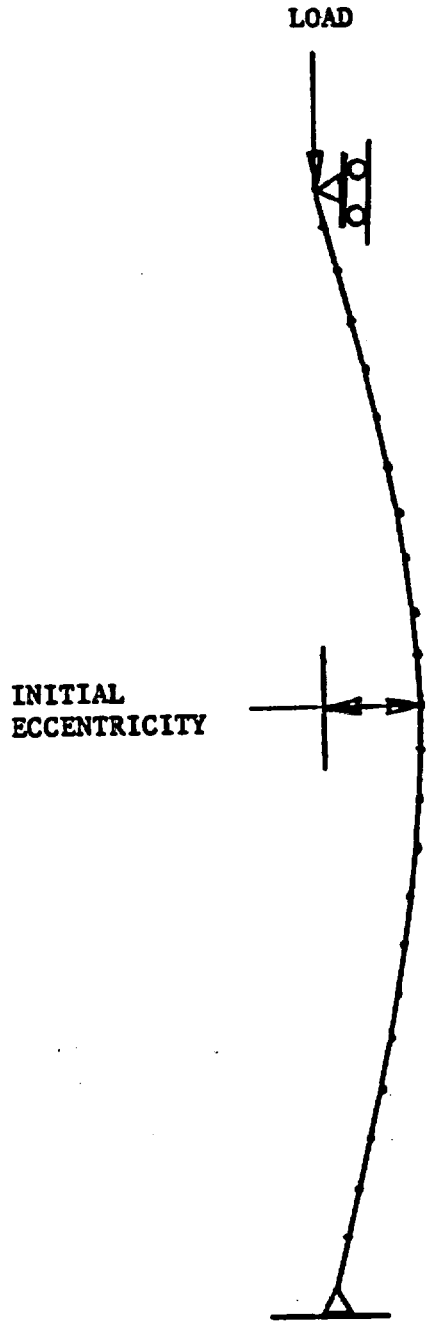

FIGURE V-26. ADINA FINITE ELEMENT TIE ROD MODEL

curves used to represent the tie rod mechanical properties have an elastic modulus of 26.2×10^6 psi and a tangent modulus of 2.9×10^5 psi. A yield strength of 58.4 ksi (200°F) or 65 ksi (room temperature) is used. The criteria for showing that the tie rods do not buckle is that the lateral deflections resulting from the design basis load remain stable over the time required for the cask's momentum to be dissipated.

The peak and plateau forces applied to the top of a single tie rod are determined by multiplying the total fuel basket static weight of 5675 lbs times the peak and plateau decelerations shown in Figure V-22 for a bottom end drop, then dividing by 4. These forces are shown in Table V-24.

Table V-24. Peak and Plateau Tie Rod Forces

Peak Force	= 407.2 kips
Plateau Force	= 180.2 kips

In this analysis, no multiplier is required to account for variations from perfect rigid body motion because the cask bottom head and fins form an extremely rigid structure. In addition, the tie rods are located at the periphery of the cask cavity so that the fuel basket is insensitive to motion of the cask bottom head, should it occur. These features are depicted in Figure V-27.

In addition to the initial conditions described above, the tie rod analysis includes an initial eccentricity of 0.030-inch. This eccentricity includes manufacturing tolerances plus the effect created (momentarily) by the inertia of the spacer disk imparting a bending moment to the tie rods. The latter effect was conservatively calculated to be 0.022-inch based on a statically applied deceleration of 287 G's and a summation of moments about axes through the tie rods.

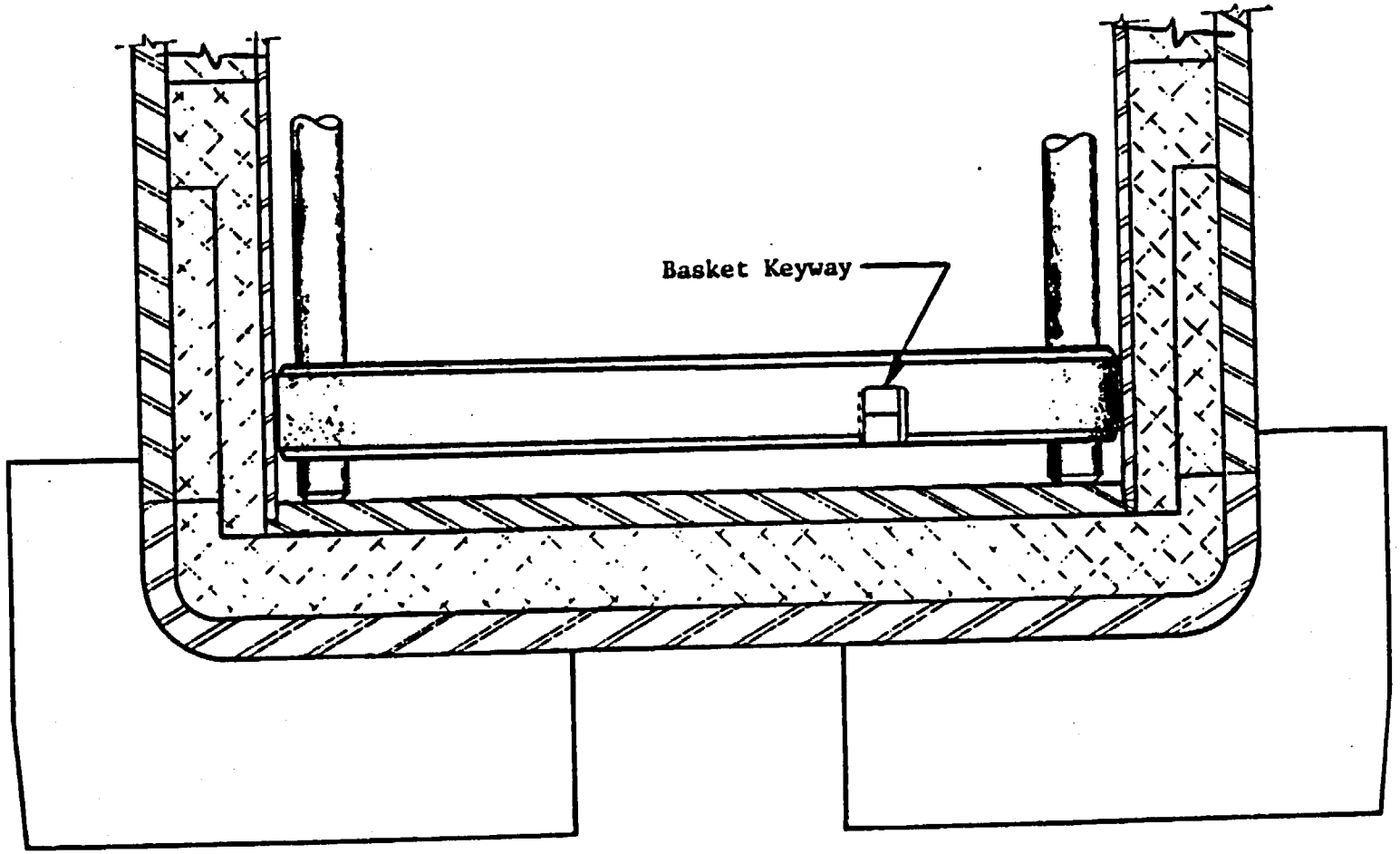

FIGURE V-27. RELATIONSHIP OF FUEL BASKET TIE RODS TO CASK BOTTOM HEAD

Lateral Deflections. Figure V-28 shows lateral deflections versus time at the tie rod midspan for the nominal design basis case described above (Case 4) and four other cases (1, 2, 3 and 5). From the principle of impulse and momentum, the momentum of the cask is fully dissipated 10.1 milliseconds after impact for a vertical bottom end drop. Cases 1 and 3 were run for 7.5 milliseconds, Cases 2 and 5 were run for 10.0 milliseconds, and Case 4 was run for 15.0 milliseconds, with the plateau load ramped down to zero between 10.0 and 19.0 milliseconds.

All five cases show the same oscillating pattern with the peak lateral deflections remaining constant with succeeding cycles. A peak lateral deflection of 54 mils occurs for the nominal case, while the other cases show the effect of various changes in the initial conditions. A comparison of the nominal case with the others shows a relatively high sensitivity to changes in initial eccentricity and applied load, and a relatively low sensitivity to changes in the assumed yield strength of the tie rod material.

Not shown in Figure V-28 is the reduction in displacements and stresses that occurs in the nominal case as the applied load is cecreased after 10.0 milliseconds. Similar reductions are expected from the other four cases after 10.0 milliseconds.

Two additional cases were run which show the effect of increasing the applied load beyond 120 percent of the nominal design basis value. Figure V-29 shows lateral deflections versus time at the tie rod midspan for Cases 6 and 7 (123 and 130 percent of nominal load, respectively) and Cases 4 and 5 (100 and 120 percent of nominal load, respectively). Cases 6 and 7 show large and uncontrolled lateral deflections as are expected for the tie rod when the critical buckling load is reached.

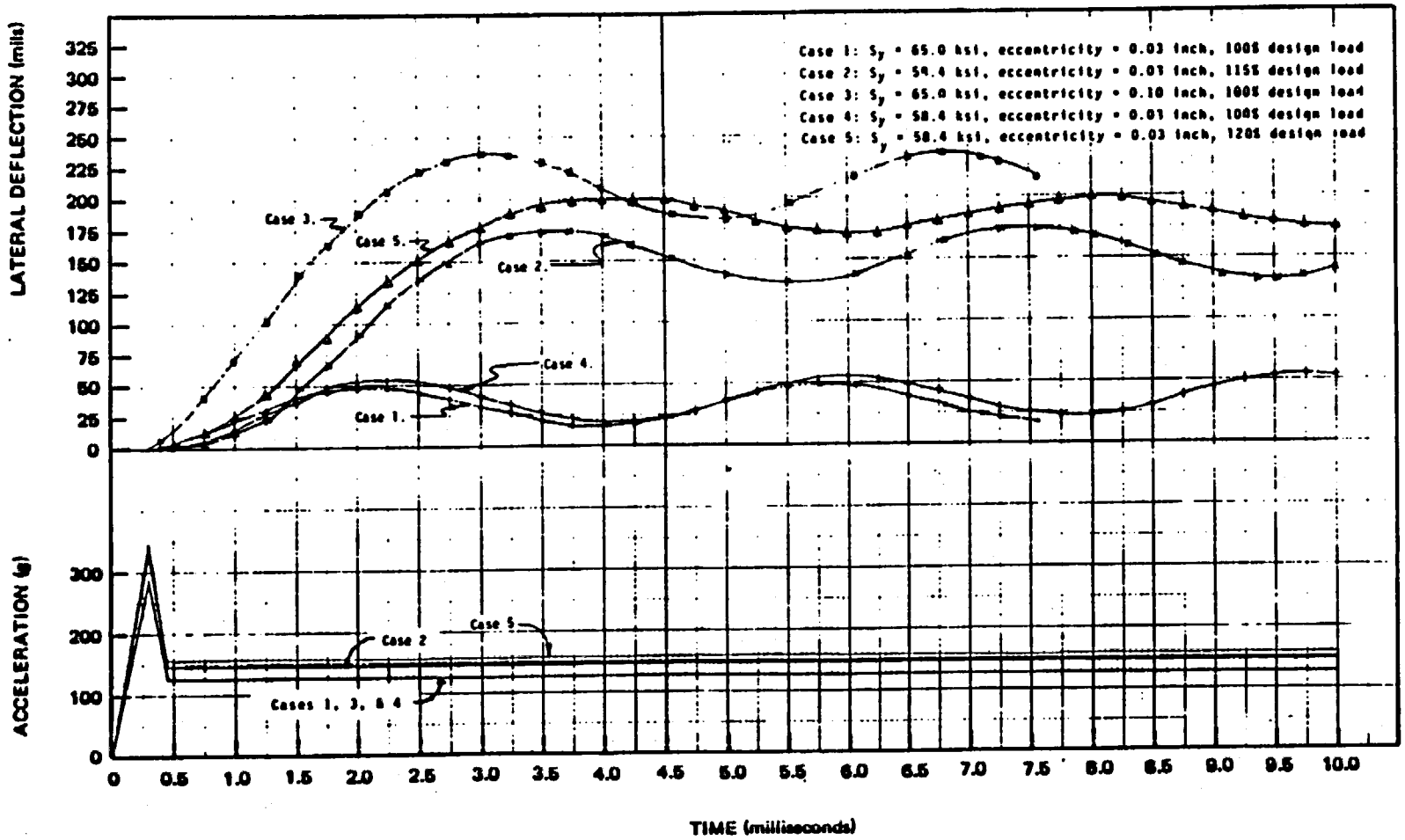

FIGURE V-28. LATERAL DEFLECTIONS VS TIME AT TIE ROD MIDSPAN

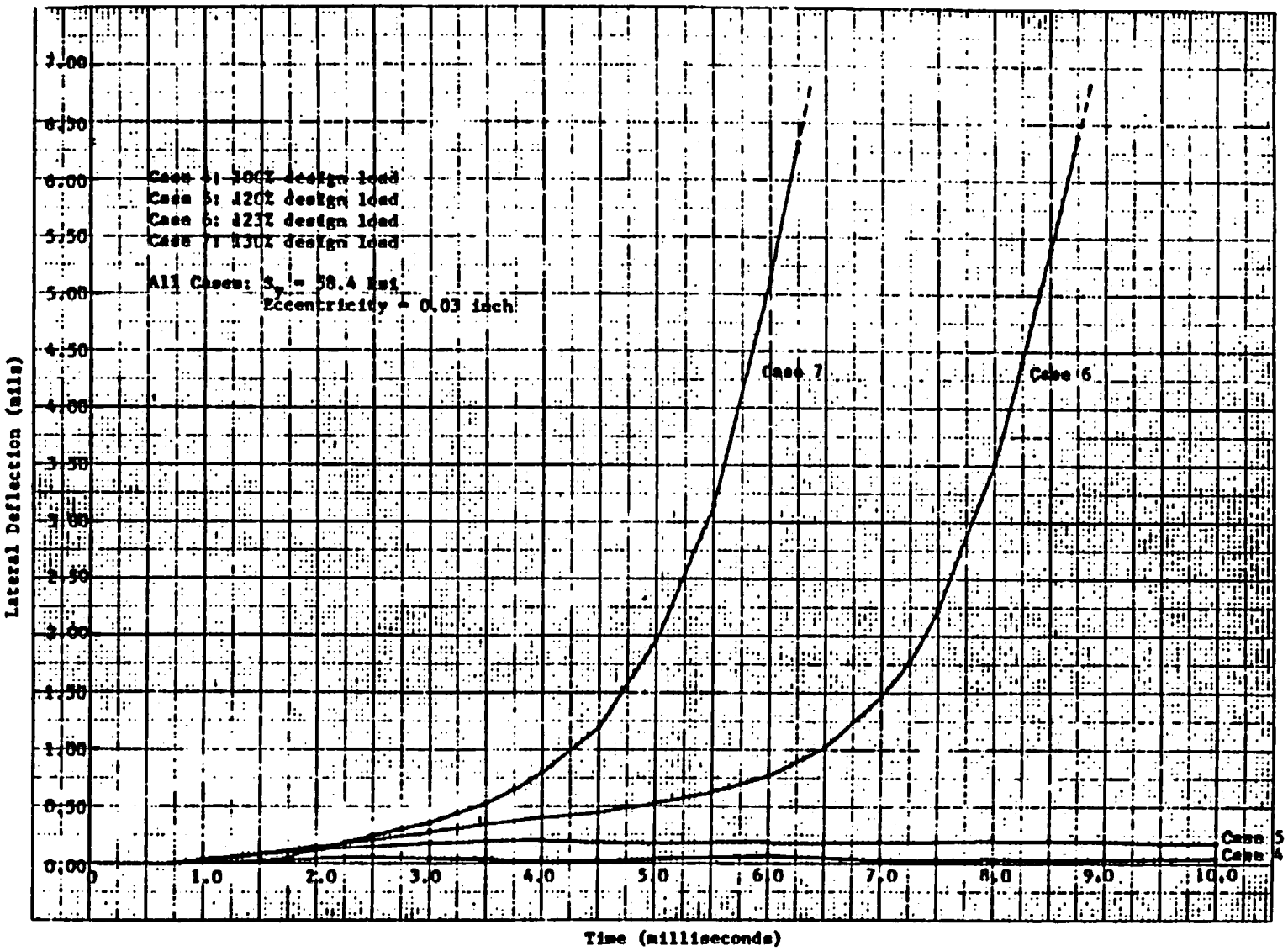

Figure V-29 Lateral Deflection vs Time At Tie Rod Midspan

Based on the results presented above, it is concluded that the tie rods will not buckle under the design basis 30-foot vertical drop of the cask. Furthermore, tie rod buckling is not predicted until the applied load exceeds 120 percent of the nominal design basis load or three times the nominal initial eccentricity.

Stresses. Figures V-30A through V-30E show the axial stress response versus time at the tie rod midspan for Cases 1-5. Three stress values are plotted, one for each of the following midspan locations:

- the surface on concave side of the rod
- the tie rod center line
- the surface on convex side of the rod

In this instance the concave and convex side of the tie rod refer to the shape the rod takes due to the assumed initial eccentricity. The surface stresses include bending and membrane stress components. The centerline stress is an arithmetic average of four integration points across the tie rod cross-section. The centerline stress is only an approximation of the axial stress; a precise evaluation of this stress requires the data from all twelve of the midspan integration points and the use of Newton-Cotes weighting functions.

A review of the axial stress versus time data for Cases 1-5 reveals the following additional pertinent facts about the question of tie rod buckling.

- For all five cases, the bending stress is small initially and increases with time according to the resulting lateral deflections. Maximum and minimum outer surface stresses are observed to occur at approximately the same frequency as maximum and minimum lateral deflections.

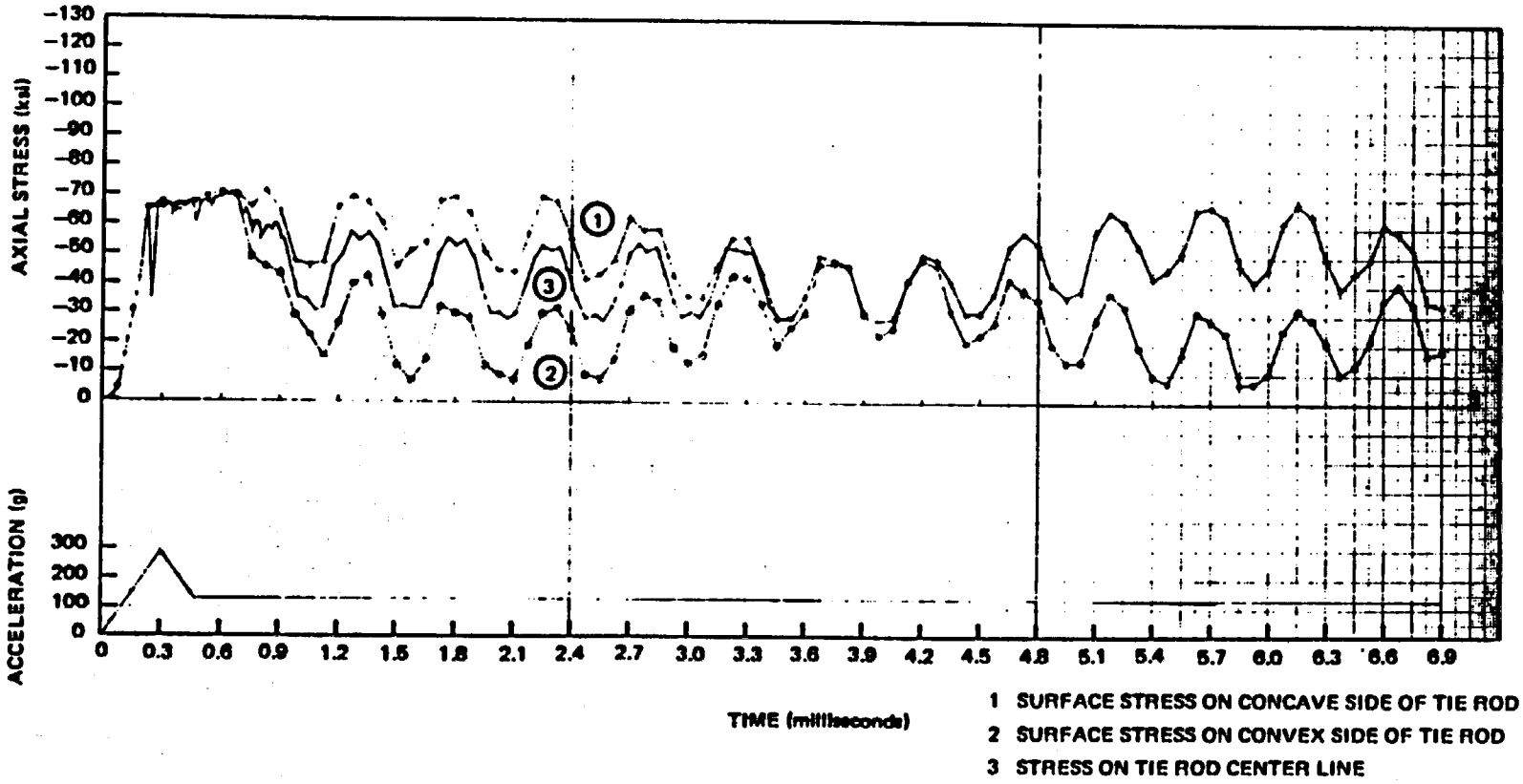

FIGURE V-30A. TIE ROD AXIAL STRESS AT MIDSPAN VS. TIME 0.03 INCHES INITIAL ECCENTRICITY
Sy = 65 ksi; E = 26.2 x 10^6 psi; 100 Percent Load
Case 1

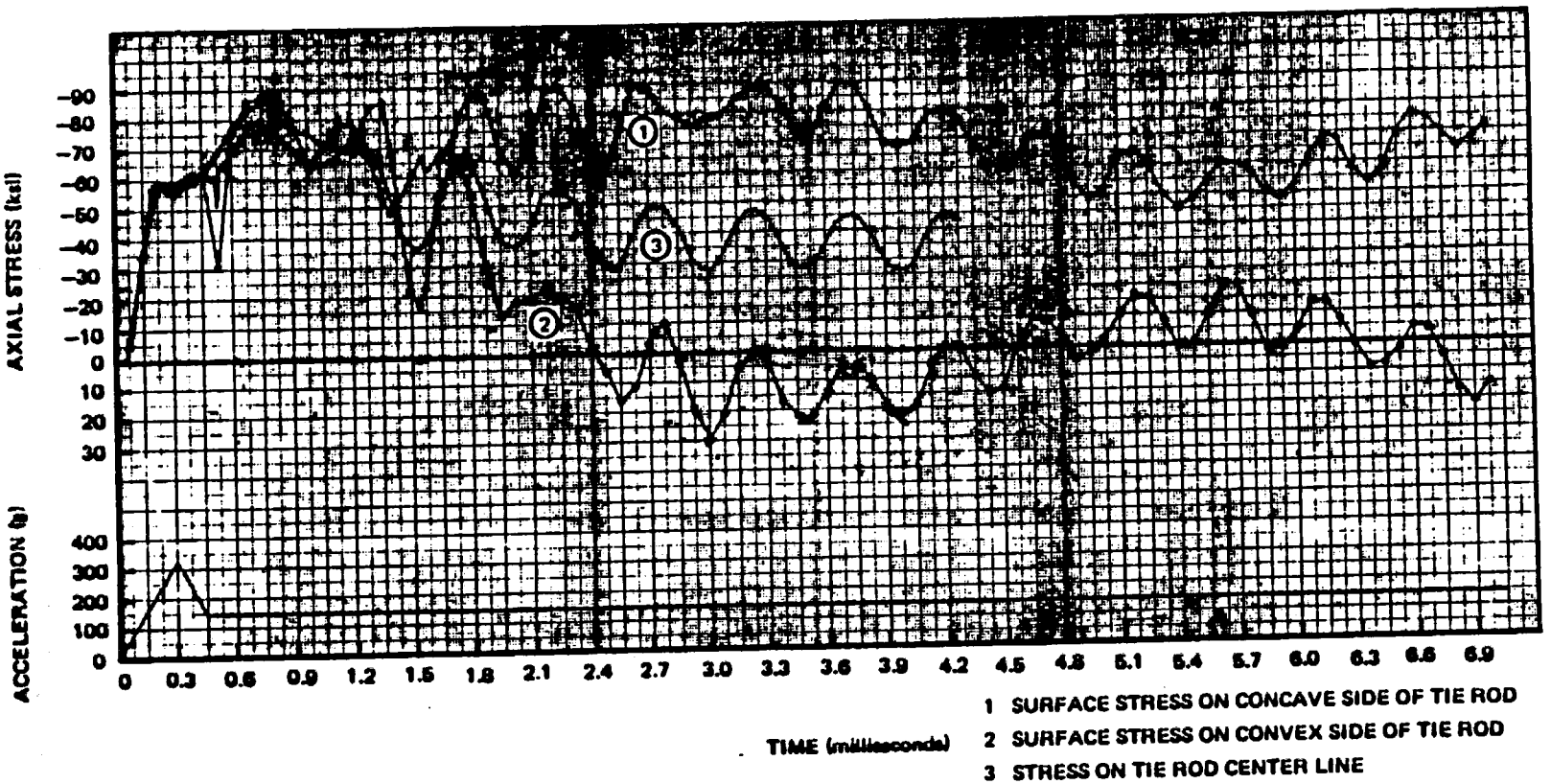

FIGURE V-30B. TIE ROD AXIAL STRESS AT MIDSPAN VS. TIME 0.03 INCHES INITIAL ECCENTRICITY
Sy = 58.4 ksi; E = 26.2 x 10^6 psi; 115 Percent Load
Case 2.

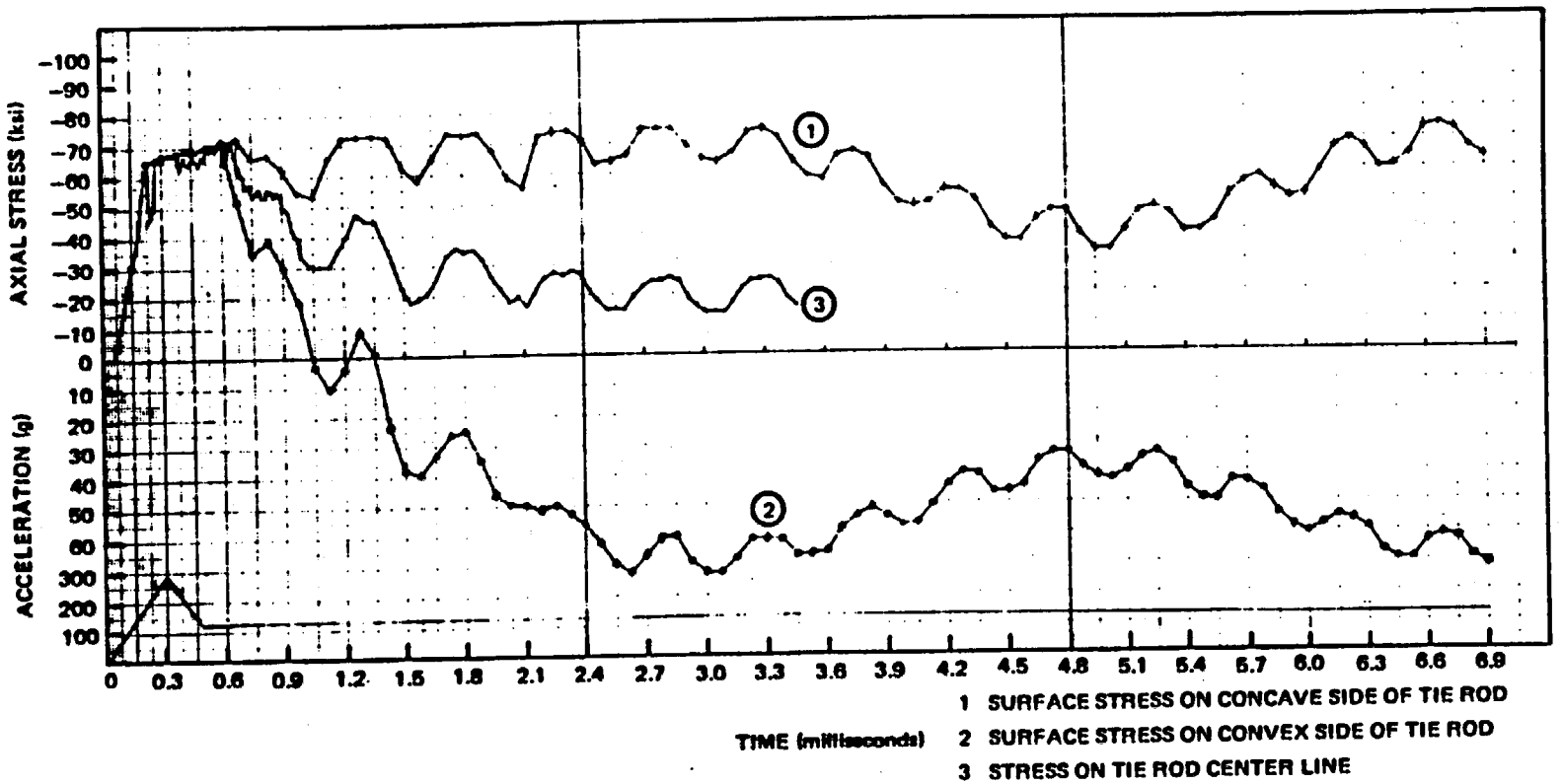

FIGURE V-30C. TIE ROD AXIAL STRESS AT MIDSPAN VS. TIME 0.10 INCHES INITIAL ECCENTRICITY
Sy = 65 ksi; E = 26.2 x 10^6 psi; 100 Percent Load
Case 3.

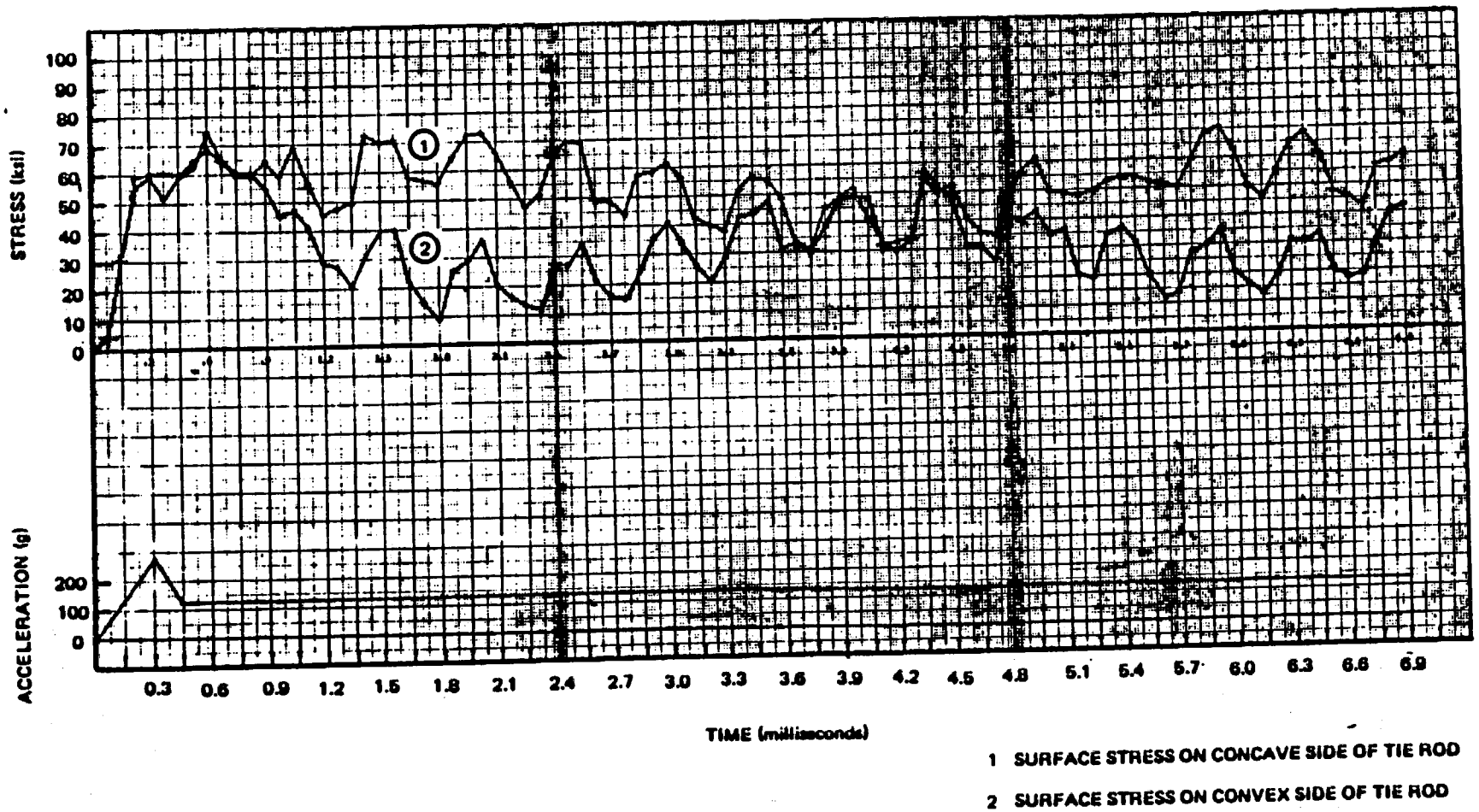

FIGURE V-30D. TIE ROD AXIAL STRESS AT MIDSPAN VS. TIME 0.03 INCHES INITIAL ECCENTRICITY
Sy = 58.4 ksi; E = 26.2 x 10^6 psi; 100 Percent Load
Case 4.

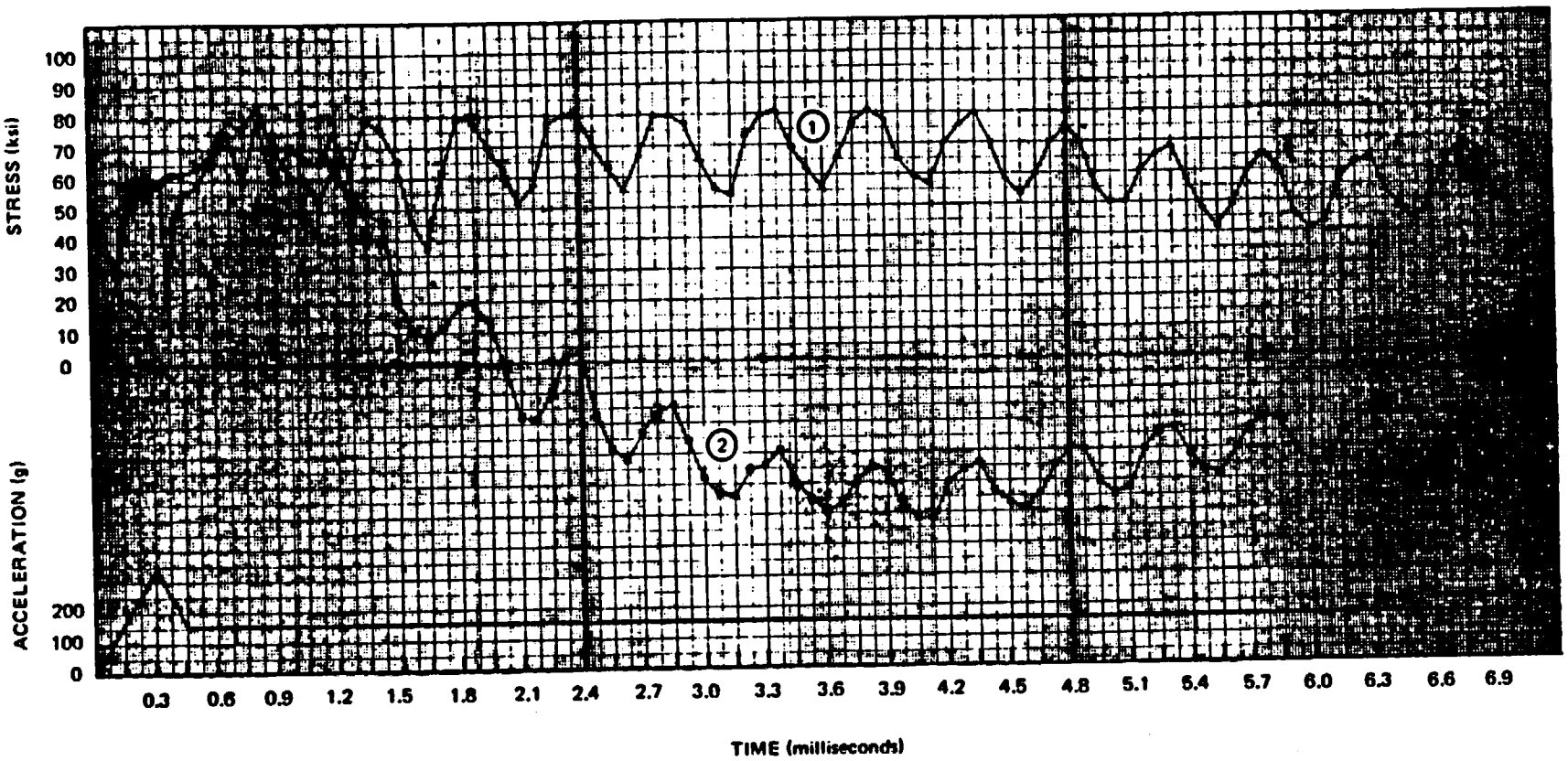

FIGURE V-30E. TIE ROD AXIAL STRESS AT MIDSPAN VS. TIME 0.03 INCHES INITIAL ECCENTRICITY
Sy = 58.4 ksi; E = 26.2 x 10^6 psi; 120 Percent Load
Case 5.

- The maximum variation in stress for a given surface, after initial yielding, occurs for the 115 percent of nominal design basis load case shown in Figure V-30B. For this case, the maximum stress variation is approximately 50 ksi. Since the endurance limit at 10^6 cycles for austenitic stainless steel (ASME Code, Section III, Figure I-9.2) is ± 25 ksi, cyclic fatigue is of no consequence.

- Stresses and lateral deflections show no net decrease with time over the plateau phase of the applied load. This is a direct result of having conservatively assumed that the fuel basket structure has no internal damping. With damping, the results would be decreasing with each cycle since the system has been shown to be stable up to 120 percent of the design basis load.

- The nominal design basis case is shown in Figure V-30D. A peak surface stress of 75 ksi is predicted for this case. Although not plotted, additional data shows similar stress results from 6.9 to 10.0 milliseconds, after which the stresses begin to decrease as the plateau load is ramped down to zero over the time interval between 10.0 and 19.0 milliseconds. As stated in the discussion of lateral deflections, the transient is actually over in 10.1 milliseconds, based on the principle of impulse and momentum.

- The high frequency stress oscillation which is observed in all four of the cases analyzed corresponds to the elastic axial vibration of the tie rod at its fundamental frequency of about 2100 Hz.

The results of Cases 2, 3 and 5 show that margin exists against buckling of the tie rods for both the design basis eccentricity and applied load. In addition to that margin, the tie rod analysis has several other conservatisms that provide additional margin against the possibility of tie rod buckling. These conservatisms are as follows:

- The load applied to the tie rod is taken to be one fourth of the maximum fuel basket weight, as determined by actual measurement. This weight is 9 percent conservative since the weight of certain components at the bottom of the fuel basket is not transmitted thru the tie rod section in question.

- The tie rod is assumed to be pinned at each end. For determination of buckling this is the most conservative assumption that can be made, consistent with the lateral restraint provided by the spacer disks. In reality, the tie rod ends have some rotational resistance due to the spacer disk interface.

- The length of the tie rod is assumed to be 22 3/4-inches, equal to the distance between spacer disk centerlines. When the spacer disk and weld bead thickness is accounted for the true unsupported column length is 21 1/4-inches.

- The design basis eccentricity of 0.030-inches is based on two factors:

  - As-installed eccentricity: The tie rods are centerless ground bars. Eight measurements of as-installed eccentricity over a 17-inch span have shown a maximum eccentricity of 0.002-inch. A conservative assumed accentricity of 0.008-inches has been used for the 22 3/4-inch span of this analysis.

  - Lateral deflection resulting from spacer disk inertia effects: A static calculation based on the peak deceleration of 287 G's was conservatively used to determine the lateral deflection resulting from spacer disk inertia effects. Actual lateral deflections would be less due to the short duration of the peak deceleration.

- The structural capability of the poison rods, after a nominal 3/16-inch decrease in the distance between spacer disks is not considered. In reality, the poison rods can absorb a fair amount of the energy of the fuel basket deceleration by adding approximately 20 percent more cross-sectional area to that of the tie rods (excluding the boron carbide contained within). While the very bottom section of the tie rods would see the total applied load, its free length is only 3 5/8-inches.

- The fuel basket section (between spacer disks) that was analyzed, is the most limiting location on the fuel basket because of the greater load and the greater tie rod length (approximately 13 percent) at that location.

- The increase in yield strength that is normally associated with high strain rates is ignored. The dynamic critical buckling stress has been estimated to be at least twice as high as the static critical buckling stress if a 7 ksi increase in yield strength per decade of strain rate from 10^{-5}-in/in/sec to 10^{2}-in/in/sec is assumed.

- The post-buckling capabilities that would resist collapse if the buckling point was encountered are nor accounted for.

Therefore, it is again concluded that the BWR fuel basket tie rods will not buckle as a result of the design basis loading conditions.

ii. Tie Rod-to-Spacer Disk Weld Analysis

Stresses in the welds between the tie rods and the spacer disks have been analyzed to determine whether the spacer disks will maintain their axial position in a vertical cask drop. A statically applied deceleration of 287 G's was used to calculate the peak shearing force. The configuration of the weld is shown in Figure V-23, section B-B. Using a weld throat depth of 0.265-inch, a weld quality factor of

0.6, and a static load of 100 lbs, the weld shear stress is calculated to be 17.2 ksi. When compared to a maximum allowable shear stress of half the yield strength (maximum shear stress theory), the factor of safety for this calculation is 1.70. This result confirms that there will not be any axial displacement of the spacer disks relative to the tie rods, for the vertical drop case.

5.6.3.2 PWR Basket

The PWR basket design concept is identical to the BWR basket concept in that it consists of spacer disks, thin-walled square channels, and four 2-1/4-inch diameter support bars. The PWR basket has 7 fuel channels, as compared to the BWR basket with 18 channels (Figures V-20 and V-21).

a. PWR Basket Horizontal Drop Analysis

The horizontal decelerations shown in Figure V-22 apply to both the BWR and PWR baskets, as does the 5 percent amplification factor for cask motion. The maximum basket weight with fuel is about the same for both baskets (16,925 lbs-BWR; 15,370 lbs-PWR), so that the loadings and distribution will be equivalent. (If the PWR basket load includes control rod clusters/assemblies, the PWR basket weight will be approximately the same as in the BWR case.) Based on the similarity between the basket designs and weights of the loaded baskets, it can be concluded that a 30-foot horizontal drop of the PWR basket would result in deformation similar to that found for the BWR basket and that no degradation in criticality safety provided by the basket would occur.

b. PWR Vertical Drop Analysis

As noted for the horizontal drop analysis, the PWR fuel basket is designed similarly to the BWR fuel basket, except that it provides space for 7 (PWR) fuel bundles. Tie rods of the same (2-1/4-inch)

diameter as those used in the BWR basket extent from the bottom of the cask cavity to the closure head when the fuel basket is installed in the cask. Also, the same vertical drop decelerations of Figure V-22 apply. The BWR fuel basket, however, constitutes the limiting case for the 30-foot vertical cask drop. The reasons for this are:

- The PWR basket weights 4520 pounds maximum versus 5675 pounds to the BWR basket.

- The maximum length between PWR basket spacer disks is 20-7/8-inches versus 22-3/4-inches for the BWR basket.

Since the PWR applied load and tie rod column length are less than the BWR applied load and column length and buckling of the BWR basket tie rods has been shown not to occur, it can be concluded that buckling of the PWR basket tie rods does not occur either.

5.6.3.3 Conclusions

The analyses of subsection 5.6.3 demonstrate the integrity of both the BWR and the PWR basket configurations under the 30-foot side and end drop decelerations.

Other than minor localized deformation, each basket retains the ability to provide support, separation and criticality control for the contained fuel bundles under severe accident conditions.

5.6.4 Fuel Basket Poison Rods - 30-Foot Drop

As described in Section IV, the poison rods for the 7-cell PWR and 18-cell BWR fuel baskets licensed prior to 1991 are 1/2-inch diameter by 0.020-inch wall 304 stainless steel tubes filled with boron carbide. These tubes are retained by cage plates attached to the spacer disks between adjacent elements. They run parallel to the axis of the fuel basket. (The borated stainless steel poison plates used in the 17-cell channelled BWR fuel basket licensed in 1991 are described in Volume 3, Appendix A.)

5.6.4.1 Side Drop

For the purpose of analysis, a single rod was examined since the failure of one rod will not lead to the failure of any other. The first 3/4 inch on each end of the rod is the supported length. Each rod is unsupported along its length. The maximum unsupported span is less than 20 inches. These tunes can be assumed to act as a beam built in at both ends. The span length (L) is assumed to be 20 inches for conservatism (see Figure V-31).

The maximum side drop deceleration is 122,3G's. The tube and born carbide act as a distributed loaf having a linear weight (W) of 1.92×10^{-2} pounds per inch. The maximum bending moment is given by:

$$M = \frac{WL^2}{12}$$

$$M = \frac{1.95 \times 10^{-2}}{12} (20)^2 = 0.65 \text{ inch-lb @ 1 G}$$

For 1/2 inch diameter tubing:

$$C = \frac{0.5}{2} = 0.25 \text{ inch}$$

Moment of inertia is given by the following:

$$I = \frac{\pi (r_o^4 - r_i^4)}{4}$$

$$I = \frac{\pi}{4} (0.25^4 - 0.23^4) = 8.78 \times 10^{-4} \text{ inch}^4$$

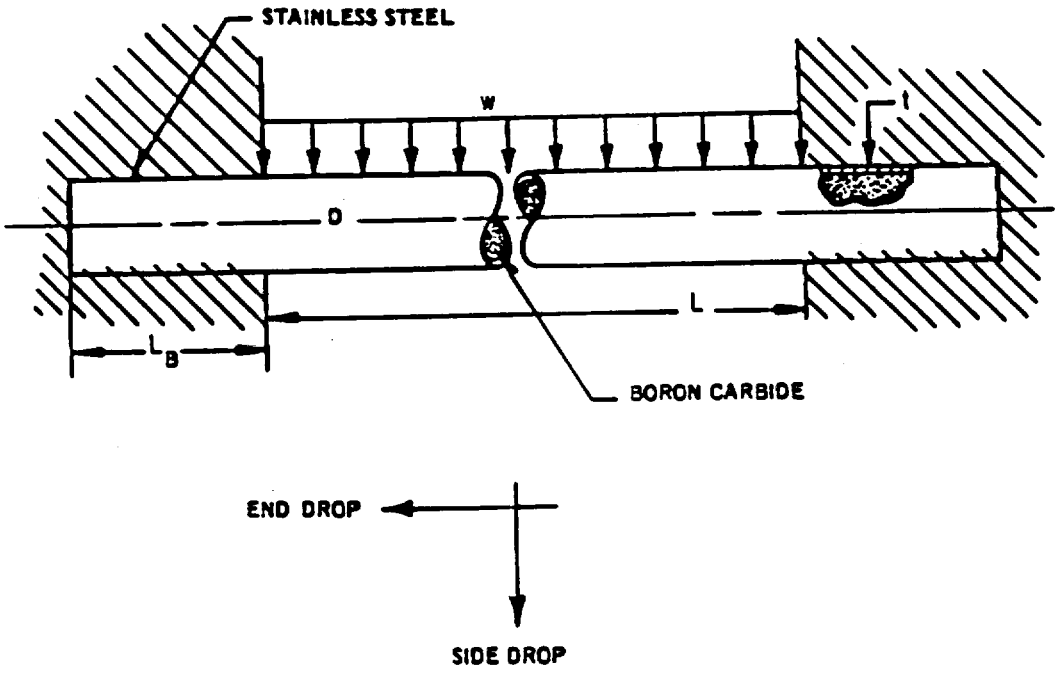

FIGURE V-31. POISON TUBE

Maximum bending stress at 1 G is:

$$\sigma_B = \frac{MC}{I}$$

$$= \frac{(0.65)\ (0.25)}{8.7 \times 10^{-4}} = 185 \text{ psi}$$

Maximum bending stress at 122.3 g's

$$\sigma_B = (122.3)\ (185) = 22{,}626 \text{ psi}$$

From ASME Code, Section III @ 200°F (Reference 1)

$$\sigma_Y = 25{,}600 \text{ psi}$$
$$SF = \frac{25{,}600}{22{,}626} = 1.13 \text{ (min)}$$

The poison rods are capable of sustaining the maximum side drop deceleration without failure.

5.6.4.2 End Drop

Each rod is captured between the 1-inch thick basket spacer disks. Therefore, in an end drop circumstance, they cannot axially displace without penetrating the disk. Under maximum (234) "G" loading each rod has an equivalent weight of:

$$W_{EQ} = (234)\ (0.507) = 119 \text{ pounds}$$

Rod cross sectional area is:

$$A = \frac{\Pi}{4}(d)^2 = \frac{\Pi}{4}(0.5)^2 = 0.196 \text{ in.}^2$$

thus the contact stress is:

$$\sigma_c = \frac{119}{0.196} = 606 \text{ psi}$$

This is an extremely low value, hence the poison rods are capable of sustaining the end drop without failure or displacement.

5.6.5.A Fuel Bundles - Group I

This section examines the Group I PWR and BWR fuel bundles under both the normal transport one-foot horizontal drop and the accident 30 foot drop, side and end. To adequately and accurately describe fuel rod behavior under these various impact conditions, General Electric has done the following:

- Generated dynamic spring-mass models of the most highly stressed fuel rods and computed strains under maximum "g" loading.

- Evaluated the fuel deflection restraints provided by the cask and fuel basket which assure that the fuel rod deflections and resulting strains are less than those calculated.

- Performed a detailed literature study of irradiated material behavior under the conditions present in the 30-foot drop.

- Performed bending tests on actual samples of high burn-up fuel to impose deflections and strains more severe than either those calculated or those possible considering the basket restraint.

The results show that all fuel rods are capable of sustaining the various drop conditions without breaching cladding integrity.

5.6.5.A.1 Fuel Support Description

As described on drawing 153C5238 sheet 6 (Section IV), the fuel bundles are held in the cask cavity by a compartmented structure referred to as a basket. The IF-300 cask design has two types of baskets, a BWR model which holds 18 bundles and a PWR model which holds 7 bundles. These baskets are all stainless steel weldments. They consist of circular plates, which fit the cavity diameter and are at fixed intervals along the cavity length.

These plates are slotted to accept square channels which run axially through the basket. Each channel is designed to hold a single fuel bundle.

A typical BWR or PWR fuel bundle consists of a square array (7 x 7, 14 x 14, 15 x 15) of fuel rods retained at both ends by some type of nozzle or tie-plate. Spacing of the rods is provided by a series of integral grids positioned at intervals along the bundle length.

Under side drop loadings (1 foot or 30 foot drop) the fuel rods deflect downward (drop direction). Due to the small (0.223") fuel bundle-to-fuel basket channel and rod-to-rod (0.141") gaps the rods become supported along a portion of their length by basket components which limit the amount of deflection. The maximum unsupported length of a fuel rod is set by the spacing between the fuel basket spacer disks. For the PWR fuel this distance is 18.5 inches; for BWR fuel it is 19.75 inches. In the PWR case the spacing of the fuel basket spacer disks (18.5") is less than the spacing of the fuel bundle grid spacers (26"). In the BWR case the fuel basket spacer disk span and the grid spacer span are approximately the same.

To allow for thermal expansion, the fuel bundles are not restrained in the axial direction. Spacers are mounted to the underside of the cask head, as needed, and in the basket bottom to provide minimum free movement of the bundle consistent with expansion requirements.

5.6.5.A.2 Material Properties

The use of Zircaloy tubing as a containment for the uranium fuel pellets is practically universal in LWR applications (a few exceptions use stainless steel cladding). There is some loss of Zircaloy cladding ductility due to neutron irradiation. Nevertheless, the material behaves as a metal and the available elongation

before failure is sufficient to accommodate the maximum fuel rod strains under peak decelerations. Furthermore, the values of yield and tensile strength are elevated with increasing strain-rate while the elongation parameters are reasonably unaffected. Both of these points plus some additional measures of material toughness will be presented in the following discussions.

a. Zircaloy Stress-Strain Curve

A typical PWR irradiated Zircaloy cladding stress-strain curve is shown in Figure V-32, temperature corrected to 400°F (static) and strain-rate corrected for dynamic loading (125% static). The basic curve is extracted from Westinghouse document WCAP-3017-6094 which is a summary of the Yankee fuel irradiation program. WCAP-3017-6093 is an interim document in the Yankee fuel study, which shows two additional stress-strain curves. These curves as well as the one in the summary publication all have similar shape and magnitude characteristics. The basic curve is described by Westinghouse on Page 11-4 third paragraph as "a typical stress-strain curve..." The following subsection contains all three curves.

b. Physical Properties - Discussion

This section contains an analysis of those physical properties of irradiated Zircaloy which pertain to the drop loadings. As indicated previously, ductility is the prime factor affecting the integrity of the fuel rods. The data presented below indicates that highly irradiated (high fluence) cladding has the capacity for (1) a yield stress in excess of 85 Ksi, (2) an ultimate tensile strength in excess of 90 Ksi, (3) uniform elongation including elastic strain averaging 2.7 and a total elongation including elastic strain averaging 5.1%. High fluence Zircaloy cladding will accommodate >0.8% elastic strain in tension. This work was performed by Dr. C. D. Williams of General Electric Company.

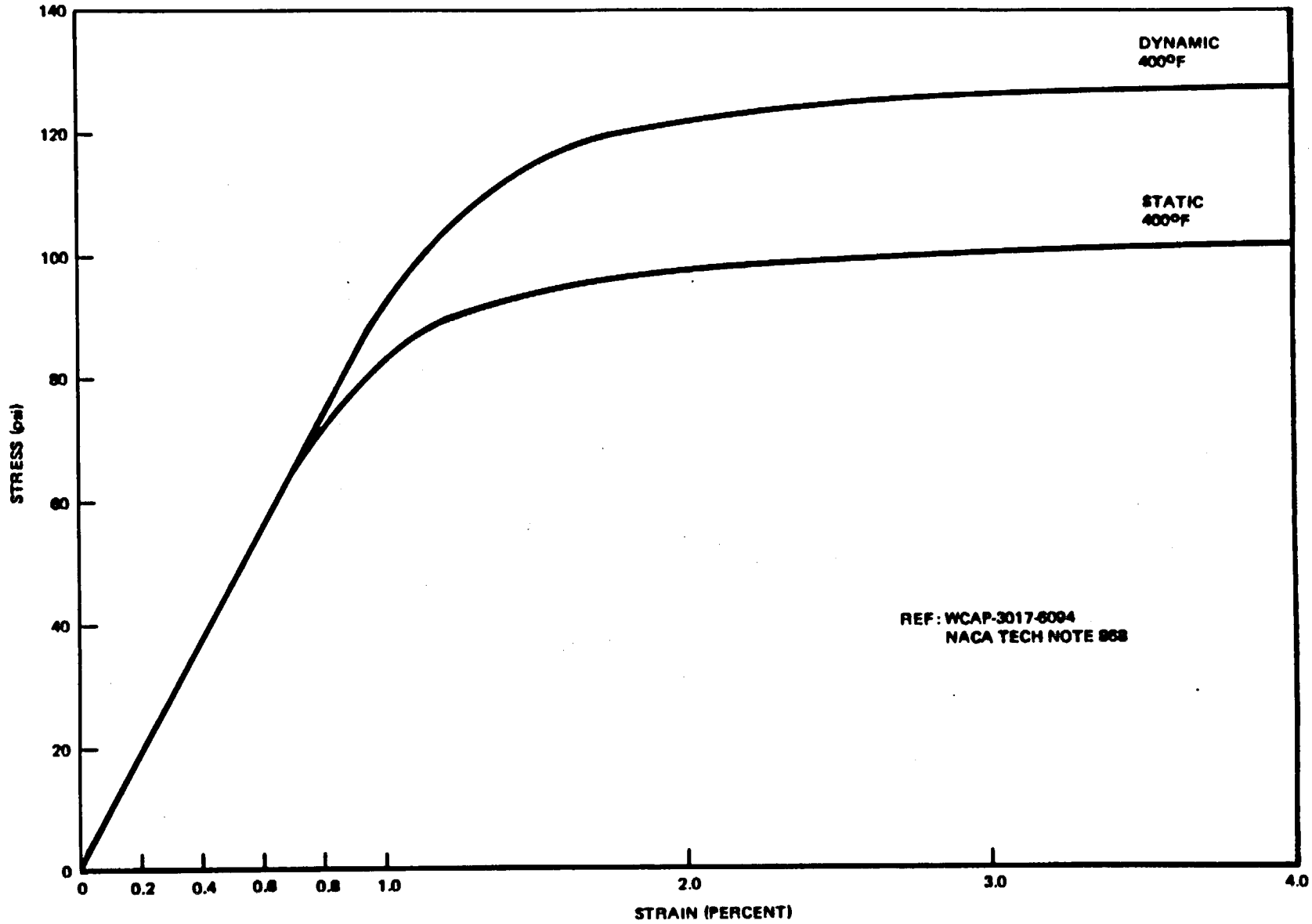

FIGURE V-32. STRESS-STRAIN CURVES FOR IRRADIATED ZIRCALOY CLADDING REPRESENTATIVE OF PWR FUEL

The following information is compiled in connection with analysis of the behavior of irradiated Zircaloy-2 cladding in the high strain-rate conditions imposed during the hypothetical "cask-drop". The data covers available data on yield strength, uniform and total elongation and fracture toughness.

c. Conclusions

1. Relative to Brittle Failure:

Available data indicate that typical Zircaloy-2 cladding containing a hydrogen concentration (<100 ppm) commensurate with exposure in a BWR environment for the full lifetime of a fuel rod and with worst case specification hydride orientation will not fracture in a brittle mode under high strain rate mechanical loading. The alloy's fracture toughness is not markedly reduced by neutron irradiation and irradiation does not remove its capacity for ductile fracture even at loading temperatures far below room temperature (-140°C).

2. Relative to Ductile Rupture:

Available data from tests on tubes show that typical Zircaloy-2 cladding as defined, after irradiation to fluences in the range of 5-10 x 10^{21} nvt (E > 1 Mev) has the following tensile properties at high strain rates at ∿300°F; (1) a yield stress in excess of 85 Ksi, (2) an ultimate tensile strength in excess of 90 Ksi and a capacity for (3) uniform elongation (including elastic strain) averaging 5.1%.

d. Review of Data

1. Consideration of Fracture Mode in Irradiated Zircaloy

Two sets of observations on fracture of irradiated Zircaloy-2 of normal hydrogen concentration show that the material is not subject to brittle failure when subjected to mechanical stress. The first is the well documented observation of necking to fracture, which occurs in uniaxial tensile and biaxial pressurized tests. As noted above, total elongation values and reduction of area values are reduced by irradiation but to a much smaller extent than uniform elongation. This is a consequence of the change in damage distribution of the irradiated material which occurs when it is deformed; dislocations moving through the neutron-damaged structure are able to sweep up the small lattice defects caused by irradiation, leaving "channels" of damage-free material within which further slip can occur at a reduced stress. These channels have essentially the flow stress and work hardening properties of the unirradiated alloy. The channels broaden with increasing deformation, and with work hardening the material approaches fracture, and in due course fails, in the same ductile manner as unirradiated material. This ductile fracture is shown by examination of the fracture surfaces which evidence ductile dimple rupture. Total elongation and reduction of area values are reduced somewhat below the unirradiated values because the volume of material within which this necking and fracture occurs is relatively small and is constrained by the bulk of material which, in the irradiated, undeformed state, has a much higher flow stress than the channeled regions. Details of this "channeling" effect in irradiated Zircaloy are shown for example in Reference 5.

The second, well documented observation is that the fracture toughness of Zircaloy is not markedly reduced by high fluence irradiation. The most commonly used criterion of fracture toughness is the plane strain stress intensity factor K_{Ic} [6]. This is a measure of the stress intensity required to propagate a crack under well defined conditions of stress. The K_{Ic} parameter cannot be strictly applied to fuel cladding because the plain strain condition required in derivation of K_{Ic} requires that the material section thickness is equal or greater than 2.5 $(K_{Ic}/\sigma_{ys})^2$ where σ_{ys} is the yield stress. This condition cannot be satisfied in thin walled fuel cladding at elevated temperatures. However, the concept of fracture toughness as the resistance of the material to crack propagation can be applied to irradiated tubing since similar fracture mechanisms are involved at the crack tip. It is, therefore, of importance to the present question to note that extensive studies of fracture toughness of Zircaloy carried out on thick-walled tubing and plate material show that K_{Ic} values are not greatly reduced by fast neutron irradiation. Thus, the irradiated alloy is, like unirradiated Zircaloy, resistant to brittle failure. Hoagland and Rowe have reported that some reduction in K_{Ic} is caused by irradiation in the fluence range $<5 \times 10^{20}$ but a saturation occurs in the effect at approximately this fluence [7]. Figure V-33 shows their data obtained from plate material with specimens cut so that cracking occurred parallel with, (RD), and normal to, (TD), the rolling direction.

An estimation of the effect of strain rate on fracture toughness may be obtained using the rate temperature

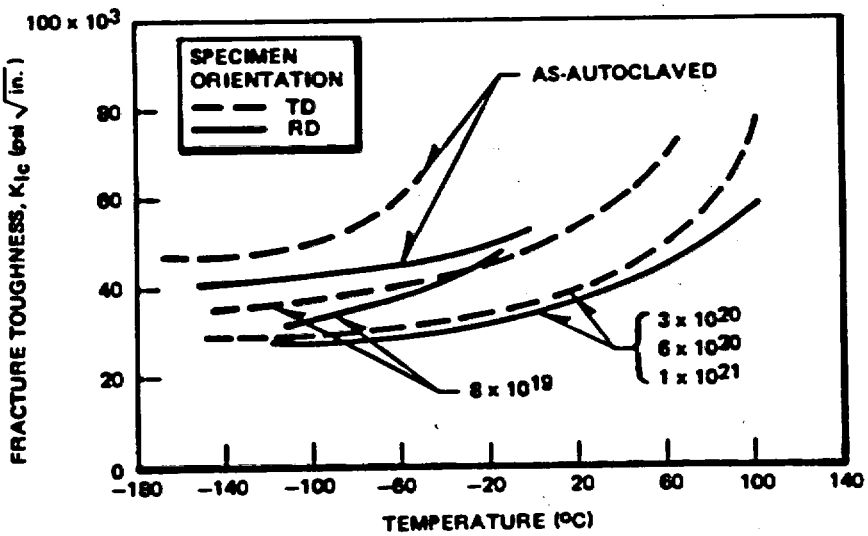

Effect of neutron fluence to 1 X 10^{21} n/cm^2 (E > 1 MeV) in 280°C water on the temperature dependence of the fracture toughness of annealed Zircaloy-2 for both cracking orientations. At fluence levels of 3 X 10^{20} n/cm^2 and above no further change in the fracture toughness occurs. Specimens were autoclaved prior to irradiation.

FIGURE V-33. EFFECT OF NEUTRON FLUENCE

parameters $T \times \ln(A/\dot{\varepsilon})$ where T is the strain temperature in °Rankine, A is a constant = 10^8 sec^{-1} and $\dot{\varepsilon}$ is the strain rate[8]. This relationship has been used to correlate data obtained in tests on a number of steels over a wide range of strain rates. Application to the available Zircaloy data indicate that raising the strain rate by four orders of magnitude to ∿6 sec^{-1} in the present "drop event" will reduce the K_{Ic} value at 200°F from ∿55 Ksi $\sqrt{in}$ (Figure V-34) to ∿35 Ksi $\sqrt{in}$.

An alternative estimate may be obtained from the relationship $K_{Ic} = M\sigma_{ys}^{-1.5}$ where M is a material constant.[9] Allowing for an increase in yield stress from 100 Ksi to 125 Ksi obtained with the increase in strain-rate, a reduction in K_{Ic} at 200°F from 55 Ksi $\sqrt{in}$ to 40 Ksi is expected.

In either case, the fracture toughness at high strain rates is representative of a ductile or tough material.

In further studies of irradiation effects, Watkins et al[10] found no decrease in critical crack length of 0.2 in. wall Zircaloy-2 pressure tubes irradiated to 10^{21} nvt (>1 Mev). (The critical crack length is the minimum length of a through wall defect which will propagate under internal stress in an unstable manner). Cowan and Langford have also reported, Figure V-34, little change in critical crack length of Zircaloy-2 tubing at 20°C with irradiation to a fast fluence of 7 x 10^{20} nvt[11]. These observations again indicate that irradiation does not render Zircaloy-2 brittle.

2. Tensile Strength and Ductility of Irradiated Zircaloy

The effect of increasing strain rate through the range of 10^{-2} - 1 in/in/min is to increase the yield and ultimate

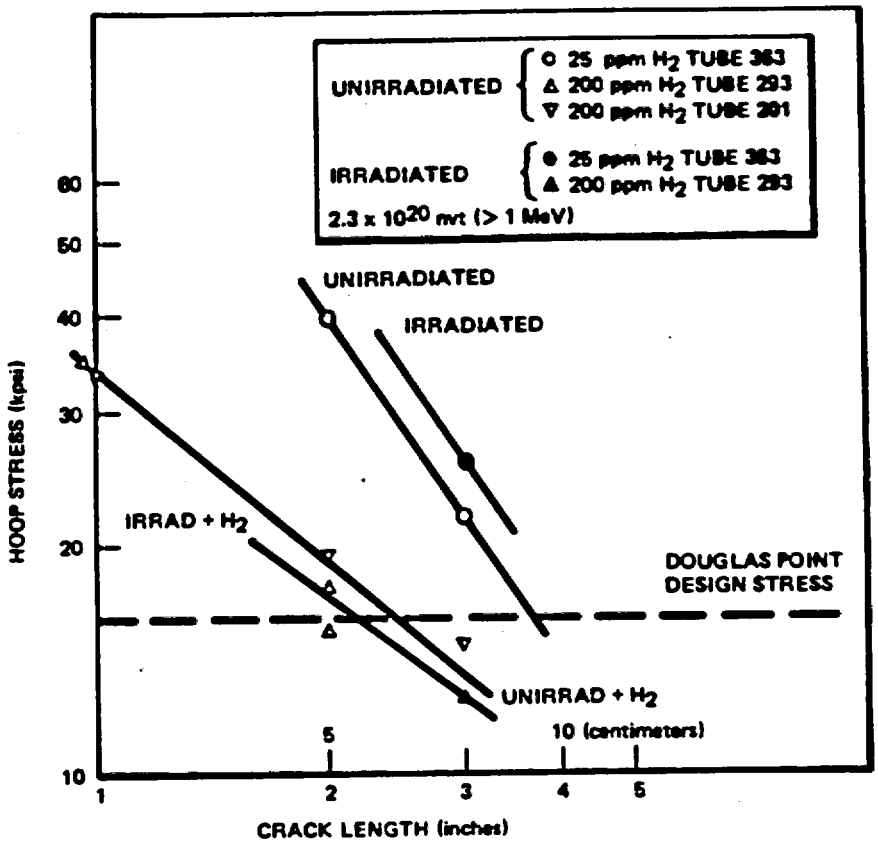

FIGURE V-34. CRITICAL CRACK LENGTH OF ZIRCALOY-2 PRESSURE TUBING AT 20°C.

strength of Zircaloy-2. Figures V-35[12] and V-36[13] show this effect for unirradiated Zircaloy at room temperature and irradiated Zircaloy at 600-675°F respectively. The effect of fast neutron fluence on Zircaloy-2 is illustrated by Figure V-37, Ref (13) and Table V-29, from cladding specimens tested at 500-700°F and at strain rates near 0.05 in/in/min. Values at 300°F will be approximately 20 Ksi higher than the values at 650°F. It is expected that with increasing strain rates the strength levels will increase following the trend shown in steels[18], Figure V-38.

Typical load elongation curves for highly irradiated BWR and PWR cladding are shown in Figures V-39A through C_1 and V-40.

The uniform and total elongation values shown in Figure V-36 change little with increasing strain rate. The absence of a downward trend at high rates is noted and a slight upward trend in elongation values is apparent in results obtained on unirradiated Zircaloy-2, Figure V-41[14]. It is expected that the elongation values obtained at the high strain rates imposed in the "drop event" will be similar to those at the conventional test rates of ∿0.05 in/in/min. The collection of data shown in Figure V-42, V-43, and V-44 confirm that for a variety of alloys having a range of tensile strengths from 45-200 Ksi the elongation values do not change significantly over a range of very high impact velocities up to 1800 in/in/sec.[15] Therefore, although the yield stress for highly irradiated Zircaloy-2 is expected to be ∿25% higher at a strain rate of ∿1 in/in/sec than at 0.05 in/in/min, the elongation values will be similar at the two strain rates.

The strain capacity within the stable deformation range, i.e., before the onset of plastic instability or necking,

Table V-29

DNPS TYPE I CLADDING LONGITUDINAL TENSILE TESTS ON COUPON SPECIMENS, GAGE LENGTH 0.634 IN. THESE SPECIMENS WERE MACHINED FROM CLADDING

Fast Neutron Fluence nvt is 1 MEV x 10^{-21}	Test Temperature (°F)	Strain Rate (in/in/min)	Yield Stress (psi)	Ultimate Stress (psi)	Uniform in 0.634 in. (%)	Total in 0.634 in. (%)
2.0	650	0.0315	73,700	75,300	1.7	3.5
2.0	↓	↓	70,500	72,300	1.9	4.1
2.5			65,800	68,700	1.5	3.6
2.5			69,700	70,300	0.5	2.7
1.9	650	0.0315	47,000	52,600	1.3	3.6
1.9	↓	0.0315	76,400	80,400	1.6	4.1
1.9		0.315	61,200	67,400	2.1	4.4
1.9		0.315	75,500	76,900	1.2	3.2
2.0		0.00315	63,900	66,600	1.2	3.2
2.0		0.00315	63,400	67,000	1.6	3.9
2.0	800	0.0315	58,600	61,000	0.9	4.6
2.0	800	0.0315	59,600	61,900	0.9	4.3
DNPS Type I Cladding Longitudinal Tensile Tests on Full Tube Specimens (gage length 2 ins.)						
2.1	Room	0.025	100,000	112,100	4.8	6.8
2.0	↓	↓	92,500	109,900	4.0	5.4
2.1	650		62,800	74,800	2.0	3.2
2.0	↓		58,100	74,500	2.9	4.6
2.6			50,900	71,900	2.3	2.8
2.5	750		50,500	68,200	2.6	3.9
2.7	750		48,900	69,500	-	-

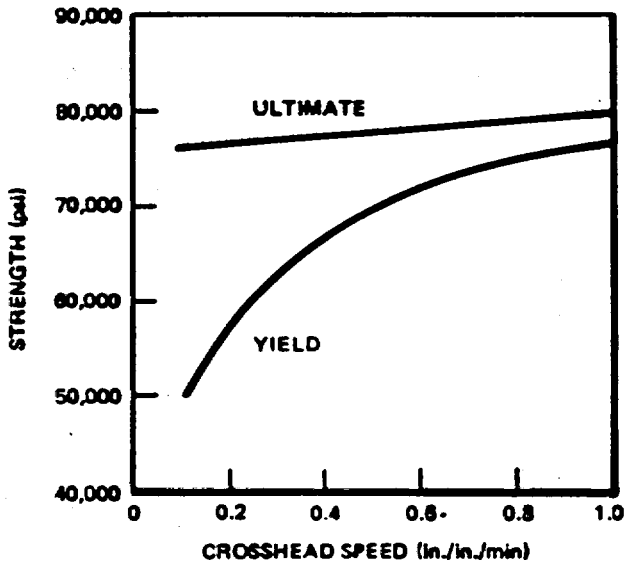

Plot showing the variation of ultimate and yield strength of Zircaloy sheet with increasing cross-head speed.

FIGURE V-35. VARIATIONS OF ZIRCALOY ULTIMATE AND YIELD STRENGTH

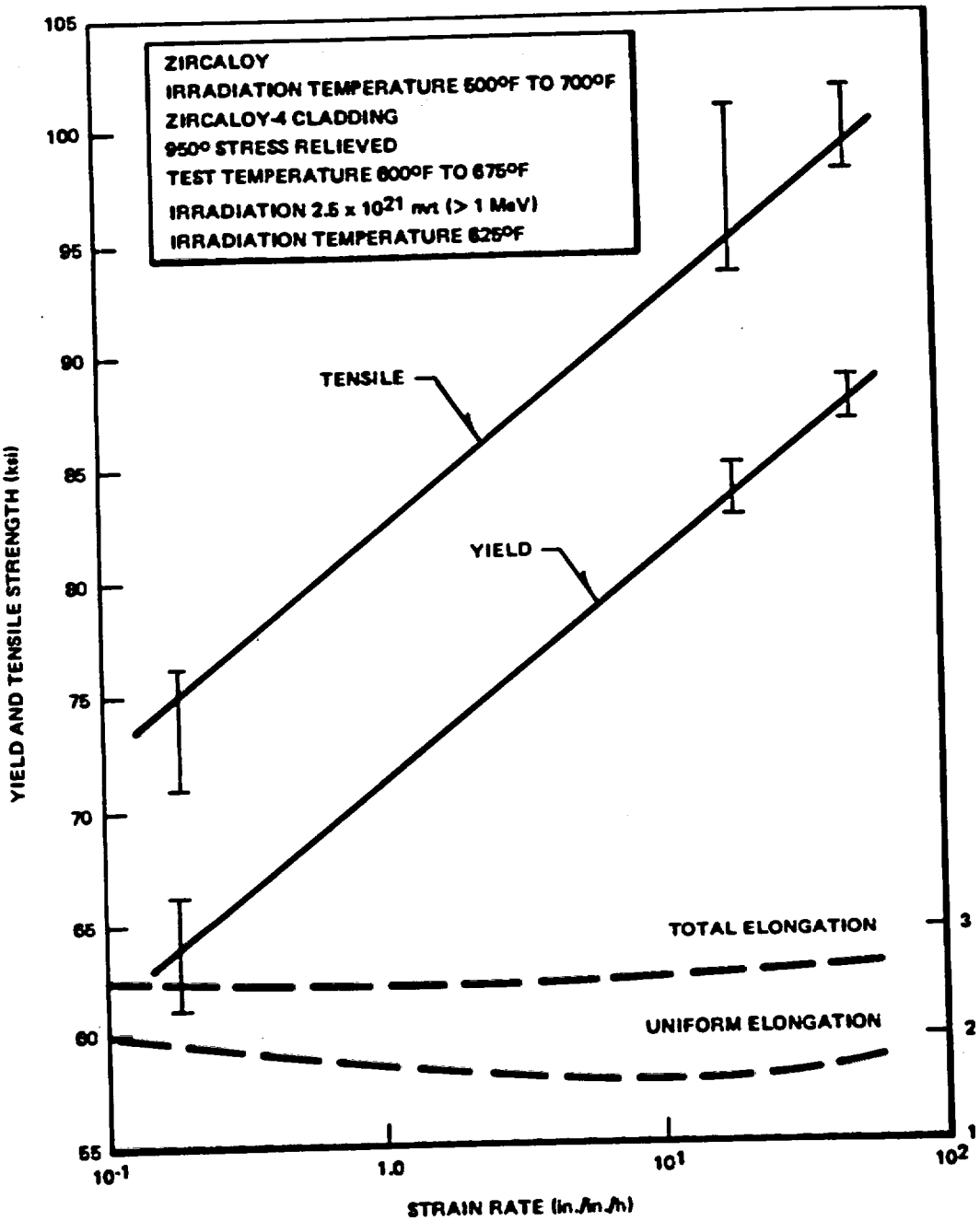

FIGURE V-36. ZIRCONIUM ELONGATION, YIELD STRENGTH AND TENSILE STRENGTH VERSUS STRAIN RATE

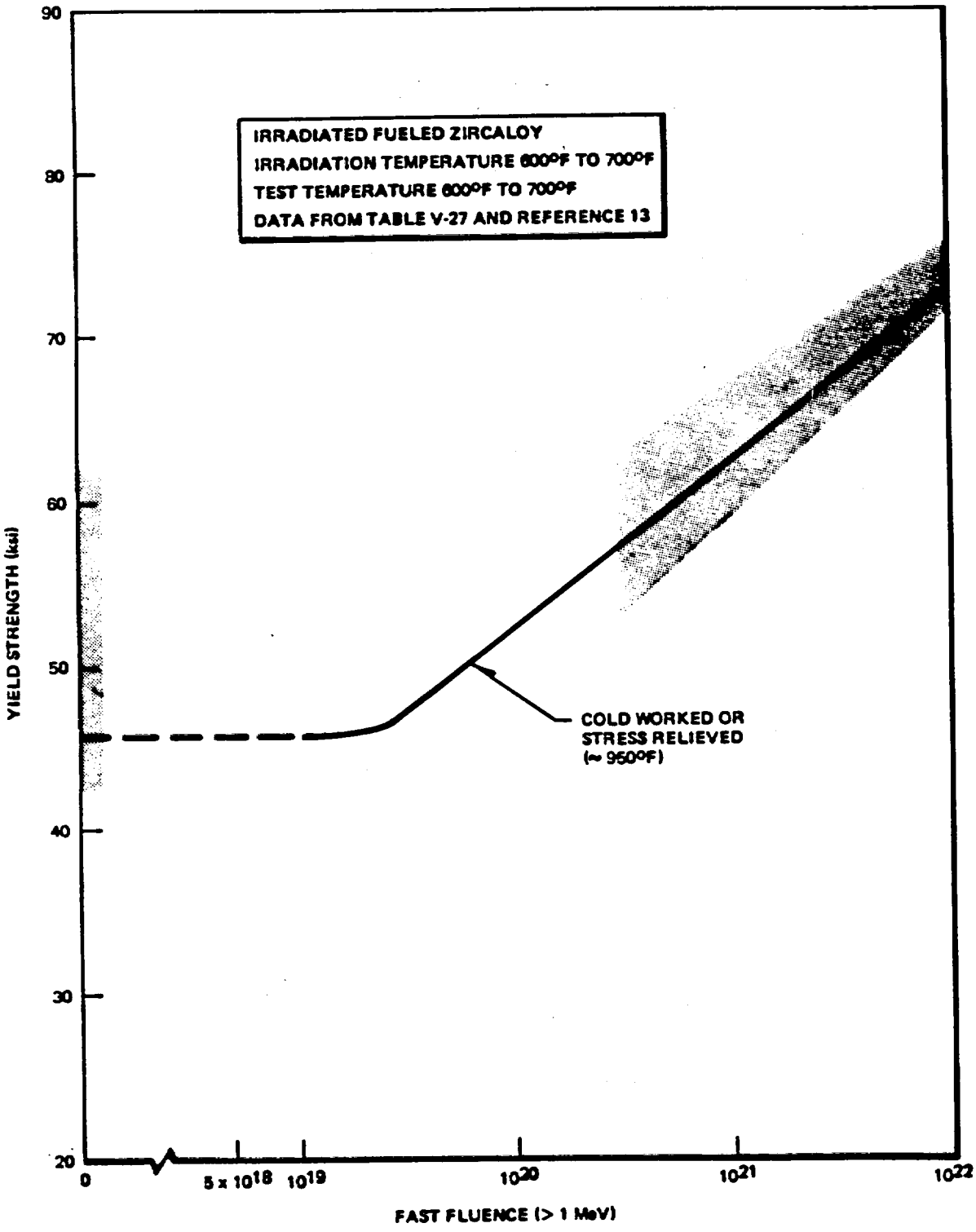

FIGURE V-37. DATA FROM TABLE V-27 AND REFERENCE (13)

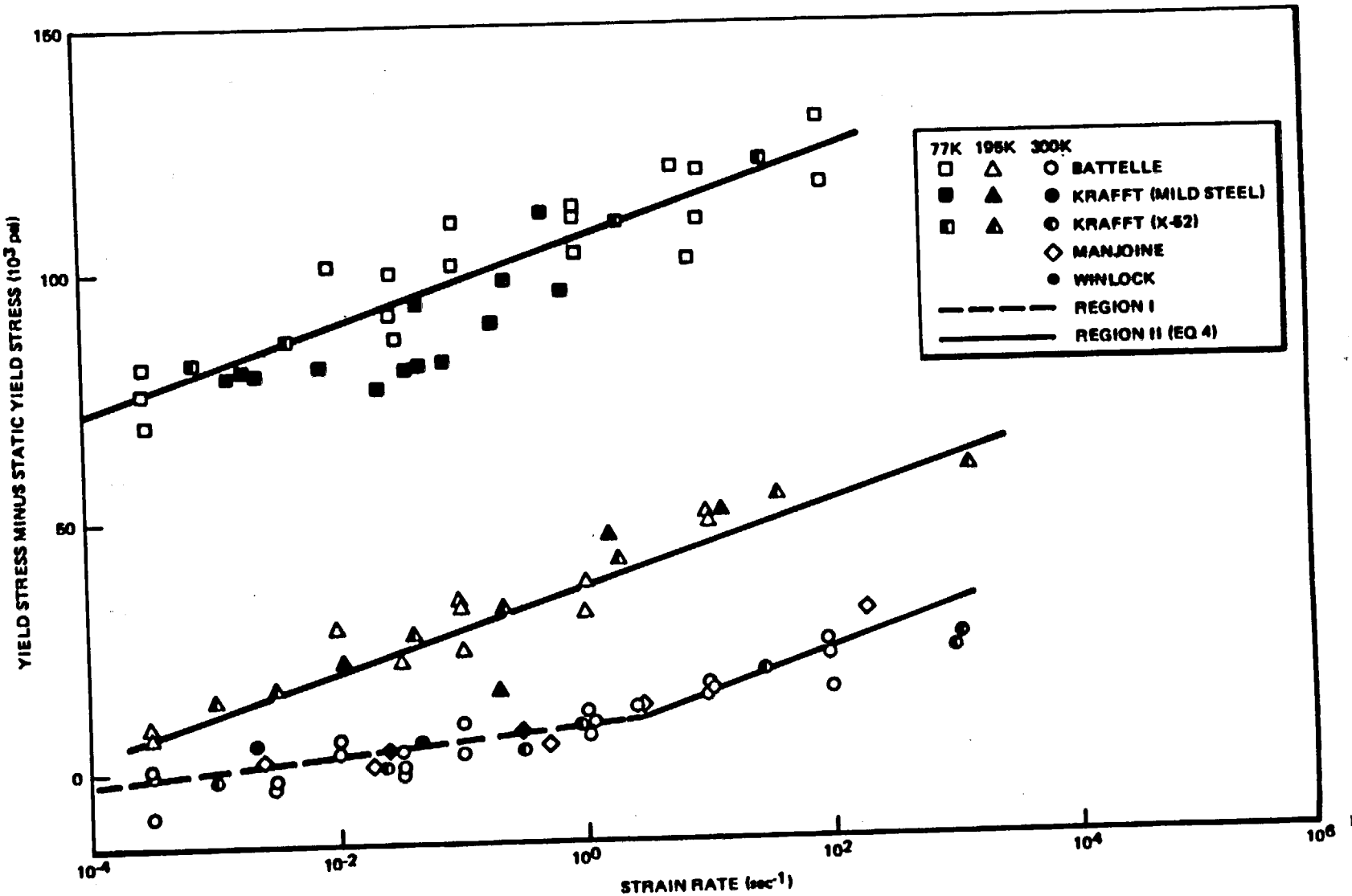

The graph reports the difference between the yield stress at the indicated strain rate and the room temperature value at 10^{-3} sec^{-1} (the static yield stress). Included are results of Krafft[18,14], Manjoina[15], Winlock[19], and Meiehan[13].

FIGURE V-38. INFLUENCE OF STRAIN RATE AND TEMPERATURE ON THE LOWER YIELD STRESS OF STEEL

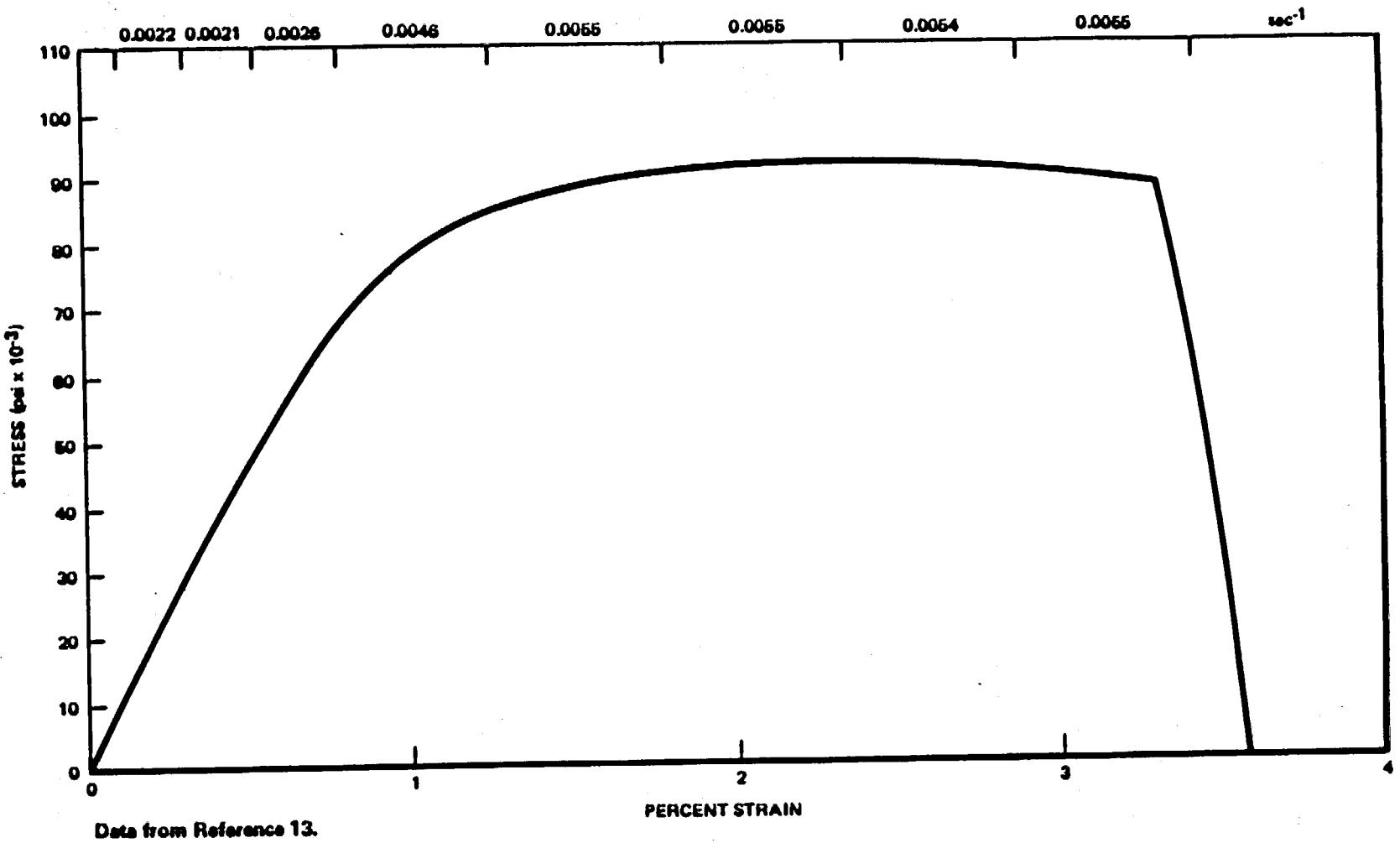

Data from Reference 13.

FIGURE V-39A. TYPICAL STRESS TRAIN CURVE FOR PWR CLADDING, FAST FLUENCE 2.5 X 10^{21} NVT (E > 1 Mev) TUBULAR SPECIMEN, GAGE LENGTH 2 IN. TESTED AT 625°F AT STRAIN RATE OF 5 X 10^{-3} SEC^{-1}

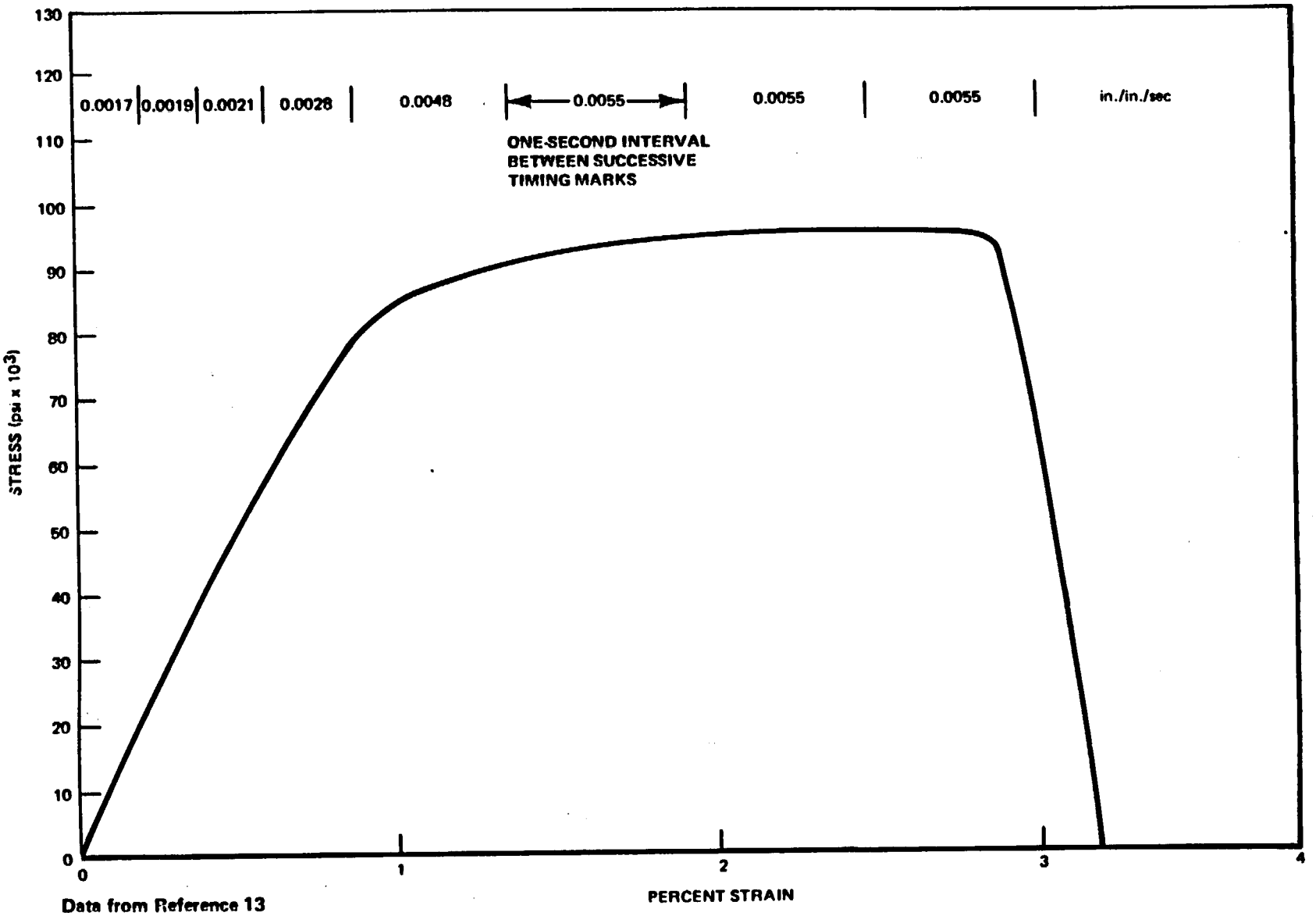

FIGURE V-39B. SPECIMEN T1-17-1 AT 625° AT A CROSSHEAD SPEED OF 1.2 IN./MIN. FAST FLUENCE IS 2.2 X 10^{21} NVT

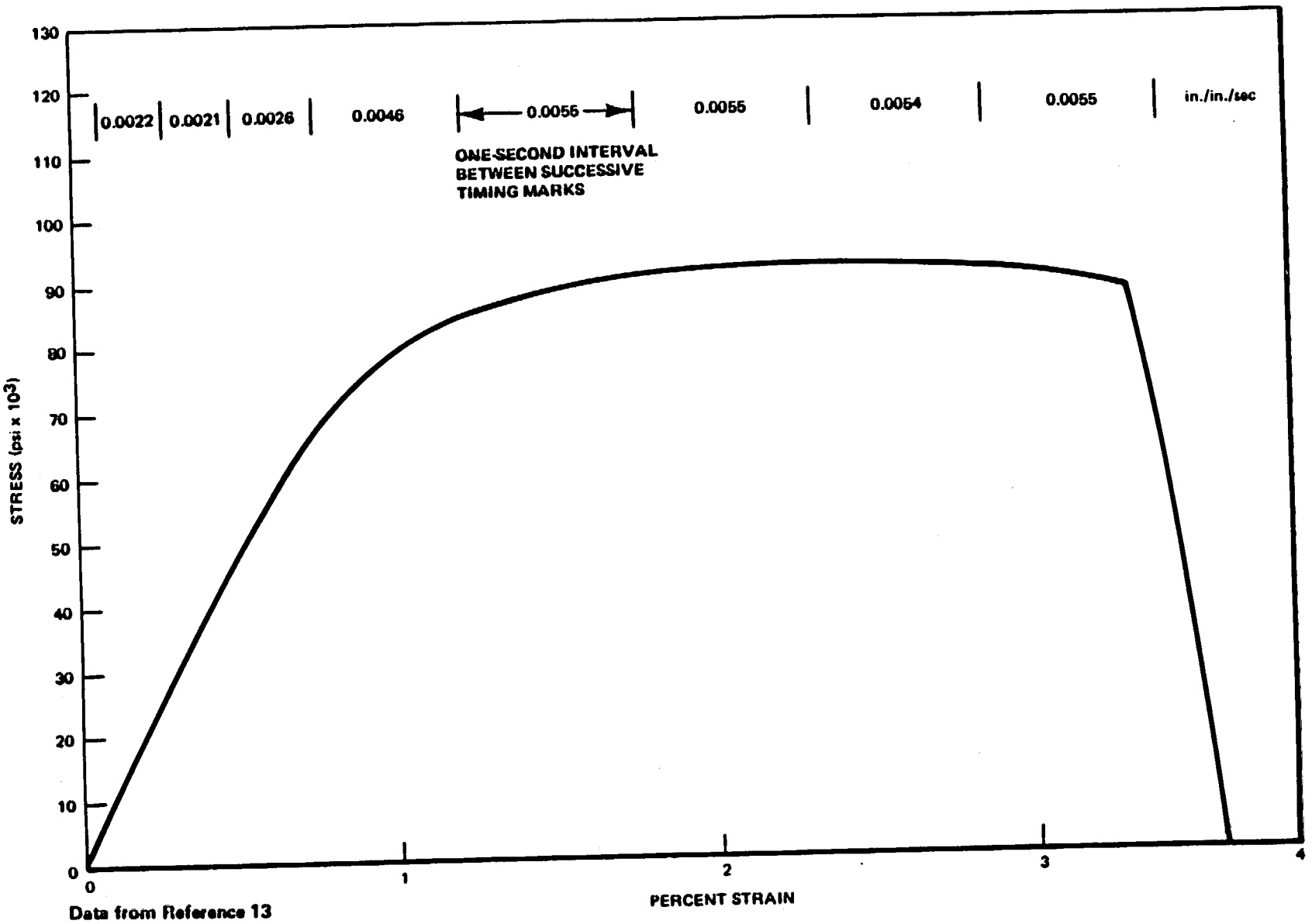

FIGURE V-39C. SPECIMEN T1-15-2 TESTED AT 625°F AT A CROSSHEAD SPEED OF 1.2 IN./MIN. FAST FLUENCE 2.5 X 10^{21} NVT

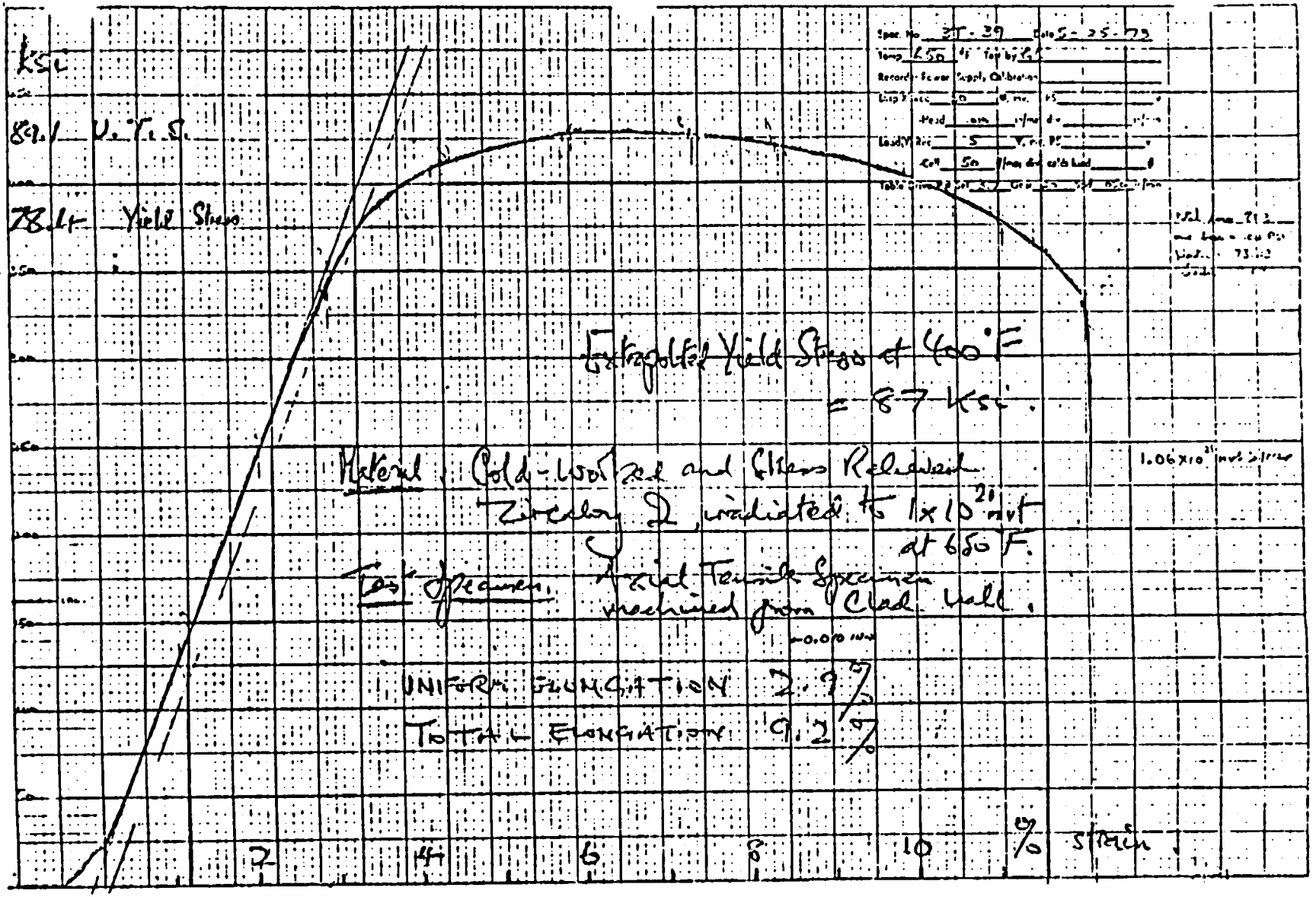

FIGURE V-40. SAMPLE OF ORIGINAL DATA: STRESS STRAIN CURVE FOR BWR CLADDING, FAST FLUENCE 1 X 10^{21} NVT AT 650°F UNIAXIAL TENSILE SPECIMEN, GAGE LENGTH 1 IN., CUT FROM TUBING

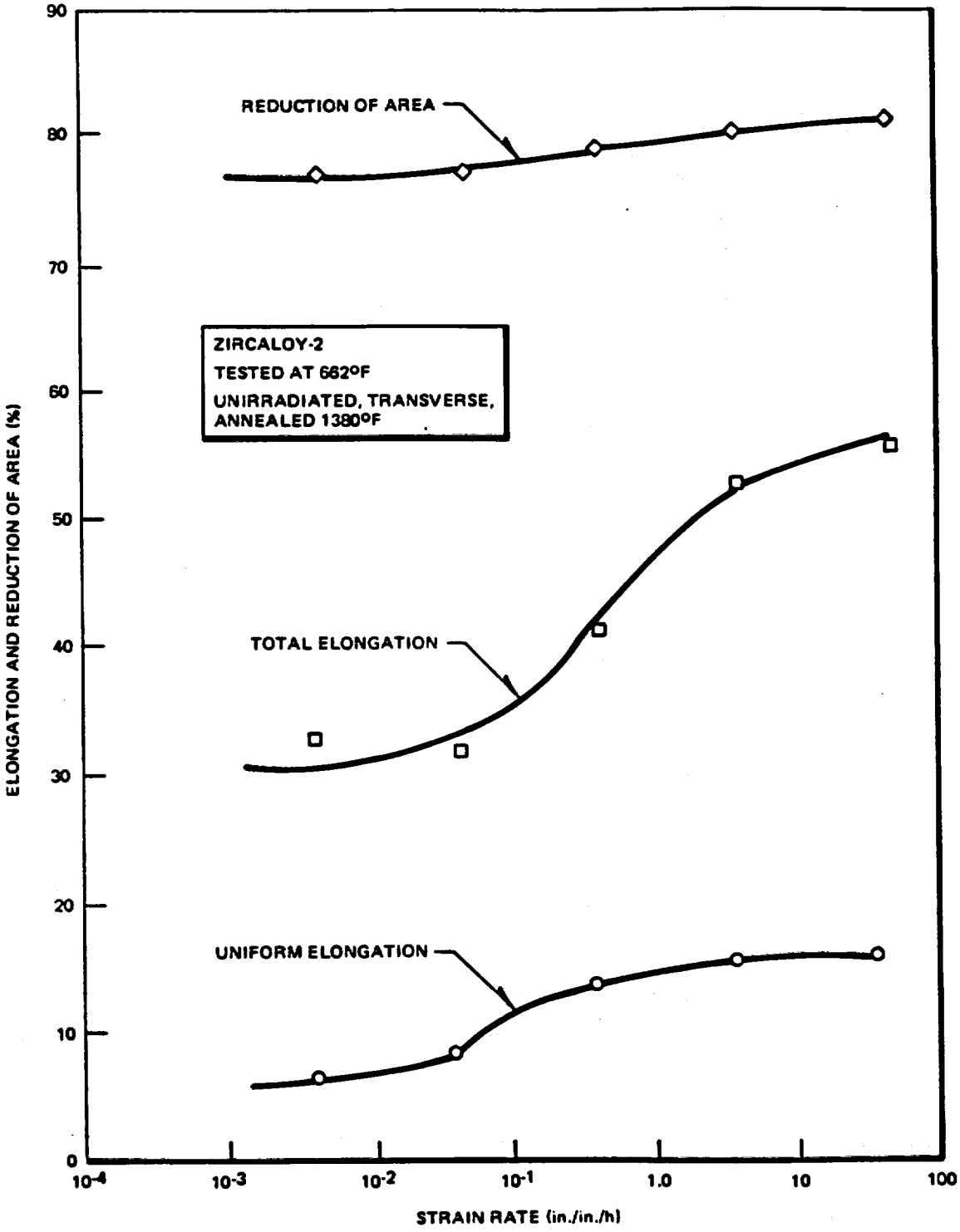

FIGURE V-41. DUCTILITY PARAMETERS VERSUS STRAIN RATE

TENSION CHARACTERISTICS AGAINST IMPACT VELOCITY. ALUMINUM

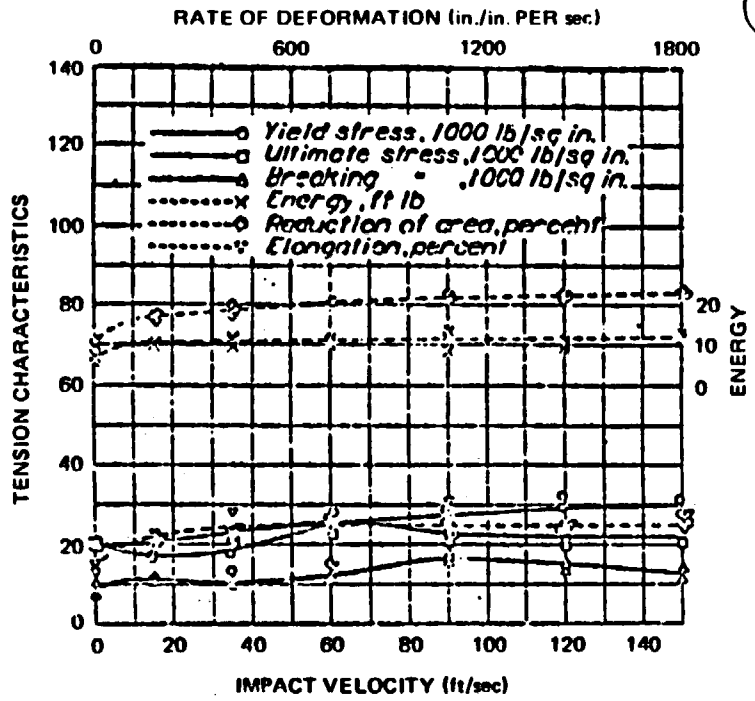

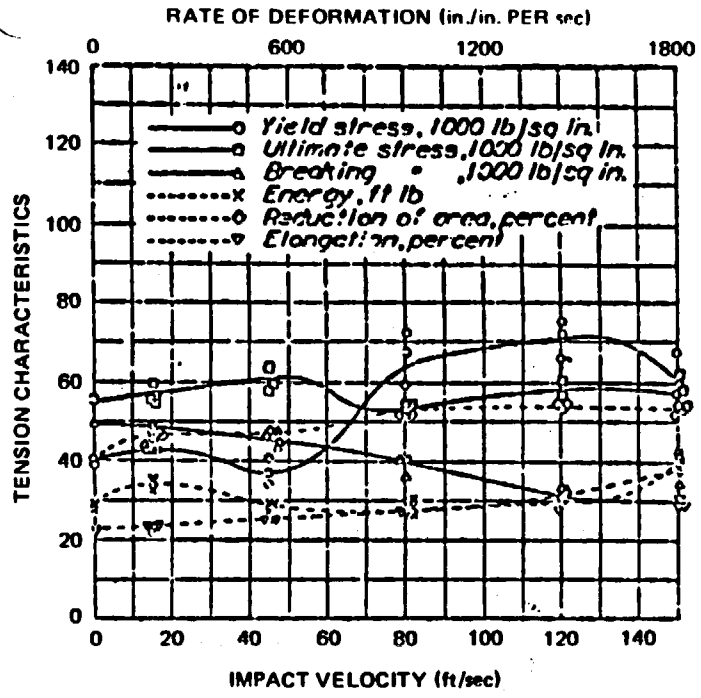

TENSION CHARACTERISTICS AGAINST IMPACT VELOCITY. 17ST DURALUMIN

TENSION CHARACTERISTICS AGAINST IMPACT VELOCITY. 24ST ALUMINUM ALLOY

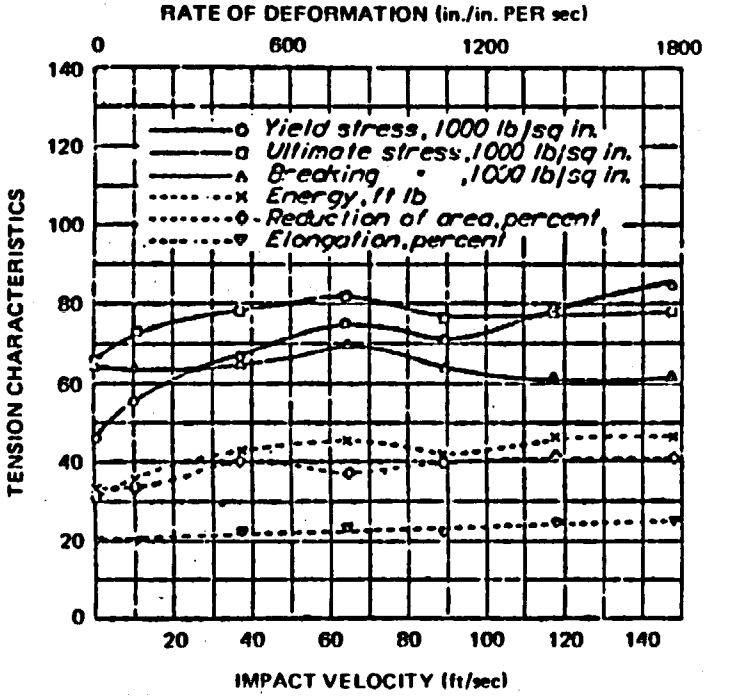

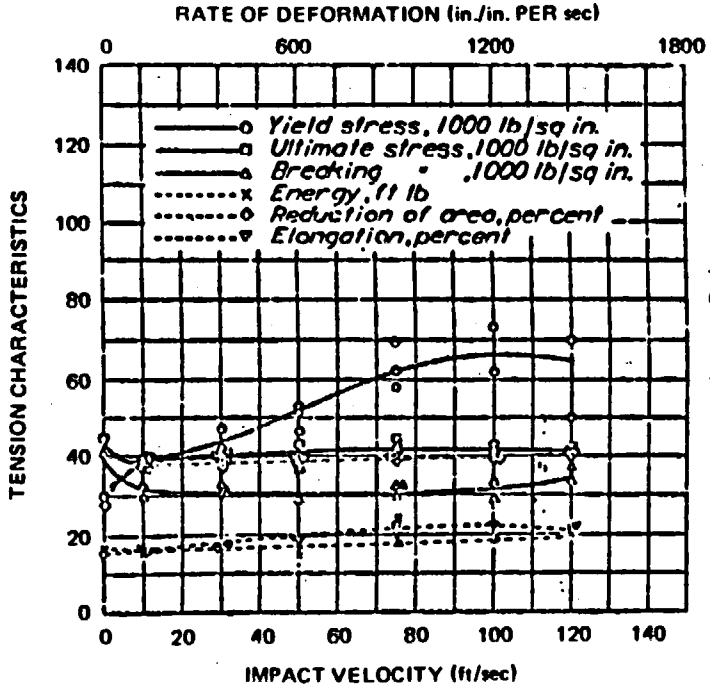

TENSION CHARACTERISTICS AGAINST IMPACT VELOCITY. DOW METAL J

FIGURE V-42. TENSION CHARACTERISTICS

TENSION CHARACTERISTICS AGAINST IMPACT VELOCITY. SAE X4130 DRAWN 600°F

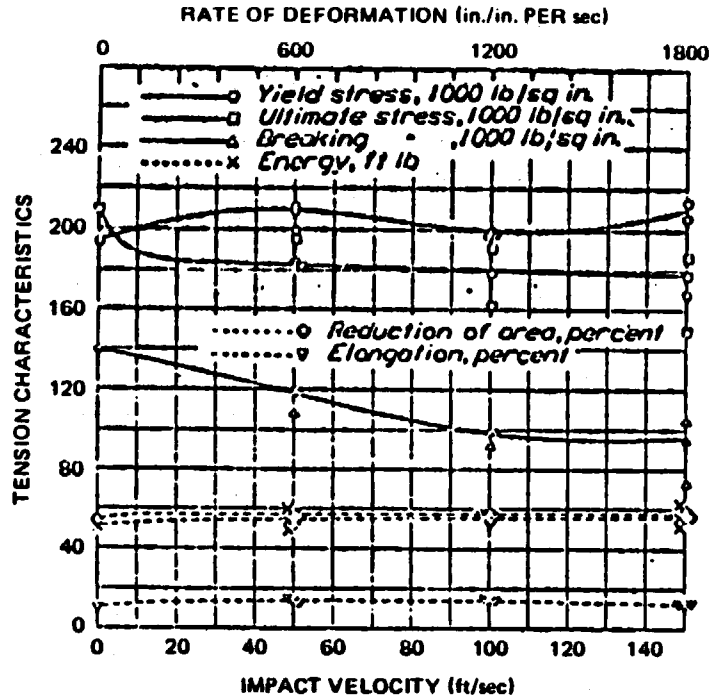

TENSION CHARACTERISTICS AGAINST IMPACT VELOCITY. SAE X4130 DRAWN 800°F

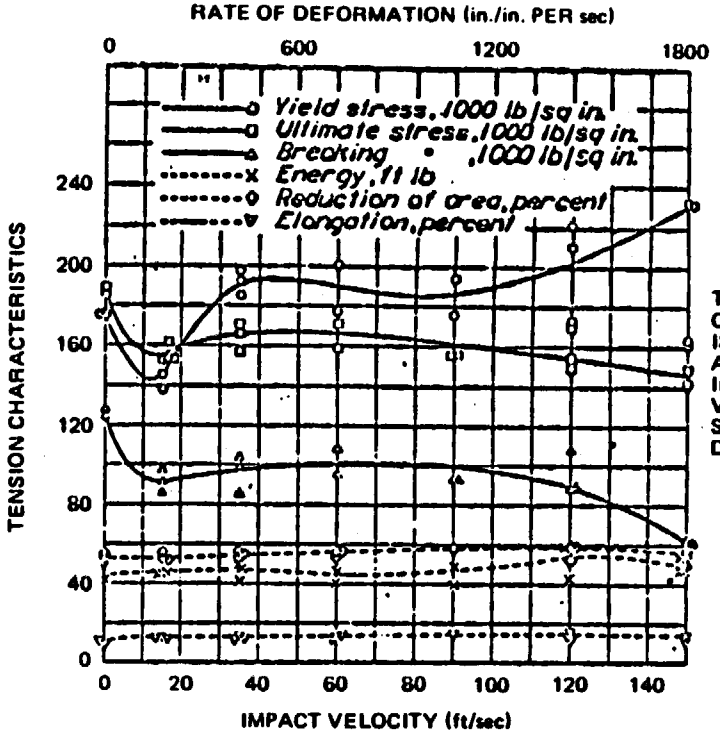

TENSION CHARACTERISTICS AGAINST IMPACT VELOCITY. SAE X4130 DRAWN 1000°F

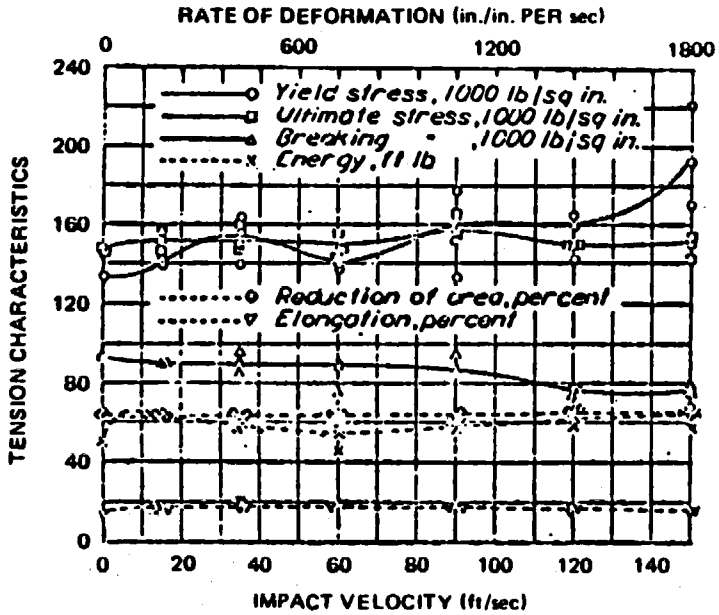

TENSION CHARACTERISTICS AGAINST IMPACT VELOCITY. SAE X4130 ANNEALED

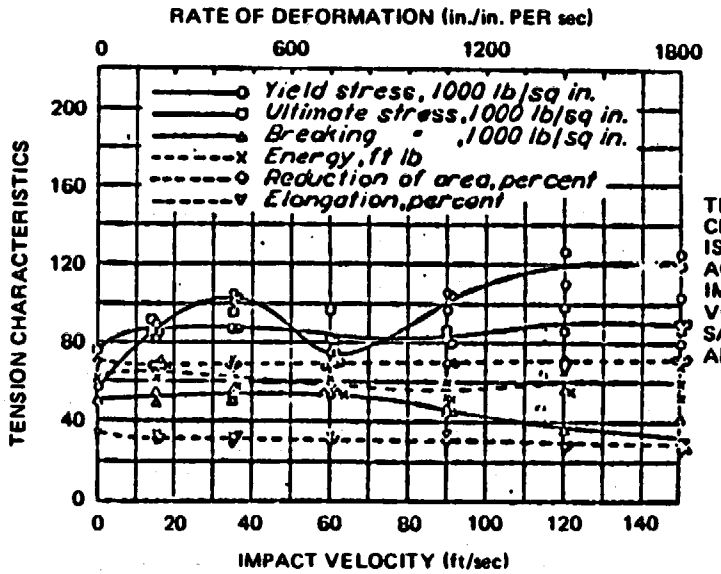

FIGURE V-43. TENSION CHARACTERISTICS

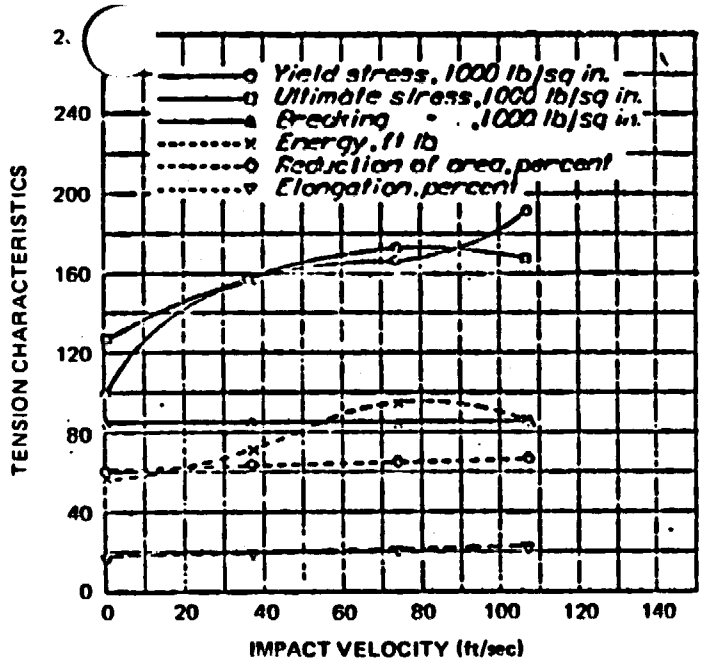

TENSION CHARACTER-ISTICS AGAINST IMPACT VELOCITY. 16-2 STAINLESS STEEL, OIL QUENCHED, DRAWN 1200°

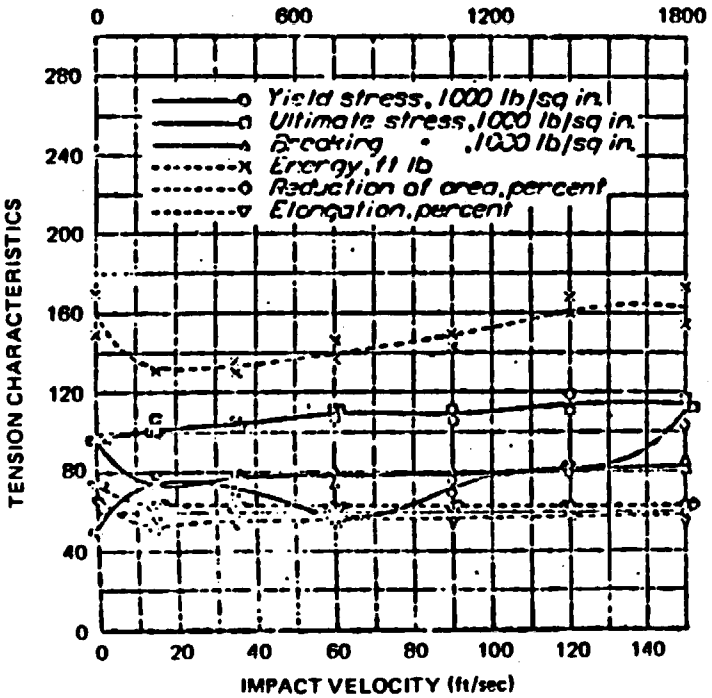

TENSION CHARACTER-ISTICS AGAINST IMPACT VELOCITY. 18-8 STAINLESS STEEL

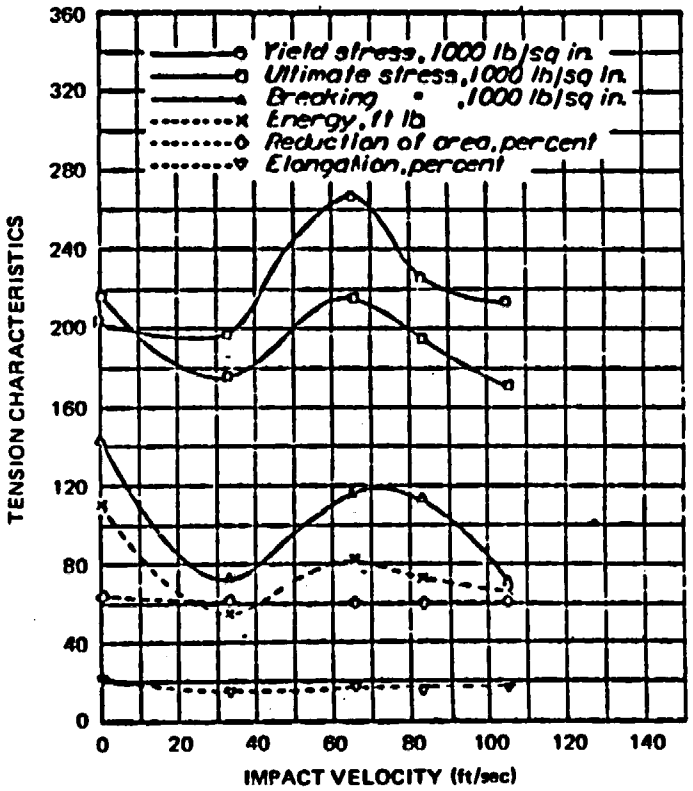

TENSION CHARACTERISTICS AGAINST IMPACT VELOCITY. 16-2 STAINLESS STEEL, OIL QUENCHED, DRAWN 900°

FIGURE V-44. TENSION CHARACTERISTICS

is the sum of the elastic and uniform plastic strains. Inspection of the load-elongation curves shown in Figures V-38, V-39A through C, and V-40 and confirmed by the load-elongation curves for lower fluence Zircaloy reported by Hardy in Figure 3 of his paper[19], shows that the elastic strain component is at least 0.7%. The calculated elastic strain at 400°F for the cladding having a yield stress of 85 Ksi is 0.68%, using $E = 12.4 \times 10^6$ lbs/in^2[16]. An increase in elastic strain of 0.16% will be obtained if the yield stress is raised 20 Ksi by the high-strain-rate in the drop event.

After high fluence irradiation, uniform elongation values, Table V-29 and Ref. (13) obtained in tensile tests on cladding tubular specimens average 2.7% including elastic strains. Total elongation values average at 5.1% including elastic strains. Data obtained from tensile specimens of similar texture irradiated to 7×10^{21} nvt show similar plastic strain values[17] over the range of fluences $1 \times 10^{21} - 1 \times 10^{22}$.

e. Strain-rate Phenomena

The stress-strain curve used in the fuel rod computer model was a static curve at 400°F elevated in strength by 25% to account for the property changes experienced under dynamic conditions (high strain-rate). The computer model results shown in following sections indicate a maximum strain rate of $\sim$6 in/in/sec. The discussion of tensile strength and ductility contained in the physical properties discussion above demonstrates that irradiated Zircaloy strength values increase with increasing strain-rate while elongation values remain essentially unchanged. A value of 25% increase in strength levels is a reasonable estimate of this strain-rate effect. The consistency of elongation values is derived from a study of numerous alloys having a wide range of properties. Although

irradiated Zircaloy was not in the study, there is no reason to believe that it would not behave in a manner similar to that of the other alloys.

f. Temperature Correction

The temperature correction for the stress-strain curve to 400°F from 625°F is made by adding 10 Ksi to the yield stress to allow for the reduction in temperature. An example plot showing the regular dependence of yield stress of Zircaloy on test temperature is shown in Figure 7.4, page 7.8 of Reference (19).

5.6.5.A.3 Clad Bending Tests

To verify the literature survey on irradiated Zircaloy properties General Electric performed a series of tests on actual fuel specimens. Highly irradiated fuel segments cut from Dresden I reactor bundles were available for testing purposes, however equipment to perform dynamic tests was not readily obtainable. Based on studies showing that elongation is not a function of strain rate, it was elected to perform quasi-static tests on these irradiated segments with equipment available at the Radioactive Materials Laboratory (RML) at General Electric's Vallecitos Nuclear Center.

a. Process

The irradiated material was Zircaloy cladding (containing uranium dioxide pellets) cut from Dresden I power reactor fuel bundles. The rod segments were approximately 12 inches long, and eleven such segments were tested. Bending of each segment was performed by placing the rod in a guided fixture and then driving a hydraulically actuated sem-circular ram of 5 1/2 inches in diameter into the rod mid span.

The wheel and bearing surfaces were coated with light lubricating oil to minimize frictional effects. Deflections were monitored visually with the aid of a scale beneath the ram.

Photographs were taken at selected displacement intervals and also when the rods were removed from the device; the photographs were used to measure the deflections and to show the state of the surface on the deformed section. The local strain in the bend region and the deflection capacity of the rod was estimated by simple geometrical considerations as shown below. It was noted that the deflections (elastic and plastic) under load considerably exceeded the plastic deflection measured after unloading. An approximate evaluation of the rate of deformation was obtained by recording the time intervals during which the deflections were applied.

b. Material

The material used was a Zircaloy-2 cladding manufactured by RMI, cold-rocked to size, and stress relieved at 960°F for 2 hours. This is typical of LWR fuel cladding.

Eight specimens were cut from fuel having a burn-up of 14,298-17,079 MWd/T (fast neutron exposures 2.2 - 2.8 x 10^{21} nvt). Four sections were cut from fuel having a burn-up of 11,819-14,598 MWd/T (fast neutron exposures 1.7-2.3 x 10^{21} nvt).

Mechanical properties at room temperature typical of Zircaloy cladding of neutron exposures in this range are:

Yield strength:	∿110 Ksi	
U.T.S.	∿120 Ksi	obtained in axial
Uniform elongation:	1.0-3.0%	tensile tests[13] [17]
Total elongation:	3.5%	

Literature data e.g. Reference (13) and (17) show that although the yield and ultimate strengths of Zircaloy cladding show some small increase over the fluence range 10^{21} - 10^{22} nvt there is little change in uniform or total elongation values with increasing fluence above 1 x 10^{21} nvt.